EXPERIMENTAL INVESTIGATIONS OF FROSTING AND DEFROSTING OF EVAPORATOR COILS AT FREEZER TEMPERATURES

By

NAWAF KHALID MISHARI AL-MUTAWA

A DISSERTATION PRESENTED TO THE GRADUATE SCHOOL
OF THE UNIVERSITY OF FLORIDA IN PARTIAL FULFILLMENT
OF THE REQUIREMENTS FOR THE DEGREE OF
DOCTOR OF PHILOSOPHY

UNIVERSITY OF FLORIDA

1997

In the Name of Allah The Ever-Merciful,
The Bestower of Mercy

This Dissertation is Dedicated to

My Father Khalid Mishari and My Mother Um Marzouq

My Wife Um-Mishari

My Sons, Mishari, Abdullah, Abdulrahman and Abdelilah

My Brothers Abu-Faisal and Abu-Khalid

My Sisters, Kawakeb, Um-Nasser, Um-Abeer and Um Essa

My Nephews, Nasser, Mohammed O., Faisal, Bader, Khalid,

Essa, Abdulaziz, Yousef and Mohammed S

My Nieces, Abeer, Samar, Ghada, Dalal, Dina, Amal,

Basmah, Mariam and Dalia

ACKNOWLEDGMENTS

Praise be to Allah, the Lord of the Universe. His help I seek and His guidance I search for, who blessed me by extending my life to complete this dissertation and earn my degree of Doctor of Philosophy in the field of mechanical engineering.

I would like to express my sincere appreciation, gratitude and thanks to my advisor Dr S.A. Sherif, chairman of the supervisory committee, for his invaluable guidance, criticism, and encouragement during the course of my studies. I have learned so much from the graduate courses that he taught in refrigeration, air-conditioning and thermal systems design. I have been delighted to be his student, his advisee and most of all his brother.

I also would like to extend my sincere appreciation and thanks to Dr W.E. Lear, Dr. H.A. Ingley III, Dr A.A. Seireg and Dr F.T. Najafi for serving on my supervisory committee. Their suggestions and remarks have helped in putting the dissertation the way it looks right now.

My sincere thanks go to several other individuals for helping in the construction and operation of the experimental facility employed in this project. The list includes John West, Jason Tiedeman, Jeff Urlaub, Justin Steadham, Steven MacFarlane, Robert Harker, and Dr G.D. Mathur. We formed a great work team that ended in the success of the project.

I am grateful to ASHRAE for supporting this project, and to the generous financial support provided by the Department of Mechanical Engineering which was crucial in being able to successfully complete this challenging project. I am also grateful to Kuwait University for providing me a scholarship to purse my Ph.D studies at an American university

Finally, I wish to express my gratitude and thanks to my parents, to my wife and four sons, Mishari, Abdullah, Abdulrahman and Abdelilah, for the prayers, patience, devotion, and encouragement during my studies.

TABLE OF CONTENTS

Page

ACKNOWLEDGMENTS iii

LIST OF TABLES ix

LIST OF FIGURES xi

ABSTRACT xxi

CHAPTERS

1 INTRODUCTION 1

- 1.1. Background 1
- 1.2. Review of Previous Related Work 2
- 1.3 Problem Statement 6
- 1.4. Objectives of the Research 7

2 EXPERIMENTAL FACILITY 10

- 2.1 Refrigeration/Defrost System 10
  - 2.1.1 Condensing Unit 11
  - 2.1.2. Test Fan-Coil Unit 11
  - 2.1.3 Auxilary Fan-Coil Unit 19
  - 2.1.4 Refrigeration Piping and Related Components. 26
    - 2.1.4.1 General piping system layout 26
    - 2.1.4.2 Load compensation unit. 35
    - 2.1.4.3 Surge drum 38
    - 2.1.4.4 Liquid pump 40
    - 2.1.4.5 Oil capturing system 40
    - 2.1.4.6. Compressor capacity control system 44
- 2.2. Air Distribution System 45
  - 2.2.1 Psychrometric Freezer Room 45
  - 2.2.2. General Layout of the Airflow System 52
  - 2.2.3 Air Distribution Diffuser 57
  - 2.2.4 Artificial Load Generation System 57

3 INSTRUMENTATION AND DATA ACQUISITION 63

3.1 Instrumentation System 63
3.1.1 Melt Weight Measurements 63
3.1.2 Frost Thickness Measurements 69
3.1.3 Temperature Measurements 72
3.1.4 Pressure Measurements 79
3.1.5 Refrigerant Mass Flow Rate Measurements 88
3.1.6 Humidity Measurements 95
3.1.7 Electric Power Measurements 97
3.1.8 Electrical Wiring 97
3.2. Data Acquisition System 109
3.2.1 Computer 110
3.2.2 Software 110
3.2.3 Data Acquisition Boards 111

4 TESTING PROCEDURES AND DATA REDUCTION 120

4.1 Testing Procedures 120
4.2 Data Reduction 121

5. QUALIFICATION TESTS 132

6. REFRIGERATION/DEFROST CYCLE DYNAMICS 151

6.1 Case of Entering Air Temperature of -8°F 151
6.2. Case of Entering Air Temperature of -13°F 183

7 ANALYSIS OF LOADS 215

7.1 Case of Entering Air Temperature of -8°F 215
7.2. Case of Entering Air Temperature of -13°F 224

8 A PARAMETRIC STUDY OF HOT-GAS DEFROSTING OF A CYLINDRICAL COIL COOLER 238

8.1 Introduction 238
8.2 Model Development 241
8.2.1 Pre Melting Stage 241
8.2.2 Melting Stage 250
8.3 Results and Discussion 263
8.4 Conclusions 276

9 VISUALIZATION STUDY .277

- 9.1 Psychrometrics in the Frost Zone 277
- 9.2 Visualizations of Frost Formation 284
  - 9.2.1 Subsaturated Conditions 284
  - 9.2.2. Transition from Subsaturated to Supersaturated Conditions 285
  - 9.2.3 Supersaturated Conditions 285
  - 9.2.4. Transition from Supersaturated to Subsaturated Conditions 296

10 CONCLUSIONS AND RECOMMENDATIONS 305

- 10.1 Conclusions 305
- 10.2 Recommendations 307

APPENDICES

A. DESCRIPTION OF THE CONDENSING UNIT 310

B DESCRIPTION OF THE PIPING SYSTEM 319

C DESCRIPTION OF THE COMPRESSOR CAPACITY CONTROL SYSTEM 340

D DESCRIPTION OF THE ARTIFICIAL LOAD GENERATION SYSTEM 344

E. ORIFICE METERS 352

- E.1 Performance Tests of the Orifice Meters 352
- E.2. Calculation Procedure for the Refrigerant Vapor Mass Flow Rate 354

F CALCULATION PROCEDURE FOR THE LIQUID REFRIGERANT MASS FLOW RATE 357

G TESTING PROCEDURES 359

- G.1 Initial Positions of the System Valves 359
- G.2. Setting the Psychrometric Room to the Testing Conditions 359
- G.3 Refrigeration/Hot-Gas Defrost Cycle 367
- G.4 System Shut Down 370

H. CALCULATION PROCEDURE FOR THE AVERAGE FROST TEMPERATURE 373

REFERENCES 375

BIOGRAPHICAL SKETCH 384

LIST OF TABLES

Table Page

2.1. Summary Description of the Piping System Components 30

2.2. Overall Coefficient of Heat Transfer *U* of the Front Wall. 48

2.3 Overall Coefficient of Heat Transfer *U* of the Rear and Side Walls 50

2.4. Overall Coefficient of Heat Transfer *U* of the Ceiling .51

2.5 Summary Description of the Artificial Load Generation System Components ... .61

3.1 Thermocouple Locations and the Fluids They Measure 73

3.2. Locations of the Pressure Measurements... 80

3.3 Methods of Pressure Measurements ..83

3.4 Power Transducers and the Devices They Measure 98

3.5 Specifications of the Power Transducers 99

3.6 Summary Description of the Electrical Wiring Components. 101

3.7 Functions of the Toggle Switches... 107

3.8. Summary Description of the Data Acquisition Boards.. 115

4.1 Components Contributing to the Total Sensible Internal Heat Gain ..125

5.1 Frequency and Duration of the Different Modes for the Run of (EAT = 0°F) ..133

5.2 Mass of Melt Collected From Both Fan-Coil Units for the Run of (EAT = 0°F) 135

6.1 Frequency and Duration of the Different Modes for the Run of (EAT = -8°F) 152

6.2 Mass of Melt Collected From Both Fan-Coil Units for the Run of (EAT = -8°F) 155

6.3 Frequency and Duration of the Different Modes for the Run of (EAT = -13°F) 184

6.4 Mass of Melt Collected From Both Fan-Coil Units for the Run of (EAT = -13°F) 185

7.1 Total Refrigeration Load Rate with Components and the Average Load Sensible Heat Ratio for the Run of (EAT = -8°F) 223

7.2 Defrost Heat Input, Heat Required to Melt FCU-T Frost, Defrost Heat Load Rate and Defrost Efficiency for the Run of (EAT = -8°F) 225

7.3 Average Coil Performance Load Rate and Fan-Defrost Contribution for the Run of (EAT = -8°F) 226

7.4 Total Refrigeration Load Rate with Components and the Average Load Sensible Heat Ratio for the Run of (EAT = -13°F) 233

7.5 Defrost Heat Input, Heat Required to Melt FCU-T Frost, Defrost Heat Load Rate and Defrost Efficiency for the Run of (EAT = -13°F) 235

7.6. Average Coil Performance Load Rate and Fan-Defrost Contribution for the Run of (EAT = -13°F) 236

A.1 Summary Description of the Condensing Unit Auxiliaries 312

E.1 Data From the Performance Tests 353

E.2. Polynomial Coefficients 355

G.1 Initial Positions of the Solenoid Valves 363

G.2 Initial Positions of the Gate and Ball Valves 364

LIST OF FIGURES

Figure Page

2.1 An isometric view of the refrigeration/defrost system 12

2.2. A different isometric view of the refrigeration/defrost system 13

2.3 Condensing unit 14

2.4 Front view of the test fan-coil unit (FCU-T) 16

2.5 Back view of the test fan-coil unit (FCU-T) 17

2.6 Schematic diagram of the test fan-coil unit (FCU-T) 18

2.7 Schematic diagram of the auxiliary fan-coil unit (FCU-A) 21

2.8 Exterior panels of the FCU-A 22

2.9 Location of the FCU-A on top of the psychrometric freezer room 23

2.10. Schematic diagram of the piping system 29

2.11 Components of the piping system inside the psychrometric freezer room 32

2.12 Schematic diagram of the load compensation unit (LCU) 37

2.13 Schematic diagram of the surge drum 39

2.14 Load compensation unit (LCU) and surge drum 41

2.15 Oil pump 43

2.16 The psychrometric freezer room 46

2.17 The psychrometric freezer room doors 47

2.18 General layout of the airflow system 53

2.19 Supply and return air duct connections with FCU-A 55

2.20 A top view of the airflow system inside the psychrometric freezer room 56

2.21 Schematic diagram of the special discharge diffuser 58

2.22. Plenum air outlets of the special discharge diffuser 59

2.23 Schematic diagram of the artificial load generation system 60

3.1 Melt weighing system 65

3.2 Digital scale for melt weight measurement 66

3.3 Melt return lines 68

3.4. Demand defrost system mounted on FCU-T 70

3.5 Frost detector head of the demand defrost system 71

3.6 Locations of FCU-T refrigerant temperature measurements 74

3.7. Locations of FCU-A refrigerant temperature measurements 75

3.8. Locations of FCU-T air dry bulb temperature measurements 76

3.9. Locations of air dry bulb temperature measurements across the psychrometric freezer room walls 77

3.10 Locations of melt temperature measurement 78

3.11. Locations of FCU-T refrigerant pressure measurements 81

3.12. Locations of refrigerant pressure measurements 82

3.13. Pressure gages mounted on the instrumentation board 84

3.14. Pressure gage on the hot-gas line for pressure measurement P4 85

3.15. Differential pressure measurement of the air across the FCU-T coil 87

3.16. Locations of refrigerant mass flow rate measurements 89

3.17 Schematic diagram of the orifice meter 91

3.18 Signet analog flow meter 94

3.19 Locations of relative humidity measurements 96

3.20 Schematic diagram of the electrical wiring 100

3.21 Control panel 106

3.22. Computer monitoring of several different blocks 112

3.23 Schematic diagram of the data acquisition boards layout 114

3.24 Solid state relay mounting and interface rack 117

3.25 Analog input multiplexors 119

5.1 FCU-A inlet and outlet refrigerant temperatures versus time during FCU-A initial refrigeration mode for the run of (EAT = 0°F) 136

5.2. FCU-A inlet and outlet refrigerant temperatures versus time during FCU-A final refrigeration mode for the run of (EAT = 0°F) 137

5.3 Air dry bulb temperatures across the freezer walls versus time during FCU-A initial refrigeration mode for the run of (EAT = 0°F) 139

5.4 Air dry bulb temperatures across the freezer walls versus time during FCU-A final refrigeration mode for the run of (EAT = 0°F) 140

5.5 FCU-T inlet and outlet refrigerant temperatures versus time during FCU-T refrigeration mode for the run of (EAT = 0°F) 142

5.6 Air dry bulb temperatures across the freezer walls versus time during FCU-T refrigeration mode for the run of (EAT = 0°F) 143

5.7 Air dry bulb temperatures across FCU-T versus time during FCU-T refrigeration mode for the run of (EAT = 0°F) 144

5.8 TD across FCU-T versus time during FCU-T refrigeration mode for the run of (EAT = 0°F) 145

5.9 FCU-T inlet and outlet refrigerant temperatures versus time during FCU-T hot-gas defrosting mode for the run of (EAT = 0°F) 146

5.10 Refrigerant pressures versus time for the run of (EAT = 0°F) 147

5.11 FCU-T coil after the hot-gas defrosting mode has been completed for the run of (EAT = 0°F) 149

5.12 A close up of the FCU-T coil after the hot-gas defrosting mode has been completed for the run of (EAT = 0°F) 150

6.1 FCU-A inlet and outlet refrigerant temperatures versus time during FCU-A initial refrigeration mode for the run of (EAT = -8°F) 156

6.2. FCU-A inlet and outlet refrigerant temperatures versus time during FCU-A refrigeration mode No. 1 for the run of (EAT = -8°F) 157

6.3 FCU-A inlet and outlet refrigerant temperatures versus time during FCU-A refrigeration mode No. 2 for the run of (EAT = -8°F) 158

6.4. FCU-A inlet and outlet refrigerant temperatures versus time during FCU-A refrigeration mode No. 3 for the run of (EAT = -8°F) 159

6.5 Air dry bulb temperatures across the freezer walls versus time during FCU-A initial refrigeration mode for the run of (EAT = -8°F) 160

6.6 Air dry bulb temperatures across the freezer walls versus time during FCU-A refrigeration mode No. 1 for the run of (EAT = -8°F) 161

6.7 Air dry bulb temperatures across the freezer walls versus time during FCU-A refrigeration mode No. 2 for the run of (EAT = -8°F) 162

6.8 Air dry bulb temperatures across the freezer walls versus time during FCU-A refrigeration mode No. 3 for the run of (EAT = -8°F) 163

6.9. FCU-T inlet and outlet refrigerant temperatures versus time during FCU-T refrigeration mode No. 1 for the run of (EAT = -8°F) 165

6.10 FCU-T inlet and outlet refrigerant temperatures versus time during FCU-T refrigeration mode No. 2 for the run of (EAT = -8°F) 166

6.11 FCU-T inlet and outlet refrigerant temperatures versus time during FCU-T refrigeration mode No. 3 for the run of (EAT = -8°F) 167

6.12 Air dry bulb temperatures across the freezer walls versus time during FCU-T refrigeration mode No. 1 for the run of (EAT = -8°F) 168

6.13 Air dry bulb temperatures across the freezer walls versus time during FCU-T refrigeration mode No. 2 for the run of (EAT = -8°F) 169

6.14 Air dry bulb temperatures across the freezer walls versus time during FCU-T refrigeration mode No 3 for the run of (EAT = -8°F) 170

6.15 Air dry bulb temperatures across FCU-T versus time during FCU-T refrigeration mode No 1 for the run of (EAT = -8°F) 171

6.16 Air dry bulb temperatures across FCU-T versus time during FCU-T refrigeration mode No 2 for the run of (EAT = -8°F) 172

6.17 Air dry bulb temperatures across FCU-T versus time during FCU-T refrigeration mode No 3 for the run of (EAT = -8°F) 173

6.18 TD across FCU-T versus time during FCU-T refrigeration mode No. 1 for the run of (EAT = -8°F) 174

6.19 TD across FCU-T versus time during FCU-T refrigeration mode No 2 for the run of (EAT = -8°F) 175

6.20 TD across FCU-T versus time during FCU-T refrigeration mode No. 3 for the run of (EAT = -8°F) 176

6.21 FCU-T inlet and outlet refrigerant temperatures versus time during FCU-T hot-gas defrosting mode No 1 for the run of (EAT = -8°F) 177

6.22 FCU-T inlet and outlet refrigerant temperatures versus time during FCU-T hot gas defrosting mode No. 2 for the run of (EAT = -8°F) 178

6.23 FCU-T inlet and outlet refrigerant temperatures versus time during FCU-T hot gas defrosting mode No 3 for the run of (EAT = -8°F) 179

6.24 Refrigerant pressures versus time for the run of (EAT = -8°F) 180

6.25 FCU-A inlet and outlet refrigerant temperatures versus time during FCU-A initial refrigeration mode for the run of (EAT = -13°F) 187

6.26 FCU-A inlet and outlet refrigerant temperatures versus time during FCU-A refrigeration mode No 1 for the run of (EAT = -13°F) 188

6.27 FCU-A inlet and outlet refrigerant temperatures versus time during FCU-A refrigeration mode No 2 for the run of (EAT = -13°F) 189

6.28 FCU-A inlet and outlet refrigerant temperatures versus time during FCU-A refrigeration mode No 3 for the run of (EAT = -13°F) 190

6.29 Air dry bulb temperatures across the freezer walls versus time during FCU-A initial refrigeration mode for the run of (EAT = -13°F) 191

6.30 Air dry bulb temperatures across the freezer walls versus time during FCU-A refrigeration mode No 1 for the run of (EAT = -13°F) 192

6.31 Air dry bulb temperatures across the freezer walls versus time during FCU-A refrigeration mode No 2 for the run of (EAT = -13°F) 193

6.32 Air dry bulb temperatures across the freezer walls versus time during FCU-A refrigeration mode No 3 for the run of (EAT = -13°F) 194

6.33. FCU-T inlet and outlet refrigerant temperatures versus time during FCU-T refrigeration mode No 1 for the run of (EAT = -13°F) 196

6.34. FCU-T inlet and outlet refrigerant temperatures versus time during FCU-T refrigeration mode No 2 for the run of (EAT = -13°F) 197

6.35 FCU-T inlet and outlet refrigerant temperatures versus time during FCU-T refrigeration mode No 3 for the run of (EAT = -13°F) 198

6.36. Air dry bulb temperatures across the freezer walls versus time during FCU-T refrigeration mode No 1 for the run of (EAT = -13°F) 199

6.37 Air dry bulb temperatures across the freezer walls versus time during FCU-T refrigeration mode No 2 for the run of (EAT = -13°F) 200

6.38. Air dry bulb temperatures across the freezer walls versus time during FCU-T refrigeration mode No 3 for the run of (EAT = -13°F) 201

6.39 Air dry bulb temperatures across FCU-T versus time during FCU-T refrigeration mode No. 1 for the run of (EAT = -13°F) 202

6.40. Air dry bulb temperatures across FCU-T versus time during FCU-T refrigeration mode No. 2 for the run of (EAT = -13°F) 203

6.41 Air dry bulb temperatures across FCU-T versus time during FCU-T refrigeration mode No 3 for the run of (EAT = -13°F) 204

6.42 TD across FCU-T versus time during FCU-T refrigeration mode No 1 for the run of (EAT = -13°F) 205

6.43 TD across FCU-T versus time during FCU-T refrigeration mode No 2 for the run of (EAT = -13°F) 206

6.44. TD across FCU-T versus time during FCU-T refrigeration mode No. 3 for the run of (EAT = -13°F) 207

6.45 FCU-T inlet and outlet refrigerant temperatures versus time during FCU-T hot-gas defrosting mode No. 1 for the run of (EAT = -13°F) 208

6.46 FCU-T inlet and outlet refrigerant temperatures versus time during FCU-T hot-gas defrosting mode No. 2 for the run of (EAT = -13°F) 209

6.47 FCU-T inlet and outlet refrigerant temperatures versus time during FCU-T hot-gas defrosting mode No. 3 for the run of (EAT = -13°F) 210

6.48 Refrigerant pressures versus time for the run of (EAT = -13°F) 211

7.1 Total sensible transmission heat gain and components versus time during FCU-T refrigeration mode No. 1 for the run of (EAT = -8°F) 216

7.2 Total sensible transmission heat gain and components versus time during FCU-T refrigeration mode No. 2 for the run of (EAT = -8°F) 217

7.3 Total sensible transmission heat gain and components versus time during FCU-T refrigeration mode No. 3 for the run of (EAT = -8°F) 218

7.4 Total natural sensible heat gain and components versus time during FCU-T refrigeration mode No. 1 for the run of (EAT = -8°F) 219

7.5 Total natural sensible heat gain and components versus time during FCU-T refrigeration mode No. 2 for the run of (EAT = -8°F) 220

7.6. Total natural sensible heat gain and components versus time during FCU-T refrigeration mode No. 3 for the run of (EAT = -8°F) 221

7.7. Total sensible transmission heat gain and components versus time during FCU-T refrigeration mode No. 1 for the run of (EAT = -13°F) 227

7.8 Total sensible transmission heat gain and components versus time during FCU-T refrigeration mode No. 2 for the run of (EAT = -13°F) 228

7.9 Total sensible transmission heat gain and components versus time during FCU-T refrigeration mode No. 3 for the run of (EAT = -13°F) 229

7.10 Total natural sensible heat gain and components versus time during FCU-T refrigeration mode No. 1 for the run of (EAT = -13°F) 230

7.11 Total natural sensible heat gain and components versus time during FCU-T refrigeration mode No. 2 for the run of (EAT = -13°F) ... 231

7.12 Total natural sensible heat gain and components versus time during FCU-T refrigeration mode No. 3 for the run of (EAT = -13°F) ... 232

8.1 Pre-melting stage ... 242

8.2. Melting stage ... 251

8.3 Sublimation heat rate versus time at different defrost heat input fluxes. ... 265

8.4 Evaporation heat rate versus time at different defrost heat input fluxes ... 266

8.5 Melting heat rate versus time at different defrost heat input fluxes ... 267

8.6 Frost thickness versus time at different defrost heat input fluxes ... 268

8.7 Sublimation heat rate versus time at different tube diameters ... 270

8.8 Evaporation heat rate versus time at different tube diameters. ... 271

8.9 Melting heat rate versus time at different tube diameters ... 272

8.10 Frost thickness versus time at different tube diameters ... 273

8.11 Sublimation, evaporation and melting heat rates versus time at different initial frost thicknesses ... 274

8.12. Frost thickness versus time at different initial frost thicknesses ... 275

9.1 Psychrometric chart ... 278

9.2. Encountered conditions at a typical freezer due to infiltration/exfiltration problems ... 279

9.3 Fog and haze formation at an actual freezer entrance. ... 281

9.4 Snow-like frost accumulations on an actual freezer coil ... 282

9.5 Infiltration/exfiltration air path typically encountered at actual freezer doorways ... 283

9.6 Frost formation on the FCU-T coil ($S_f = 0.031"$) ... 286

9.7 Frost formation on the FCU-T coil ($S_f = 0.069"$) 287
9.8 Frost formation on the FCU-T coil ($S_f = 0.107"$) 288
9.9 Fog formation at $S_f = 0.107"$ 289
9.10 Frost formation on the FCU-T coil ($S_f = 0.146"$) 291
9.11 Frost formation on the FCU-T coil ($S_f = 0.184"$) 292
9.12. Airborne ice crystals at $S_f = 0.184"$ 293
9.13 Haze formation 294
9.14 Haze formation – a few seconds later 295
9.15 Supersaturated conditions 297
9.16 A close-up view of supersaturated conditions 298
9.17 Unfavorable frost formation under severe supersaturated conditions 299
9.18 Clogging of FCU-T fan outlet under severe supersaturated conditions 300
9.19 Frost sublimating 301
9.20 Frost melting after subsaturated conditions have been restored 303
9.21 Frosted FCU-T after subsaturated conditions have been restored 304
A.1 Schematic diagram of the condensing unit with auxiliary components 311
A.2 Demand cooling system diagram 317
B.1 Schematic diagram of the FCU-T under the refrigeration mode. 330
B.2 Schematic diagram of the FCU-T under the hot gas defrosting mode 331
B.3 Defrost refrigerant separator 333
B.4 Defrost refrigerant line and its components 335
D.1 Electronic diaphragm metering pump 346
D.2 Water-vapor generator 348

D.3 Artificial load generator ... 350

G.1 Operating procedures -- piping system 360

G.2. Operating procedures -- melt weighing system 361

G.3 Operating procedures -- artificial load generation system 362

Abstract of Dissertation Presented to the Graduate School
of the University of Florida in Partial Fulfillment of the
Requirements for the Degree of Doctor of Philosophy

EXPERIMENTAL INVESTIGATIONS OF FROSTING AND DEFROSTING OF EVAPORATOR COILS AT FREEZER TEMPERATURES

By

Nawaf Khalid Mishari Al-Mutawa

August, 1997

Chairman: S.A. Sherif
Major Department: Mechanical Engineering

In the field of industrial refrigeration, the heat input required to defrost coils within freezers is utilized in three parts. The first part will be used to melt the frost, while the second part warms the metal of the coil and its contents. The latter part will be transferred to the refrigerant when the evaporator switches from the defrosting mode to the next refrigeration mode. The third part of the defrost heat input transfers into the freezer space. The second and third parts represent the defrost heat loads affecting the refrigeration system.

The heat loads associated with defrosting of coils have not been fully quantified as a function of the various parameters which affect the system. The current rule of thumb is to simply assume that the coil defrosting load added to the fan heat exceeds 15% of the net refrigeration load with no clear direction as to how a designer may determine what the actual defrosting load may be

In this research, a method is outlined for determining and quantifying the heat loads associated with freezer coil defrosting using the hot refrigerant vapor defrost method. This dissertation will outline this method in detail. It will also describe an experimental test facility which was designed and constructed for that purpose in addition to describing the experimental procedures employed in the data acquisition and reduction stages. Based on the testing results obtained for several coil entering air dry bulb temperatures (EAT) the defrost heat load is found to be in a good order-of-magnitude agreement with the 15% rule of thumb.

The dissertation also examines the time-dependent dynamics of a refrigeration/defrost system. This involves the delicate task of generating time profiles of a host of variables which are bound to change as the system cycles from the refrigeration mode to the defrosting mode and back to the refrigeration mode again several consecutive times. A visualization study of frost formation at freezer temperatures is also described in this dissertation. This study is intended to provide a qualitative assessment of psychrometric processes typically encountered in true-to-life industrial freezers. Last but not least, the dissertation describes a mathematical model for predicting the evaporation and sublimation rates on a frosted cylindrical coil cooler during hot gas defrosting of the coil.

CHAPTER 1
INTRODUCTION

1.1. Background

When refrigerant freezer coils (unit coolers) are exposed to moist air conditions due to infiltration, doorways and other forms of external exposure, frost forms on the coil surfaces. This frost is detrimental to the thermal performance of the coils and needs to be periodically cleared. A variety of methods are used to clear the frost but the more common type is the "hot-gas defrost" where the hot refrigerant vapor from the compressor discharge flows through the coil, raises the coil temperature and thereby removes the frost.

The heat loads associated with defrosting of the coils have not been fully quantified as a function of the various parameters which affect the system. The current rule of thumb is to simply assume that the coil defrosting load added to the fan heat exceeds 15% of the net refrigeration load with no clear direction as to how a designer may determine what the actual defrosting load may be

This dissertation explains the research conducted in order to experimentally investigate the frosting and defrosting of finned-tube evaporator coils at freezer temperatures. This research was sponsored by ASHRAE under contract number RP-622, and represents the first phase of a projected multiphase investigation on refrigeration in low temperature environments. The performed research outlines a method for determining and quantifying the heat loads associated with freezer coil defrosting using the hot refrigerant vapor defrost method The dissertation will outline details of the experimental facility along with the instrumentation and data acquisition systems employed. It will also outline the testing procedures employed and data reduction methodology used, qualification tests performed the dynamics of the refrigeration/defrost cycle and the analysis of defrost loads Finally, a visualization study of frost formation at freezer temperatures is also described in this dissertation. The latter study is intended to provide a qualitative assessment of psychrometric processes typically encountered in true to-life industrial freezers.

1.2. Review of Previous Related Work

There has been considerable amount of work done in the area of frost formation and defrosting in heat exchange equipment. While the coils of specific interest in this research are freezer coils used in the refrigeration industry, coil frosting is also a problem faced by the air conditioning industry - heat pumps to be more specific. There appears to have been more work done in relation to heat exchangers used more commonly in the air conditioning industry - heat pumps and high fin density tube fin heat exchangers.

Previous studies on frosting in finned tube heat exchangers have been described by Kondepudi and O Neal (1987) in which only a handful dealt with coils with large fin spacings similar to those in freezer coils Kondepudi (1988) and Kondepudi and O'Neal (1988, 1989a, 1989b 1989c 1990, 1991a, 1991b) also did their own studies on the thermal effects of frosting for a variety of fin surfaces--smooth, wavy, corrugated and louvered. They found that the general observations of performance deterioration as a result of frost were true only if the air flow rate was allowed to dwindle with the increase in pressure drop. If the airflow was maintained constant, there was little appreciable drop in thermal performance.

Other investigators who have studied the effects of frosting on coils with large fin spaces include Sanders (1974), Niederer (1976), Stoecker (1957, 1960), Hosoda and Uzuhashi (1967), and Gatchilov and Ivanova (1979). These investigators examined coils with fin densities ranging from 2 to 8 fins per inch and mainly dealt with the heat transfer and pressure drop aspects of the frosting process. More recently, Smith (1989) analyzed cooling-coil load calculations at freezer temperatures. His analysis was based on the psychrometrics at low temperatures, the entering air and refrigerant temperatures and sensible heat ratio. He recognized the need for and suggested that more studies on the evaluation of cooling-coil performance under a full range of sensible heat ratios be performed.

While the aforementioned studies are very important in that they help establish a more fundamental basis as to the thermal and airside pressure drop characteristics of the frost formation process on the coils along with the factors affecting frost formation and the effects of fin geometry on the frosting process, they do not address the heat loads associated with defrosting the coils themselves. Among the investigators who examined defrosting of freezer coils are Kerschbaumer (1971), Niederer (1976), Stoecker et al. (1983), Coley (1983) and more recently Cole (1989). Niederer (1976) attempted to determine the amount of heat required for defrost by measuring the amount of hot-gas condensing and the power (kW) input during the defrost cycle. He found that only 15 to 25% of the total heat went to melt the frost. He observed that the remaining 75 to 85% of the heat went to heat the surrounding environment and the coil/cabinet surfaces. Kerschbaumer (1971) defined the defrost efficiency (η_D) to be the ratio of the total heat required to melt the frost alone (including sensible warming) to the total amount of defrost heat input (including any refrigeration load effects) Stoecker et al. (1983) conducted a study which considered the effect of hot gas defrost in industrial refrigeration systems They presented an itemization of the various components which were heated by the hot gas defrost--melting of the frost and warming of the coil surfaces (fins and tubes) themselves. The component of the load which heats the coil metal surfaces themselves is important in that when the system goes back into the refrigeration mode, the surfaces need to be cooled down again, thereby representing an additional load on the refrigeration system.

Coley (1983) suggested that during a defrost cycle in freezers, at least 15% of the frost sublimes (directly transforms into vapor) into the surrounding refrigerated air space. This represents an additional amount of load to be subsequently removed by future refrigeration cycles. Cole (1989) showed that Coley's (1983) assertions were valid with data presented by Stoecker et al (1983) He presented data obtained from a manufacturer which gave a breakdown of the various heat loads during typical defrost of an ammonia based unit. He also presented a graphical analysis of the estimated costs associated with coil defrosting.

In summary previous studies have established the various parameters which affect frosting and defrosting of coils. Some have concerned themselves with the loads associated with defrost, but there has been no full-fledged study on the latter The following general conclusions can be drawn from previous studies

a. Frost formation is detrimental to the overall thermal performance of heat exchanger coils

b. The density of the frost layer is constantly varying approaching that of ice for the lower sections of the layer This causes the thermal properties of the frost to vary

c. A distinction has been made between the more dense ice-like coil frost and the less dense snow like coil frost by referring to them as favorable and unfavorable frost, respectively (Smith 1989)

d. Coils with low fin densities tend to perform better to the presence of frost than those with high fin densities.

e. Pressure drop across the coils and hence the "blockage effect" is a very influential parameter in the frosting process.

f. Louvered and waffled fin types have more frost accumulation than smooth flat fin types.

g. The latent component in the energy transfer process during frosting is substantial.

h. There is a lack of good complete model which addresses the overall thermal behavior of coils under frosting conditions.

i. One of the major driving factors in frost formation in cooling coils is the difference between entering air and coil refrigerant temperatures.

j Approximately 15 to 25% of the defrost heat input is actually used to melt the frost, with the remaining energy returning to the refrigeration system as additional load.

k. The two major thermal loss mechanisms during defrost are the heat and mass transfer to the air and refrigerant vapor bypass as it enters the compressor suction

The manner in which the defrosting process impacts the refrigeration load is not fully understood and has not been quantified. There has been no study to date which clearly establishes the heat loads due to defrosting geared towards the design engineer's needs. A set of design tools which clearly correlates the various loads, sensible heat ratio, refrigerant, coil surface, and air temperatures, and air humidity is yet to be developed in a clear and simple easy to use manner. It is hoped that the work performed in this research will provide the necessary direction and basis for the development of such design tools.

1.3. Problem Statement

Field observations of the performance of evaporator coils employed in industrial freezers suggest that the heat loads created by the refrigerating equipment in the process of extracting moisture from air at freezer temperatures are significantly larger than the latent heat gain from which the moisture results (Smith 1992). These observations also suggest that these equipment related loads (defrost heat loads) may sometimes be larger than all other components of the total refrigeration load. The latter load components are the transmission load, product load, internal load, and the infiltration load. Rules of thumb pertaining to estimating the magnitude of the different load components exist (ASHRAE 1994). However, these rules of thumb do not account for the psychrometric conditions prevailing in the freezer during both the refrigeration and defrost portions of the complete refrigeration/defrost (R/D) cycle. Apparently, the refrigeration industry decided years ago that applied psychrometrics of air-cooling processes could safely be ignored. For example, Smith (1992) reports that the refrigeration industry's decision may have been justified at the time because the latent heat gain to storage freezers of the day tended to be minor and the need for accounting for psychrometric effects may have been negligible. When these storage freezers evolved into distribution-type freezers with heavy-usage doorways with the associated increase in infiltration air, the latent heat gain tended to be major and the psychrometric effects throughout the complete R/D cycle became important.

Additional field observations in industrial freezers with high latent heat load components suggest that the nature of the frost forming on freezer coils do affect the heat required to defrost the coil. When warmer and more humid outer-room air mixes with much colder and much drier freezer air in the freezer temperature range, the air-mixing process line is likely to invade the supersaturated zone. This, in turn, results in the formation of airborne ice crystals which if precipitated on the coil would result in snow-like frost. This type of frost has poorer thermal conduction properties than the ice-like frost which normally forms if the air mixing process line did not invade the supersaturated zone. Thus, one of the issues that needed to be resolved in this research project was providing some additional insight into the defrost heat gain in freezer coils and the interrelationship with applied psychrometrics. Thus, coupled with the need to understand the dynamic nature of the refrigeration/defrost cycle, and the analysis of the different load components, exemplified the rationale behind performing the research.

1.4. Objectives of the Research

The objective of this research was to obtain quantitative and reliable data on the heat loads associated with defrosting a freezer coil of frequently used design employing the hot-gas refrigerant method. It was intended that tests be conducted under conditions which are representative of true-to-life operating conditions of freezers in the field.

The scope and emphasis of this research was to perform the following tasks:

1- Building a liquid overfeed refrigeration/defrost system capable of operating under true-to-life conditions of industrial freezers in the field.

2- Instrumenting the system along with designing a data acquisition system in order to obtain quantitative and reliable data required for the load calculations.

3- Operating the system, collecting data, and analyzing the heat loads associated with defrosting the evaporator coils for several complete runs of typical values of coil entering air dry bulb temperature (EAT) in the range of 0°F to -20°F where a complete run of the system consists of three consecutive refrigeration/defrost (known as R/D) cycles.

4- Studying the dynamics of the refrigeration/defrost system for the complete R/D cycle. Examination of the dynamics of a refrigeration/defrost system involves the delicate task of generating time profiles of a host of variables (such as refrigerant temperatures and pressures and air temperatures) which are bound to change as the system cycles from the refrigeration mode to the defrosting mode and back to the refrigeration mode again several consecutive times.

5- Performing a visualization study of frost formation at freezer temperatures. This task is specifically designed to provide a qualitative assessment of psychrometric processes typically found in industrial freezers. Laboratory simulation of air-mixing and air-cooling processes at freezer temperatures should help understand the psychrometric issues associated with operating industrial distribution freezers with heavy-usage doorways and corresponding high latent load component associated with it.

CHAPTER 2
EXPERIMENTAL FACILITY

The purpose of this chapter is to provide a description of the experimental facility. In its simplest form, the test facility is comprised of a refrigeration/defrost system consisting of a condensing unit, auxiliary and test fan-coil units, and refrigeration piping and related components (load compensation unit, surge drum, oil capturing system, liquid pump, etc.) and an air distribution system consisting of a psychrometric freezer room, an air distribution diffuser, ducts, and an artificial load generation system (sensible heat generator and water vapor generator). In what follows more detailed descriptions of the aforementioned systems will be provided.

2.1. Refrigeration/Defrost System

The refrigeration/defrost system has been designed to provide the same refrigerant and air-cooling conditions that are found in a real-life industrial freezer. The top feed hot-gas defrosting method is used in this system since it is one of the most popular methods in the refrigeration industry. This task is very important since the testing required must project what is happening inside an actual industrial freezer. The system consists of a condensing unit, two fan-coil units and the refrigeration piping system. Two schematic drawings showing different isometric views of the refrigeration/defrost system can be seen in Figures 2.1 and 2.2 The coils used in the two fan coil units are identical to those used in industry

2.1.1. Condensing Unit

The condensing unit employed in this investigation is a R-22 (Chlorodifluoromethane, $CHClF_2$) packaged Krack unit (model number KBD15L2K33E) which is a vertical discharge air-cooled condensing unit. A picture of the condensing unit can be seen in Figure 2.3 The unit is designed for low temperature applications ranging from 0°F to -40°F saturated suction temperature (Krack 1992a) It is also capable of achieving a cooling capacity of 2.6 tons at -40°F saturated suction temperature, when the ambient temperature is 95°F (Krack 1992b)

The condensing unit is employed with a 15-hp Copeland compressor (model number 4DL3-1500-TSK) that has four cylinders. It is also employed with a large storage capacity liquid receiver that is capable of storing up to 192 pounds of R-22. A detailed description of the condensing unit layout and its associated auxiliaries is shown in Appendix A.

2.1.2. Test Fan-Coil Unit

The test fan-coil unit (FCU T) is a liquid overfeed recirculating evaporator with an overfeed ratio of 3 It is this unit that has been tested to determine the heat loads due to coil hot-gas defrosting The FCU-T manufactured by Colmac Coil Manufacturing, Inc., is a Colmac 4HF1 Special with a model number RB/RTL-21x29-8R-4F FF R/L, and is designed to follow industry practice as close as possible This unit has a refrigerating

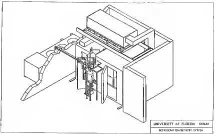

Figure 2.1 An isometric view of the refrigeration/defrost system

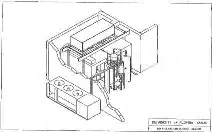

Figure 2.2. A different isometric view of the refrigeration/defrost system

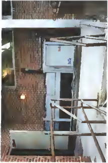

Figure 2.3 Condensing unit

capacity of about two tons and a basic capacity of about 330 Btuh/ft^2 TD, where TD is the difference between the coil entering air dry bulb temperature (EAT) and the coil refrigerant temperature (CRT) leaving the coil (Smith 1989) A front and back view of the test fan-coil unit can be seen in Figures 2.4 and 2 5 respectively

The coil finned tubes are arranged in 8 rows in the direction of air flow and in a staggered pattern of 1 5"x 1 299", where the tube material is copper having 5/8" outside diameter and 0.018" thickness. The fins are made of aluminum and have a flat pattern with flat edges The fins have a thickness of 0 01", and their spacing is 4 fins per inch. The FCU-T has a finned height of 21" and a finned length of 29"

Details of the unit are shown in Figure 2.6 where its dimensions are 40"L x 24"W x 24-3/4"H. The liquid refrigerant enters the coil through the lower 1-1/8"OD liquid connection during refrigeration and leaves the coil as wet return from the top 2-1/8"OD suction connection. The coil has 7 feeds and 16 copper tube passes. The unit is classified as a draw through unit (Stoecker 1988) since the fan draws the air against the refrigerant in a crossflow direction where each fluid flows at right angle to the other However, the tubes are circuiting in a manner that the two fluids will approach in a counterflow type heat exchanger arrangement. The FCU-T is placed inside the psychrometric freezer room, which will be described later in this chapter and it is mounted on a metal frame reinforced at the base by using angle irons

As seen in Figure 2 6, there are two 5/8"OD hot-gas connections located at the drain pan of the FCU-T During the hot-gas defrosting mode the hot gas enters the unit from the hot-gas connection next to the liquid connection and flows through the six copper tube passes located at the bottom of the drain pan. The hot gas then leaves FCU-

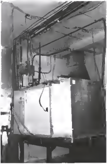

Figure 2.4. Front view of the test fan-coil unit (FCU T)

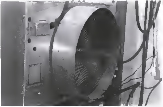

Figure 2.5 Back view of the test fan-coil unit (FCU-T)

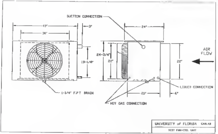

Figure 2.6. Schematic diagram of the test fan-coil unit (FCU-T)

T from the other hot-gas connection, where this process is necessary to remove the frost that had accumulated in the drain pan during refrigeration The hot gas then enters FCU-T again through the suction connection, since this is a top hot-gas feed unit, and leaves the unit from the liquid connection where this process will remove the frost that had accumulated on the coil tubes during refrigeration. The frost removal from the drain pan and the coil tubes will be in two forms, melt, and moisture that escapes to the space inside the freezer (Cole 1989) The top hot gas feed method has been used in order to have a fast defrosting process and to force the oil from accumulating inside the unit tubes (Refrigerating Specialties 1984) The produced melt will leave the unit through the bottom drain connection and is then collected using a special mechanism that will be explained later in Chapter 3

The test fan-coil unit is employed with one fan that has a diameter of 20" and a speed of 1075 rpm and is operated by a 1/4-hp motor This unit has a face area of 4.23 square feet and a face velocity of 750 feet per minute, while its capacity is 3172 cfm The fan material is aluminum, while its hub is steel.

2.1.3. Auxiliary Fan-Coil Unit

The auxiliary fan-coil unit (FCU-A) was assembled by HCR, Inc., while the coil itself was manufactured by Colmac Coil Manufacturing Inc The unit is designed to collect all the moisture-escape from the FCU-T when the latter is operating under the hot-gas defrosting mode. This unit contains a coil a blower, two heater elements used for electrical defrosting, a light fixture, two duplex receptacles and two dampers with their linear actuators. These components are housed in an insulated sheet-metal frame as shown in Figure 2.7 where the frame is internally insulated with 1 inch thick of Armaflex. The FCU A frame panels and their openings are shown in Figure 2.8 where the unit's dimensions are 115"L x 42.5"W x 26.5"H and the cut-out on the top panel has been used for a double pane window.

The FCU-A is placed on top of the psychrometric freezer room by a specially designed wooden frame structure as can be seen in Figure 2.9 The unit is mounted on the wooden frame by six compression vibration insulators from McMaster-Carr Supply Company (model number 64875K79) that are screwed in the wooden structure These insulators are made from neoprene rubber and each has a maximum load of 375 pounds and a maximum deflection of 0 125" This action has helped in protecting the freezer from the FCU-A vibrations.

The FCU-A is a draw-through unit and has a Colmac coil (Item 4 in Figure 2.7) that is identical with the one in the FCU-T except for the fact that the tubes of the FCU-A coil are circuiting in a manner that the heat exchange between the air and the refrigerant will approach that of a parallel type heat exchanger arrangement. The coil of the FCU-A is defrosted electrically where the FCU A is equipped with two defrosting heater elements (Item 3 in Figure 2 7) that are located below the coil. Each defrosting heater element has a power of 1500 Watts.

The unit is employed with one Dayton blower (model number 5C198A) that has a wheel of 12-5/8" diameter and a width of 9-1/2"(Item 1 in Figure 2 7) The blower is operated by a 1 hp motor mounted to the body of the blower in order to reduce vibrations This motor operates at three different speeds. The blower has a capacity of 2780 cfm when the motor is operating at a speed of 1075 rpm (Dayton 1992) As can be

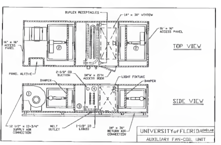

Figure 2.7. Schematic diagram of the auxiliary fan-coil unit (FCU A)

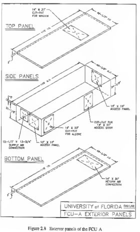
14" X 30" CUT-OUT FOR WINDOW
TOP PANEL
42-1/2" I.D.
115" I.D.
2"
SIDE PANELS
42-1/2" O.D.
119" O.D.
24-1/2"
2"
20-1/2"
18" X 18" ACCESS PANEL
CUT-OUT FOR 14" X 21" ACCESS DOOR
18" X 20" CUT-OUT FOR ALCOVE
12-1/2" X 13-3/4" SUPPLY AIR CONNECTION
18" X 18" ACCESS PANEL
BOTTOM PANEL
42-1/2" I.D.
115" I.D.
14" X 30" RETURN AIR CONNECTION
2"
UNIVERSITY of FLORIDA CAD LAB
FCU-A EXTERIOR PANELS

Figure 2.8 Exterior panels of the FCU A

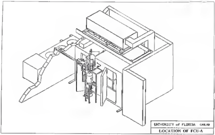

Figure 2.9 Location of the FCU-A on top of the psychrometric freezer room

seen in Figures 2.7 and 2.8 the blower supplies air to the freezer through the 12-1/2" x 13-3/4" supply air connection, while the air returns from the freezer to the FCU-A through the 14" x 30" return air connection in the bottom panel.

Two Dayton linear actuators (model number 4Z843B) are employed in the FCU-A (Item 2 in Figure 2.7), where each linear actuator is connected to one damper. These linear actuators are needed in this unit in order to open and close the dampers, where the two dampers are enclosing both the coil and the light fixture compartments. The two dampers are tight-closing dampers for zero moisture-escape during the FCU-A electric defrosting mode. The linear actuators have a nominal linear speed of 35 inches per minute when the applied load is 500 pounds. The actuators also have an adjustable switch which is used to adjust the actuator motion limits in both directions. The linear actuator motors are employed with thermal overload which can open and reset automatically (Dayton 5S2709).

The FCU-A will operate under the refrigeration mode when it is initially required to bring the freezer to the needed testing conditions. The FCU-A will also operate under the refrigeration mode when the FCU-T is operating under the hot-gas defrosting mode, where the FCU-A continues to operate in the refrigeration mode even after the termination of the FCU-T defrosting mode in order to bring back the freezer to the initial needed testing conditions. During these two FCU-A refrigeration modes, the two dampers will be open and the defrosting heater elements will be off while the coil of the FCU-A accumulates some frost on its finned tubes. As the FCU-T is switched to operate under the refrigeration mode, the FCU-A dampers will close and the FCU-A will operate under the electric defrosting mode in order to melt the frost that had accumulated on its finned tubes. The melt produced from the frost of the initial FCU-A refrigeration mode is basically the moisture removed from the freezer in order to bring the room to the needed testing conditions. The melt produced from the frost of the other FCU-A refrigeration mode, the mode during which the FCU-T hot-gas defrosting mode occurs, is basically the moisture-escape from the FCU-T when the latter is under the hot-gas defrosting mode. The melt will leave the FCU-A through the bottom melt outlet as shown in Figure 2.7 and will then be collected using a special mechanism which will be explained later in Chapter 3.

A light fixture consisting of a 75-Watt flood lamp is installed in the FCU-A as shown in Figure 2.7. Two duplex outlet receptacles are also installed in the FCU-A. The FCU-A has three Raychem self-regulating electric heating cables that are plugged into the two duplex receptacles. The length of one of these cables is 6 feet (model number W51-6P) while each of the other two has a length of 12 feet (model number W51-12P). The electric heating cables have a voltage rating of 120 Volts and their power rating is 5 Watts per foot at 40°F (Raychem 1994). These electric heating cables are laid in a way that they surround the circumference of the two fixed damper frames, where the dampers come into contact with these frames when the dampers are in the closing position. The reason for installing these cables is to heat the circumference of the damper frames during the refrigeration mode of the FCU-A where the dampers will be open during that mode. This heating process will prevent the accumulation of frost on the frames and force the frost to accumulate on the coil finned tubes. It will also protect the damper driveways from the frost so that the dampers can close safely during the FCU-A electric defrosting mode.

As shown in the top view of Figure 2.7 the FCU-A has a control panel alcove. The latter is equipped with six switches connected to it, where each switch is set to three different operating modes: the on the off, and the automatic mode of operation. The six switches are connected to control the operations of the blower, light fixture, motors of the dampers linear actuators, the defrosting heater elements, the electric heating cables, and the receptacles.

2.1.4. Refrigeration Piping and Related Components

The piping system has been constructed using type K copper tubes, since they are easy to install and have good resistance to corrosion (ASHRAE 1992a). The piping system was designed to provide low temperature bottom-feed refrigeration systems for two fan-coil units, a reliable top-feed hot gas defrosting system for the test fan-coil unit (FCU-T), and an electric defrosting system for the auxiliary fan-coil unit (FCU-A). It is a system that has easy access to every related component, and every major component can be isolated for service and maintenance.

The piping system consists of the piping layout, the load compensation unit (LCU), the surge drum, the oil capturing system, the liquid pump, different types of valves, strainers, sight glasses, vibration isolators, flow measuring devices, and other related components. A detailed description of these components is discussed in the following sections.

2.1.4.1. General piping system layout

The refrigeration/defrost system starts by operating the FCU-A under the refrigeration mode in order to bring the freezer to the required testing conditions. When the testing conditions are reached, the refrigeration mode of the FCU-A is terminated and the electric defrosting mode of the FCU-A starts During this electric defrosting mode the frost accumulated on the FCU-A finned tubes will melt and will be collected. This first collected melt represents the moisture removed from the freezer during the room conditioning period The electric defrosting mode will last until all the FCU-A frost has melted and its finned tubes have dried out, at which point the defrosting mode is terminated. The FCU-A stays unloaded until the FCU-T starts its hot-gas defrosting mode

At the same time when the testing conditions of the freezer are reached and the FCU-A starts its electric defrosting mode the FCU-T will start to operate under the refrigeration mode When the frost accumulation on the FCU-T finned tubes reaches a certain thickness, the refrigeration mode of the FCU-T is terminated, and its hot-gas defrosting mode is initiated This will be the time when the FCU-A starts to operate again under the refrigeration mode in order to capture the moisture-escape from the FCU-T due to the FCU-T hot-gas heat input. The FCU-T hot-gas defrosting mode will last until all the frost has been removed, the FCU-T melt collected, and the FCU-T finned tubes have dried out, at which point the hot-gas defrosting mode is terminated The FCU-T stays unloaded until the FCU-A is able to bring the freezer back to its initial testing conditions.

When these initial testing conditions are brought back, the refrigeration/defrost cycle (R/D cycle) is repeated two more times in a continuous manner The only difference between the last three FCU-A refrigeration modes and the initial FCU-A refrigeration mode is that the FCU-A melt collected in the former represents the moisture-escape from the FCU-T due to the FCU-T hot-gas heat input, while the FCU-A melt collected in the initial mode represents the moisture removed from the freezer during the initial room conditioning period.

The general layout of the piping system is described in a schematic that can be seen in Figure 2.10, while a summary description of the piping system components is shown in Table 2.1. Some of the piping system components are located inside the freezer while the other components are either on top or in front of it. The piping system components that are located inside the freezer are shown in Figure 2.11.

When the refrigeration/defrost system is in operation, the liquid refrigerant flows from the condensing unit receiver into the 1-1/8"OD main liquid line through the main liquid line solenoid valve (Item 18 in Figure 2.10) and continues its way to the surge drum. A Viking liquid refrigerant pump (model number SG-40550) is used to pump liquid refrigerant from the surge drum to any of the two fan-coil units when that unit is operating under the refrigeration mode.

If the FCU-T is operating under the refrigeration mode, the liquid refrigerant enters the FCU-T through the FCU-T liquid line solenoid valve (Item 2 in Figure 2.10) and leaves as wet return, where then, the latter flows in a 1-1/8" OD copper tube and passes through the FCU-T wet return stop solenoid valve and the FCU-T wet return check valve (Items 15 and 19, respectively, in Figure 2.10) before it connects to the 1-3/8" OD main wet return line.

On the other hand, when the FCU-A is operating under the refrigeration mode, the liquid refrigerant enters the FCU-A through the FCU-A liquid line solenoid valve (Item 4 in Figure 2.10) and leaves as wet return, where then, the latter flows in a 1-1/8"OD copper tube and passes through FCU-A wet return check valve, as well as the FCU-A wet

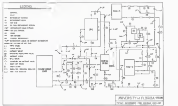

Figure 2.10. Schematic diagram of the piping system

Table 2.1. Summary Description of the Piping System Components

Item	Manufacturer	Model Number	Description
1	SUPERIOR	805C-14S	FCU-A Liquid Line Check Valve
2	SPORLAN	E19S270	FCU-T Liquid Line Solenoid Valve
3	SUPERIOR	257B-14S	Hand Operated Throttling Valve
4	SPORLAN	E19S270	FCU-A Liquid Line Solenoid Valve
5	SUPERIOR	257B-14S	Hand Operated Throttling Valve
6	SPORLAN	B10S2	Defrost Refrigerant Solenoid Valve
7	SPORLAN	B10S2	Main Hot Gas Line Solenoid Valve
8	SUPERIOR	216-10ST	Hand Operated Throttling Valve
9	SPORLAN	B10S2	Hot-Gas Bypass Solenoid Valve
10	SPORLAN	ADRPE-3	Hot-Gas Discharge Bypass Valve
11	SPORLAN	E9S240	Liquid Bypass Solenoid Valve
12	SPORLAN	EGVE 1-1/2-Z	Desuperheating Thermostatic Expansion Valve
13	SPORLAN	ORIT-20-0/75	LCU Pressure Regulating Valve
14	SPORLAN	LMC-PVE 5-1/2	Surge Drum Liquid Level Control Valve
15	SPORLAN	OE34S290	FCU-T Wet Return Stop Solenoid Valve
16	SUPERIOR	802B-6S	Oil Return Check Valve
17	RS/PARKER	A4AK	FCU-T Defrost Refrigerant Pressure Regulator
18	SPORLAN	MB25S2	Main Liquid Line Solenoid Valve
19	SUPERIOR	806C-11S	FCU-T Wet Return Check Valve
20	SUPERIOR	254A-4S	Hand Operated Throttling Valve
21	ALCO	100RB2S3	Oil Return Solenoid Valve
22	SUPERIOR	255A-8S	Hand Operated Throttling Valve
23	SUPERIOR	255A-8S	Hand Operated Throttling Valve
24	RS/PARKER	RSF SIZE 1"	FCU-T Defrost Refrigerant Strainer
25	SUPERIOR	805C-14S	FCU-T Liquid Line Check Valve
26	SUPERIOR	806C-11S	FCU-A Wet Return Check Valve
27	SUPERIOR	216-10ST	Hand Operated Throttling Valve

Table 2.1 -- continue

Item	Manufacturer	Model Number	Description
28	BROOKS	1114CJ36CSAAA	Full-View Flowmeter
29	SUPERIOR	255A-8S	Hand Operated Throttling Valve
30	SIGNET	MK-525	Turbine Flowmeter
31	SPORLAN	MB19S2	Hot-Gas Defrost Solenoid Valve
32	UF	M1	Hot-Gas Orifice Meter
33	UF	M2	Defrost Orifice Meter
34	UF	N/A	Defrost Refrigerant Separator
35	WATSCO	MS-10	Hot-Gas Line Check Valve
36	RS/PARKER	A4AK	FCU-A Heated Refrigerant Pressure Regulator
37	RS/PARKER	RSF-SIZE-1"	FCU-A Heated Refrigerant Strainer
38	SPORLAN	OE34S290	FCU-A Wet Return Stop Solenoid Valve
39	SUPERIOR	587WA-14ST	Surge Drum Liquid Line Isolation Valve
40	SUPERIOR	592WA 13ST	LCU Wet Return Isolation Valve
41	SUPERIOR	592WA 13ST	Surge Drum Suction Line Isolation Valve
42	SUPERIOR	594WA 21ST	LCU Suction Line Isolation Valve
43	SUPERIOR	587W-14ST	LCU Drain Line Valve
44	SUPERIOR	591WA-11ST	LCU Liquid Line Isolation Valve
45	SUPERIOR	586W-8ST	Liquid Refrigerant Isolation Valve
46	SUPERIOR	586W-8ST	Defrost Refrigerant Isolation Valve
47	SUPERIOR	255A-8S	Hand Operated Throttling Valve
48	N/A	N/A	Schrader Valve
49	N/A	N/A	Schrader Valve
50	PARKER	QL171R-14-14	Shut-off Valve
51	MICROPUMP	1800	Oil Pump
52	VIKING	SG-40550	Liquid Refrigerant Pump
53	VILTER	KT1018	High Side Float Valve
54	WATSCO	WAT-B1-10S	Piercing Valve

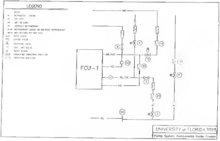

Figure 2.11 Components of the piping system inside the psychrometric freezer room

return stop solenoid valve (Items 26 and 38, respectively, in Figure 2.10) before it connects to the 1-3/8"OD main wet return line.

When the FCU-A is operating under the electric defrosting mode, the FCU-A liquid line solenoid valve and the FCU-A wet return stop solenoid valve will both be closed (Items 4 and 38, respectively, in Figure 2.10). This will increase the pressure and temperature of the refrigerant inside the FCU-A finned tubes due to the heat provided by the two defrosting heater elements of the FCU-A. This increase in pressure will force the heated refrigerant to leave the FCU-A and flow towards the FCU-A heated refrigerant pressure regulator (Item 36 in Figure 2.10) but will not be able to flow through this regulator to the 1-3/8"OD main wet return line unless the heated refrigerant pressure reaches 70 psig, which is the regulator's preset inlet pressure value. This pressurizing process is needed to hold the heated refrigerant inside the FCU-A finned tubes for a suitable period of time in order to confirm and speed the removal of all the frost accumulated on the finned tubes and also to dry out the finned tubes.

When the FCU-T is operating under the hot-gas defrosting mode, the FCU-T liquid line solenoid valve and the FCU-T wet return stop solenoid valve will both be closed (Items 2 and 15, respectively, in Figure 2.10). The hot-gas flows from the condensing unit in a 3/4"OD copper tube and passes through the main hot-gas line solenoid valve, the hot-gas defrost solenoid valve, and the hot-gas orifice meter (Items 7, 31 and 32, respectively, in Figure 2.10) before entering the FCU-T drain pan.

The hot-gas enters the FCU-T drain pan in order to remove the frost accumulated in it, and then leaves the FCU-T drain pan passing through the hot gas line check valve (Item 35 in Figure 2.10) on its way to the FCU-T wet return line. The hot-gas then enters the FCU-T again through the FCU-T wet return line, since this is a top hot-gas feed fan-coil unit, where the hot-gas mixes with the cold refrigerant inside the FCU-T finned tubes and leaves the FCU-T through the FCU-T liquid line The mixed refrigerant leaving the FCU-T will be called here "defrost refrigerant" to differentiate it from the "heated refrigerant" mentioned before when describing the electric defrosting mode of the FCU-A.

The mixing of the hot-gas with the cold refrigerant inside the FCU-T finned tubes will increase the pressure and temperature of the leaving defrost refrigerant. This increase in pressure will force the leaving defrost refrigerant to flow in a 5/8"OD copper tube towards the FCU-T defrost refrigerant pressure regulator (Item 17 in Figure 2 10) but will not be able to flow through this regulator unless the pressure of the defrost refrigerant reaches 70 psig, which is the preset inlet pressure value of the regulator

After passing through the FCU-T defrost refrigerant pressure regulator (Item 17 in Figure 2.10) the defrost refrigerant will flow into the defrost refrigerant separator (Item 34 in Figure 2.10) which works as a liquid vapor separator. The vapor leaves the top of this separator and continues its way to the 1-3/8"OD main wet return line, while the liquid leaves the bottom of the separator and passes through the high-side float valve (Item 53 in Figure 2.10) on its way to the main wet return line

All the refrigerant connections to the 1-3/8" OD main wet return line, that were discussed before will lead the refrigerant to proceed inside the main wet return line until it enters the load compensation unit (LCU) as can be seen in Figure 2.10 The load compensation unit is a pressure vessel used as a liquid refrigerant vaporizer in order to compensate for the hot-gas required during the FCU-T hot-gas defrosting mode. The LCU also serves as a liquid refrigerant storage drum and a liquid vapor separator

(Stoecker 1988) More detailed information about the LCU will be provided in a later section.

As the wet return enters the LCU, its vapor leaves the top of the LCU through the 2-1/8"OD main suction line and continues its way to the condensing unit. The liquid refrigerant accumulates inside the LCU until its level reaches the liquid overfeed outlet, where then, the overfeed liquid leaves the LCU through the 1-1/8"OD liquid line and enters the surge drum. The vapor inside the surge drum leaves the top of the latter through the 1-1/4"OD suction line and connects with the main suction line as can be seen in Figure 2.10. A more detailed description of the piping system layout and its components is provided in Appendix B.

In this refrigeration/defrost system, some of the compressor lubricating oil will have its way into the system components and piping. This will create oil rich refrigerant inside the surge drum and the oil will then be captured by an oil capturing system which will be discussed in a later section. The refrigeration/defrost system is also equipped with a compressor capacity control system which will be discussed in a later section.

2.1.4.2. Load compensation unit

In the operational practice of the hot gas defrosting systems, it is important not to defrost more than one third of the total evaporator loads, since then the system will not be able to provide the required hot-gas for the total defrosting period (Refrigerating Specialties 1984; Pita 1991). Since each of the two fan-coil units employed in this system has a refrigerating capacity of about two tons, it is clear that the FCU A cannot provide the required hot-gas to operate the FCU T under the hot gas defrosting mode. The load compensation unit (LCU) was employed in this system to serve as a source of hot-gas production when the FCU T is under the hot-gas defrosting mode, where the hot-gas is produced inside the LCU using six band heaters around the LCU.

The load compensation unit is manufactured by E. L. Nickell Co , Inc , and its details are shown in Figure 2.12 where it has an outside diameter of 20' and an overall height of 34' The LCU has two level eyes with frost shields, where the liquid overfeed level inside the LCU is designed to be in between the two eyes. The LCU's maximum allowable working pressure is 300 psig at 250°F

When the FCU T is about to operate under the hot-gas defrosting mode, the band heaters are put into operation in order to vaporize the liquid refrigerant inside the LCU The band heaters are kept on during the full duration of the FCU T hot-gas defrosting mode, and shut down at the same time when the latter is terminated. The six band heaters are manufactured by Chromalox Industrial Heating Products (model number HB-2030), where each heater has a 20" inside diameter, a width of 1-1/2", and is clamped tightly around the LCU Each heater works at 3000 Watts and 220 Volts.

The six Chromalox band heaters are power controlled by an Omega silicon controlled rectifier (model number SCR73Z-260-M) which is an extremely fast controller capable of maintaining the desired heat setting to vaporize the liquid refrigerant inside the LCU This controller can be operated by a computer, since the controller can accept an input signal of 4-20 mA, as well as manually since it is employed with a manual module and a remote potentiometer (Omega 1992a, 1993) The load compensation unit is insulated with a 2" thick fiber glass/mineral wool insulation blanket, and on top of that an additional 3" thick layer of vinyl faced fiberglass is added

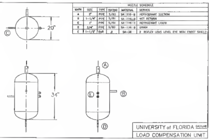

NOZZLE SCHEDULE					
MARK	SIZE	TYPE	RATING	MATERIAL	SERVICE
A	2"	PIPE	S/80	SA-106-B	REFRIGERANT SUCTION
B	1-1/4"	PIPE	S/80	SA-106-B	WET RETURN
C	1"	PIPE	S/80	SA-106-B	REFRIGERANT LIQUID
D	3/4"	PIPE	S/80	SA-106-B	DRAIN
E	1-1/2"	BAR	.2	SA-38	2 REFLEX LENS LEVEL EYE WITH FROST SHIELD

Figure 2.12. Schematic diagram of the load compensation unit (LCU)

2.1.4.3. Surge drum

A surge drum is a pressure vessel that is always used in liquid overfeed systems, where a large quantity of liquid refrigerant is required to flood the fan-coil units during refrigeration. A schematic of the surge drum is shown in Figure 2.13. The surge drum is manufactured by Ayob and Associates, Inc. (model number AV-1202), where it has an outside diameter of 12-3/4" and an overall height of 24". The surge drum's maximum allowable working pressure is 150 psig at 250°F.

As shown in Figure 2.13, the liquid refrigerant from the receiver enters the surge drum through nozzle C. It enters the surge drum in the form of a liquid-vapor mixture, since the pressure of the liquid refrigerant has dropped after passing through the surge drum liquid level control valve (Item 14 in Figure 2.10) before entering the surge drum. The vapor is separated from the liquid refrigerant inside the surge drum and is forced to flash to the top of the surge drum leaving through nozzle A to the main suction line. This action causes the liquid refrigerant to concentrate at the bottom of the surge drum, thus ensuring that only liquid refrigerant is fed through nozzle B to the fan-coil units (Pita 1991).

The insert sensing bulb of the surge drum liquid level control valve is inserted inside the surge drum through nozzle F. The horizontal centerline of nozzle F represents the desired static liquid level position. Nozzle D is the place where the oil rich refrigerant is drained by the oil capturing system. Nozzle D is located at a level that is slightly lower than nozzle F, where this change in level helps the oil capturing system to remove as much oil as possible from the surge drum, since the oil rich refrigerant is resting on top of the pure liquid refrigerant. This is due to the difference in density between the lighter oil in

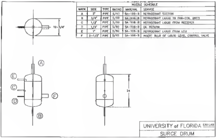

NOZZLE SCHEDULE

MARK	SIZE	TYPE	RATING	MATERIAL	SERVICE
A	2"	PIPE	S/40	SA-106-B	REFRIGERANT SUCTION
B	3/4"	PIPE	S/80	SA-106-B	REFRIGERANT LIQUID TO FAN-COIL UNITS
C	1/2"	PIPE	S/80	SA-106-B	REFRIGERANT LIQUID FROM RECEIVER
D	1/4"	PIPE	S/80	SA-106-B	OIL RETURN
E	1"	PIPE	S/80	SA-106-B	REFRIGERANT LIQUID FROM LCU
F	2-1/2"	PIPE	S/40	SA-106-B	INSERT BULB OF LIQUID LEVEL CONTROL VALVE

Figure 2.13. Schematic diagram of the surge drum

the surge drum and the heavier R-22. The location of nozzles C and E is higher than the static liquid level, since this will help in the liquid vapor separation process inside the surge drum.

The surge drum is insulated with a 2" thick fiber glass/mineral wool insulation blanket, and on top of that an additional 3" thick layer of vinyl faced fiberglass is provided. A picture of the surge drum and the load compensation unit is shown in Figure 2.14 where the former is the vessel in the front, and the insert sensing bulb is seen to its right.

2.1.4.4. Liquid pump

The liquid refrigerant pump is manufactured by Viking Pump, Inc., (model number SG-40550) and is a spur gear positive displacement pump (Item 52 in Figure 2.10) designed to rotate in a clockwise fashion (Viking 1987). The pump has a nominal capacity of 2 gpm at a motor speed of 1750 rpm. The pump is designed to operate for pressures and temperatures up to 500 psig and 225°F respectively, at a motor speed of 1750 rpm. The liquid refrigerant pump motor is manufactured by A.O. Smith Corporation (model number P48L2DA1) and has a power rating of 1-hp and a speed of 3450 rpm.

2.1.4.5. Oil capturing system

The flow of oil inside the pipes and components of an overfeed system will have a negative effect on the system performance if it is not captured and pumped back to the main suction line. The oil will raise the boiling temperature of the liquid refrigerant and reduce the heat transfer rate between the heater of the insert sensing bulb and the liquid

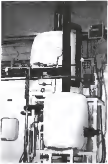

Figure 2.14 Load compensation unit (LCU) and surge drum

refrigerant inside the surge drum, which then causes an overfeeding of liquid refrigerant to the surge drum (Sporlan 1990b).

The oil capturing system can be seen in Figure 2.10 where the oil rich refrigerant flows from the surge drum through a 3/8"OD oil rich refrigerant return line and passes through the oil return solenoid valve, the oil pump, oil return check valve and a hand operated throttling valve (Items 21, 51, 16 and 22, respectively in Figure 2.10) before it connects to the 2 1/8"OD main suction line. The oil rich refrigerant captured from the surge drum is in liquid form and must be transferred to the vapor form before it enters the main suction line.

The oil return solenoid valve (Item 21 in Figure 2.10) is manufactured by Alco Controls (model number 100RB2S3). It is a normally-closed valve that is energized to open when the refrigeration/defrost system is in operation. This valve is kept closed when the system is shut down in order to prevent any surge drum liquid refrigerant from flowing to the main suction line through the oil rich refrigerant return line.

The oil pump (Item 51 in Figure 2.10) is manufactured by Micropump Corporation (model number 1800) and is a magnetic driven positive displacement gear pump used to pump the oil rich refrigerant to the main suction line. The flow rate capacity of the pump ranges from 1 to 320 milliliter per minute. The pump is designed to operate for pressures up to 300 psig and at temperatures ranging from -50°F to 225°F.

The oil pump motor is also manufactured by Micropump Corporation (model number 415) and is close coupled with the oil pump. This motor has a speed range of 0 to 9000 rpm. A picture of the oil pump is shown in Figure 2.15. The oil return check valve (Item 16 in Figure 2.10) is manufactured by Superior valve company (model number

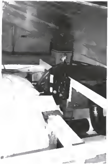

Figure 2.15 Oil pump

802C(6S) and is used in the system in order to prevent backflow of oil rich refrigerant to the oil pump discharge

The hand operated throttling valve (Item 22 in Figure 2.10) is manufactured by Superior valve company (model number 255A-8S) and is used to control the flow of the oil rich refrigerant to the main suction line such that the oil pump should not lose its prime and the fluid reaches the suction line in the form of vapor With the sight glass installed downstream of the throttling valve as can be seen in Figure 2.10, the conditions of the oil rich refrigerant can be checked

2.1.4.6. Compressor capacity control system

A compressor capacity control system is employed in this refrigeration/defrost system in order to protect the compressor from low suction pressure and high suction temperature situations. This system is represented by a 1/2"OD hot-gas bypass line connecting the main hot-gas line with the main suction line, and a 1/2' OD liquid refrigerant bypass line connecting the main liquid refrigerant line with the main suction line as can be seen in Figure 2.10 In the case of a low suction pressure the hot gas bypass line is used to raise the suction pressure by flowing hot gas to the suction line. In the case of a high suction temperature, the liquid refrigerant bypass line is used to drop the suction temperature by flowing liquid refrigerant to the suction line A more detailed description of the system and its components is provided in Appendix C.

2.2. Air Distribution System

The air distribution system is designed to provide the air-cooling conditions needed for the testing which are the same conditions found in a real life industrial freezer This air distribution system consists of a psychrometric freezer room, the ducting system and the artificial load generation system The details of the air distribution system components will be provided in the following sections

2.2.1. Psychrometric Freezer Room

The psychrometric freezer room used to conduct the testing is shown in Figure 2.16, where the dimensions of the room are 155"L x 124"W x 97"H The room has two identical access doors, where each door has a 13" x 13" square window Each door has a dimension of 30-7/8"L x 76-1/2"H, where a picture of the two doors is shown in Figure 2 17 The FCU A located on top of the freezer can be seen in Figure 2.17, where the load compensation unit (LCU) and the surge drum are shown to be stationed between the two doors There are three openings in the room ceiling. The 10" x 20" opening is for the supply air coming from the direct-drive blower of the FCU-A, while the other two 14" x 14" openings are for the return air to the FCU-A.

The construction details of the front wall and its overall coefficient of heat transfer (*U*-factor) are shown in Table 2 2 The *U*-factor of the front wall is estimated to be 0.075 Btu/(hr-ft^2-°F) The front wall has a thickness of 3-10/16" and an outside area, excluding the two doors and their windows, of 71 61 square feet. The outside area of each door is 16.4 square feet including the area of the window while each window has an outside area of 1 17 square feet. The two windows are identical and are insulated double glazing

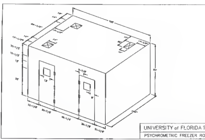

Figure 2.16 The psychrometric freezer room

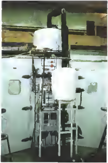

Figure 2.17 The psychrometric freezer room doors

Table 2.2. Overall Coefficient of Heat Transfer
U of the Front Wall

Construction	Resistance (R) (hr-ft^2-°F)/Btu
1- Outside surface (still air)	0.61 *
2- Aluminum sheet, 1/16 inch	0.000041 **
3- Polystyrene (molded beads), 3.5 inch	12.45 ***
4- Aluminum sheet, 1/16 inch	0.000041 **
5- Inside surface (750 fpm moving air)	0.24 *
Total thermal resistance (R_{total}): $R_{total} = \sum R = 13.30$ (hr-ft^2-°F)/Btu	
Overall coefficient of heat transfer ($U = 1/R_{total}$): $U = 1/R_{total} = 0.075$ Btu/(hr-ft^2-°F)	

* (ASHRAE 1994)
** (ASHRAE 1993)
*** This value includes the resistance of the wood studs (ASHRAE 1994)

windows with a 1/2" air space. The *U*-factor of each window is estimated to be 0.51 Btu/(hr-ft^2-°F) (ASHRAE 1993). The construction of the doors is exactly like the front wall except for the fact that the door has an additional 3/4" layer of plywood in between the outside aluminum sheet and the molded beads polystyrene insulation layer. The *U*-factor for each door is estimated to be 0.070 Btu/(hr-ft^2-°F).

Since the testing inside the freezer is performed at low temperatures (below 0°F) the two doors are equipped with good rubber seals around their contact edges with the front wall. This will protect the room and the test results from the effect of air infiltration. Two 16-foot self regulating Chromalox heating cables have been installed along the edges of the door openings between the outside aluminum sheet and the molded beads polystyrene insulation layer of the front wall. The heating cables operate at 120 Volts and their power rating is 3 Watt per foot at 40°F. One heating cable is used for each door opening. This action was found to help the door from jamming due to the low temperature and the frost that might potentially accumulate on the edges.

The construction details of the rear and side walls and their *U*-factors are shown in Table 2.3. The *U*-factor of these three walls is estimated to be 0.039 Btu/(hr-ft^2-°F). Each of the three walls represents an exact double wall of the front wall. They have a thickness of 7-1/4", while the outside area of the rear wall is 104.41 square feet and the outside area of each side wall is 83.53 square feet. The ceiling construction and its *U*-factor are shown in Table 2.4. The *U*-factor of the ceiling is estimated to be 0.028 Btu/(hr-ft^2-°F). The outside area of the ceiling, excluding the three openings, is 129.36 square feet. There are two light fixtures hung on the ceiling where each fixture has two 60-Watt fluorescent lamps. Having metal interiors and exteriors on all the walls and the

Table 2.3 Overall Coefficient of Heat Transfer
U of the Rear and Side Walls

Construction	Resistance (R) (hr ft^2-°F)/Btu
1- Outside surface (still air)	0.61 *
2- Aluminum sheet, 1/16 inch	0.000041 **
3- Polystyrene (molded beads) 3.5 inch	12.45 ***
4- Aluminum sheet, 2/16 inch	0.000081 **
5 Polystyrene (molded beads), 3.5 inch	12.45 ***
6- Aluminum sheet, 1/16 inch	0.000041 **
7 Inside surface (750 fpm moving air)	0.24 *
Total thermal resistance (R_{total}) $R_{total} = \sum R = 25.75$ (hr ft^2 °F)/Btu	
Overall coefficient of heat transfer ($U = 1/R_{total}$) $U = 1/R_{total} = 0.039$ Btu/(hr ft^2-°F)	

* (ASHRAE 1994)

** (ASHRAE 1993)

*** This value includes the resistance of the wood studs (ASHRAE 1994)

Table 2.4 Overall Coefficient of Heat Transfer
U of the Ceiling

Construction	Resistance (R) (hr ft^2 °F)/Btu
1- Outside surface (still air)	0.61 *
2- Galvanized sheet metal, gage 20	0.00012 **
3- Plywood 3/4 inch	0.93 **
4- Polystyrene (molded beads) 4.0 inch	15.87 *
5- Polystyrene (extruded), 1.0 inch	5.0 *
6- Aluminum sheet, 1/16 inch	0.000041 **
7- Polystyrene (molded beads), 3.5 inch	12.45 ***
8- Aluminum sheet, 1/16 inch	0.000041 **
9- Inside surface (750 fpm moving air)	0.24 *
Total thermal resistance (R_{total}) $R_{total} = \sum R = 35.10$ (hr-ft^2 °F)/Btu	
Overall coefficient of heat transfer ($U = 1/R_{total}$) $U = 1/R_{total} = 0.028$ Btu/(hr-ft^2-°F)	

* (ASHRAE 1994)

** (ASHRAE 1993)

*** This value includes the resistance of the wood studs (ASHRAE 1994)

ceiling is important in the design of the freezer, since these metal sheets will keep the moisture produced by the airborne water vapor out of the insulation (ASHRAE 1993).

The floor of the freezer is constructed of a 16-gage galvanized sheet metal on top of a 6 millimeter layer of visquene. A 4" layer of molded beads polystyrene comes beneath the visquene layer, and beneath them all comes a 1/2" layer of extruded polystyrene. These four layers constituted the floor of the freezer. Since the floor of the latter resides over an insulated floor in the laboratory which is a one foot below-grade basement floor, it is assumed that the heat transfer to the freezer through the floor is negligible.

In estimating the *U*-factors for the windows, doors, ceiling and walls, it is assumed that the outside film heat transfer coefficient (f_o) for still air is 1.65 Btu/(hr-ft^2-°F) and the inside film heat transfer coefficient (f_i) for a 750 fpm moving air is 4.12 Btu/(hr-ft^2-°F) (ASHRAE 1994). The resistance of the outside and inside surfaces is calculated by taking the reciprocal of the outside and inside film coefficients of heat transfer respectively. The four walls and the ceiling of the freezer are enforced by the existence of nominal 2 inch x 4-inch wood studs which are distributed within the 3.5-inch molded beads polystyrene layer at two feet distance on center. The resistance values of these wood studs are included in the resistance values of the 3.5-inch molded beads polystyrene layers as reported in the tables (ASHRAE 1994).

2.2.2. General Layout of the Airflow System

The general layout of the air flow system is shown in Figure 2.18 where the FCU-T is shown to be at the center of the freezer. The air flows through the 14" x 10" ducts to

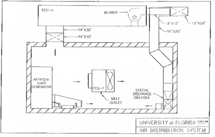

Figure 2.18 General layout of the airflow system

the inlet of the FCU-A and then leaves the FCU-A through the 8" x 12" duct. The blower of the FCU A is the driving force behind this air motion, where its capacity is 2780 cfm. The air then changes its flow direction and flows through the 10" x 20" ducts as shown in Figure 2.19. The air continues to flow downward throughout the 10" x 20" ducts as shown in Figure 2.18 and then exits to the freezer through a special discharge diffuser. In Figure 2.19 it can be seen that the two 14" x 14" duct lines coming from the freezer are both reduced to 14" x 10" ducts and then the two duct lines connect together and enter the FCU-A through a 14" x 30" duct. All the ducts in this system have been constructed from a one-inch thick duct boards equipped with fiberglass insulation.

The outlets of the special discharge diffuser and the artificial load generator are positioned in the center of the room and at a lower level beneath the FCU-T such that their flow of air is uniformly distributed in the freezer. These locations will also prevent any air currents that may adversely affect the hot-gas heat input to the FCU-T when it is operating under the hot-gas defrosting mode. The artificial load generator will be explained in detail in the sections to follow.

A top view of the airflow system inside the freezer is shown in Figure 2.20. The most important thing to realize in this figure is that the FCU-T, the special discharge diffuser and the artificial load generator are all aligned on the center line of the freezer. This is an important design requirement in order for the FCU-T to achieve symmetry of air flow right-and-left and up-and-down.

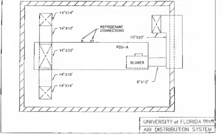

Figure 2.19. Supply and return air duct connections with FCU-A

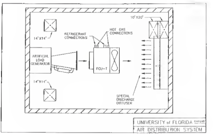

Figure 2.20 A top view of the airflow system inside the psychrometric freezer room

2.2.3. Air Distribution Diffuser

The air distribution diffuser is a special discharge diffuser built for the purpose of creating a uniform distribution of the supply air to the freezer. A schematic of the diffuser is shown in Figure 2.21, where the 6" x 67" plenum has been divided into eleven outlets. A picture showing the plenum air outlets of the special discharge diffuser is shown in Figure 2.22. It can also be seen in Figure 2.21 that there are eight vanes in the 90° elbow of the diffuser in order to preserve the momentum of the supply air to the plenum. The reduction in cross sectional area of the special discharge diffuser from 10" x 20" to 10" x 8" after it passes through the eight vanes is the key to the equal distribution of supply air to the eleven outlets. This reduction will cause the velocity of the supply air to increase as the flow reaches the farthest outlet in the plenum. This increase in the velocity is accompanied by the decrease of the mass of the supply air as it reaches the farthest outlet. The increase and decrease in velocity and mass of air, respectively, form the basis on which a uniform distribution of air in the freezer is created.

2.2.4. Artificial Load Generation System

The artificial load generation system is probably one of the most critical systems in this experimental facility. It is designed to provide the freezer with the required load in order to be able to manipulate the value of the load sensible heat ratio (LSHR) inside the freezer during the testing period. This artificial load generation system provides both sensible and latent loads. A schematic diagram describing the artificial load generation system is shown in Figure 2.23, while a summary description of the system components is provided in Table 2.5

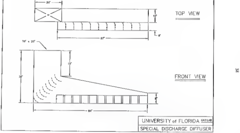

Figure 2.21 Schematic diagram of the special discharge diffuser

Figure 2.22. Plenum air outlets of the special discharge diffuser

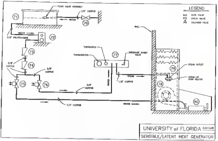

Figure 2.23 Schematic diagram of the artificial load generation system

Table 2.5 Summary Description of the Artificial Load Generation System Components

Item	Manufacturer	Model Number	Description
70	N/A	N/A	Hand Operated Line Valve
71	McMASTER-CARR	3754K71	Polyethylene Rectangular Water Tank
72	LMI MILTON ROY	A751-95T	Electronic Diaphragm Metering Pump
73	LMI MILTON ROY	A751-95T	Injection Check Valve
74	SUPERIOR	802B-6S	Check Valve
75	SPORLAN	E3S130	Water Feed Solenoid Valve
76	SPORLAN	E5S130	Water Feed Solenoid Valve
77	HCR INC	N/A	Water-Vapor Generator
78	WARREN TECHNOLOGY	HO-10.00-16X16	Electric Duct Heater With Integral Limit Control
79	DAYTON	5C093A	Direct Drive Blower
80	OMEGA	CRFC 312/240-C	Ceramic Radiant Heater

The generation of the sensible heat load is provided by an electric duct heater with integral limit control manufactured by Warren Technology (model number HO-10 00-16 x 16) with a total capacity of 10 kW (Item 78 in Figure 2.23). The artificial latent heat load is generated by the water-vapor generator (WVG) shown as Item 77 in Figure 2.23, which is a liquid-injection type water-vapor generator. It is a 1/4" thick steel constructed vaporizer that has a rectangular shape and is equipped with three heating elements strapped to its sides and bottom, and each heating element works at 700 Watts and 240 Volts.

City water is injected inside the water vapor generator (WVG) by the electronic diaphragm metering pump (Item 72 in Figure 2.23), where the metering pump can be adjusted to the required water mass flow rate. The injected water is heated to the desired temperature inside the vaporizer and is allowed to leave the WVG as steam through a 7/8" copper tube to the steam outlet inside the freezer as shown in Figure 2.23.

An alternate water-vapor generation technique has also been tried in this research. This system is shown in Figure 2.23, and is represented by a 1400 Watts Omega formed ceramic radiant heater (Item 80 in Figure 2.23) which surrounds a 2"OD copper tube. As the water is injected inside the heated 2"OD copper tube, it vaporizes and leaves the 2"OD copper tube to the inside of the freezer. A more detailed description of the artificial load generation system and its components is provided in Appendix D.

CHAPTER 3
INSTRUMENTATION AND DATA ACQUISITION

The purpose of this chapter is to describe the instrumentation and data acquisition systems employed in the experimental program. The instrumentation system includes devices for measuring the refrigerant pressures, temperatures, and flow rates; air dry-bulb temperatures, and differential pressure across the coil of the test fan-coil unit; electric power measurements, melt weight measurements, and frost thickness. The data acquisition system employed includes a computer, data acquisition boards, and associated software. Details of the two aforementioned systems are provided in the following sections.

3.1. Instrumentation System

An instrumentation system capable of providing data for the determination of heat loads due to coil hot-gas defrosting has been designed. The system consists of devices for measuring the weight of the melt, the frost thickness, temperatures, pressures, refrigerant flow rates, air humidity, and electric power consumption. Details of the different techniques used are provided in the sections that follow.

3.1.1. Melt Weight Measurements

The weight of the melt produced in the FCU-T when it is operating under the hot-gas defrosting mode is required in order to calculate that part of the hot-gas heat input to the FCU-T coil that leaves as melt. On the other hand, the weight of the melt produced in the FCU-A when it is operating under the electric defrosting mode is also required in order to compare that part of the frost that escapes the FCU-T coil to the air inside the freezer as moisture with the part of the frost that leaves FCU-T as melt.

The system built to weigh the melt is shown in Figure 3.1. During the FCU-T defrosting mode, the FCU-T melt solenoid valve (Item 61 in Figure 3.1) is energized to open allowing the melt to flow through the 1-1/8" FCU-T melt return line and collect in the funnel. This normally-closed solenoid valve (Item 61) is manufactured by Magnatrol Valve Corporation (model number 18A44). The McMaster Carr funnel (model number 4222T1) has a capacity of 3.5 gallons and is 12-3/4" high with a 11-3/4" diameter (McMaster-Carr 1996).

When the FCU-T hot-gas defrosting mode terminates, the valve (Item 61) is de-energized to close, at which point the weight of the FCU-T melt accumulated in the funnel is measured by a precision digital scale. This digital scale (Item 63 in Figure 3.1) is manufactured by Arlyne Scale Co. (model number 610L), and has a capacity of 50 pounds with a resolution of 0.01 pounds. A picture of the digital scale is shown in Figure 3.2. The melt is then drained through the melt drain solenoid valve (Item 62 in Figure 3.1) which is a McMaster-Carr normally-closed solenoid valve (model number 4738K43). This valve (Item 62) is energized to open at that moment and then de-energized to close after all the FCU-T melt has been drained.

During the process of collecting the FCU-T melt and measuring its weight, the normally-closed FCU-A melt solenoid valve (Item 60 in Figure 3.1) is kept de-energized.

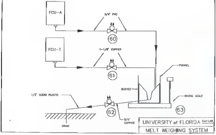

Figure 3.1 Melt weighing system

Figure 3 2 Digital scale for melt weight measurement

This action is taken due to the fact that the FCU-A is operating under its refrigeration mode at that period of time when the FCU-T is operating under its hot-gas defrosting mode. This FCU-A melt solenoid valve (Item 60) is manufactured by Magnatrol Valve Corporation (model number 18A43) and is identical with the FCU-T melt solenoid valve (Item 61), except for its smaller size.

When the FCU-A is operating under its electric defrosting mode, the FCU-A melt solenoid valve (Item 60 in Figure 3.1) is energized to open allowing the melt to flow through the 3/4" FCU-A melt return line and collect in the funnel. When the FCU-A electric defrosting mode terminates, the valve (Item 60) is de-energized to close, at which point the weight of the FCU-A melt accumulated in the funnel is measured by the precision digital scale. The melt is then drained through the melt drain solenoid valve (Item 62 in Figure 3.1) which is energized to open at that moment and then de-energized to close after all the FCU-A melt has been drained.

During the process of collecting the FCU-A melt and measuring its weight, the FCU-T melt solenoid valve (Item 61 in Figure 3.1) is kept de-energized. This action is taken due to the fact that the FCU-T is operating under its refrigeration mode at that period of time when the FCU-A is operating under its electric defrosting mode. A picture of the melt return lines showing the two Magnatrol solenoid valves is shown in Figure 3.3. As can be understood from Figure 3.3, the two melt lines are located outside the freezer, except for a portion of the FCU-T melt line (7 feet) which is located inside the freezer. The flow of melt inside this 7-foot portion is protected against freezing by two Easyheat heat cables (model number CAHB-03). Each heat cable is 3 feet long and its electrical specifications are 120 Volts and 21 Watts.

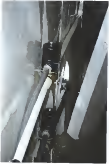

Figure 3 3 Melt return lines

3.1.2. Frost Thickness Measurements

Frost thickness measurements have been conducted employing a demand defrost system as shown in Figure 3.4, which is used to signal the time to start the defrosting mode of FCU-T. It is also used in the conduct of visualization studies of the frost thickness under subsaturated and supersaturated air conditions. This system consists of a commercial frost detector head (model number CFDH-5) to accommodate 5/8"OD tubes, and a defrost control unit switch (model number DCUS-100E). The detector head is a "U" shaped infrared sensor with optics on the inside of the open end. An infrared light beam crosses the open end of the sensor to detect the frost thickness.

The detector head is mounted vertically on a front FCU-T coil tube after cutting a portion of the coil fins and is employed with an adjusting screw to set the head to the desired frost thickness. The detector senses the thickness of 0.031" when the adjusting screw is turned all the way in, and senses the thickness of 0.375" when the adjusting screw is turned all the way out. For the other frost thickness ranging from 0.031" to 0.375", the detector's operating manual provides a table showing the number of adjusting screw turns needed for each thickness (Demand 1992). A picture of the detector head showing the adjusting screw is shown in Figure 3.5.

The defrost control unit switch is enclosed in a junction box and mounted on the outside of the freezer, where it is connected to the detector head through a 15-foot polarized plug cable. The unit switch is a normally-opened contact that closes when the frost build-up on the detector head reaches the desired adjusted frost thickness, at which point the infrared light beam is interrupted by the frost build-up (Demand 1990). The closing of the unit switch causes a small red light located on the junction box to signal the

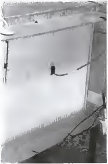

Figure 3.4 Demand defrost system mounted on FCU-T

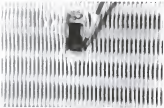

Figure 3.5 Frost detector head of the demand defrost system

beam crossing, i.e. the desired frost thickness, and also sends a 5-Volt DC analog signal to the computer.

3.1.3. Temperature Measurements

The temperatures in Fahrenheit have been measured at twenty locations using copper-constantan (type T) thermocouples for maximum accuracy. This type is suitable for low temperature applications as well as up to 700°F (ASHRAE 1993, Omega 1992b). The locations of the twenty thermocouples are identified in Table 3.1, and are shown in Figures 3.6 through 3.10, while the fluids they measure are also identified in Table 3.1. All thermocouples have been calibrated using a constant-temperature water bath manufactured by Polyscience Corporation (model number 80).

As can be seen in Figure 3.6, thermocouples (TC3 and TC7) measure the temperature at the same location, while thermocouples (TC6 and TC8) do the same thing at a different location. This practice is followed to confirm the accuracy of temperature measurements at these two locations. Temperature measurements using thermocouples TC3 and TC6 are the ones utilized in calculations for this project. Temperature measurement of thermocouple TC8 is identified as the FCU-T coil entering air dry bulb temperature (EAT), while temperature measurement of thermocouple TC10 is identified as the FCU-T coil leaving air dry bulb temperature (LV). Temperature measurement of thermocouple TC3 during the FCU-T refrigeration mode is identified as the FCU-T coil refrigerant temperature (CRT). All the temperature measurements have been recorded by a computer employing a data acquisition system.

Table 3.1 Thermocouple Locations and the Fluids They Measure

Thermocouple Number	Location	Fluid	Remarks
TC1	FCU-T melt line upstream of the valve	Water	Shown in Figure 3.10
TC2	FCU-T melt line downstream of the valve	Water	Shown in Figure 3.10
TC3	FCU-T wet return/hot gas line	R-22	Shown in Figure 3.6
TC4	FCU-T pan hot gas inlet line	R-22	Shown in Figure 3.6
TC5	FCU-T pan hot-gas outlet line	R-22	Shown in Figure 3.6
TC6	FCU-T refrigerant liquid/defrost refrigerant line	R-22	Shown in Figure 3.6
TC7	FCU-T wet return/hot gas line	R-22	Shown in Figure 3.6
TC8	FCU-T refrigerant liquid/defrost refrigerant line	R-22	Shown in Figure 3.6
TC9	FCU-T coil entrance	Air	Shown in Figure 3.8
TC10	FCU-T coil exit	Air	Shown in Figure 3.8
TC11	FCU-T blower outlet	Air	Shown in Figure 3.8
TC12	Upstream of the FCU-T coil	Air	Shown in Figure 3.8
TC13	Downstream of the FCU-T blower	Air	Shown in Figure 3.8
TC14	Inside the psychrometric freezer room next to the right wall	Air	Shown in Figure 3.9
TC15	Inside the psychrometric freezer room next to the front wall	Air	Shown in Figure 3.9
TC16	FCU-A melt line upstream of the valve	Water	Shown in Figure 3.10
TC17	FCU-A melt line downstream of the valve	Water	Shown in Figure 3.10
TC18	FCU-A refrigerant liquid line	R-22	Shown in Figure 3.7
TC19	FCU-A wet return line	R-22	Shown in Figure 3.7
TC20	Outside the psychrometric freezer room	Air	Shown in Figure 3.9

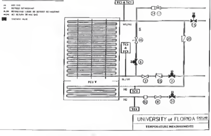

Figure 3.6 Locations of FCU T refrigerant temperature measurements

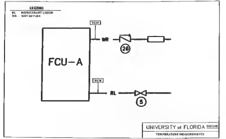

Figure 3.7 Locations of FCU A refrigerant temperature measurements

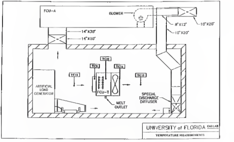

Figure 3 8. Locations of FCU-T air dry bulb temperature measurements

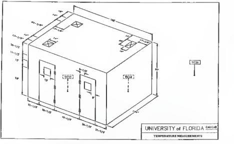

Figure 3.9 Locations of air dry bulb temperature measurements across the psychrometric freezer room walls

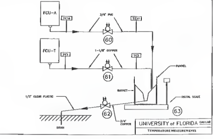

Figure 3.10 Locations of melt temperature measurements

3.1.4. Pressure Measurements

Refrigerant pressures have been measured at eight locations which are identified in Table 3.2, and are shown in Figures 3 11 and 3 12, while the types of instruments (pressure gage and/or pressure transducer) used to measure each pressure are identified in Table 3.3

The five pressure gages and the five pressure transducers for pressure measurements P1, P2, P3, P4 and P5, are all mounted on an instrumentation board outside the freezer as shown in Figure 3 13 The pressure gages and pressure transducers on the instrumentation board are connected to the refrigerant lines through 1/4"OD copper pilot lines. Each of pressures P1 and P4 is also measured by a second pressure gage mounted directly on the refrigerant line in addition to the one on the instrumentation board The pressure gage mounted directly on the hot-gas line for pressure measurement P4 is shown in Figure 3 14

The pressure gages used to measure pressures P1, P2, P3, P4 P5 and P7 are manufactured by Ritchie Engineering Company Inc , while the pressure gages used to measure pressures P6 and P8 are manufactured by Weksler Instruments. The pressure transducers used to measure pressures P1, P2, P3, P4, and P5 are manufactured by Mamac Systems Inc (model number PR-262-5-12-A-1-2-B) These transducers have a pressure range of 0 to 270 psig and can operate at a temperature limit up to 180°F The Mamac pressure transducers are accurate to ± 1% of the full-scale and need a DC power supply of 12-28 Volts to operate, while they send direct output signals of 4-20 mA (Mamac 1990a) The output signals are received by the computer through the data acquisition system

Table 3.2. Locations of the Pressure Measurements

Pressure	Location	Remarks
P1	Defrost refrigerant line downstream of the defrost orifice meter	Shown in Figure 3.12.
P2	FCU-T wet return/hot gas line	Shown in Figure 3.11
P3	FCU-T refrigerant liquid/defrost refrigerant line	Shown in Figure 3.11
P4	FCU-T pan hot gas inlet line upstream of the hot-gas orifice meter	Shown in Figure 3.11
P5	Main liquid line downstream of the liquid pump	Shown in Figure 3.12
P6	Main suction line upstream of the LCU pressure regulating valve	Shown in Figure 3.12.
P7	Main suction line downstream of the LCU pressure regulating valve	Shown in Figure 3.12
P8	Main liquid line downstream of the main liquid line solenoid valve	Shown in Figure 3.12

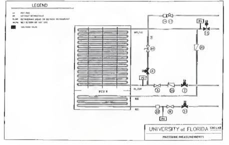

Figure 3.11 Locations of FCU T refrigerant pressure measurements

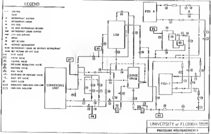

Figure 3.12 Locations of refrigerant pressure measurements

Table 3 3 Methods of Pressure Measurements

Pressure	Pressure Gage		Pressure Transducer
	On the Line	Instrumentation Board	
P1	Yes	Yes	Yes
P2	No	Yes	Yes
P3	No	Yes	Yes
P4	Yes	Yes	Yes
P5	No	Yes	Yes
P6	Yes	No	Yes
P7	Yes	No	Yes
P8	Yes	No	No

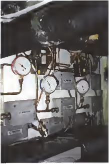

Figure 3.13 Pressure gages mounted on the instrumentation board

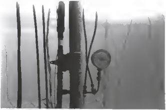

Figure 3.14 Pressure gage on the hot-gas line for pressure measurement P4

The Cole-Parmer pressure transducers (model number H 68972 12) are used to measure pressures P6, and P7 These transducers have a pressure range of 0 to 200 psig and can operate at a temperature limit up to 175°F They are accurate to ± 0 1% of the full-scale and need a DC power supply of 9 30 Volts to operate, while they send output signals of 4-20 mA (Cole-Parmer 1995) The output signals are received by the computer through the data acquisition system A Hewlett-Packard DC power supply (model number 62024C) has been used to supply the DC power required by the Mamac and the Cole-Parmer pressure transducers This DC power supply provides a voltage of 24 ± 5% Volts and an amperage of 1 75 Amps

Pressure measurement P7 represents the compressor refrigerant suction pressure, while pressure measurement P8 represents the discharge refrigerant pressure of the receiver The pressure gage for measuring P8 is only used as a safety measure to indicate the discharge refrigerant pressure of the receiver in order to confirm that this pressure does not reach a high value (greater than 250 psig) During the qualification tests of the refrigeration/defrost system pressure transducers for P3 and P6 failed to operate successfully Therefore, the pressure values for P3 and P6 have been recorded manually by reading the pressure values from the pressure gages

The differential pressure of the air (P_{air}) across the FCU-T coil has been detected as can be seen in Figure 3 15 A Mamac low pressure transducer (model number PR-272-5-12-A-1-1-A-E), and two Mamac static pressure probes (model number A-520-2-A-1) have been utilized for that purpose Each of the two 8" long aluminum probes has two orifices opposing each other on a vertical position. Each probe is attached to a 2"OD flange which is used to mount the probe on the FCU-T sheet metal frame by drilling a 1/4"

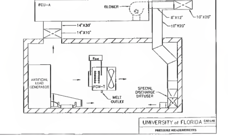

Figure 3.15 Differential pressure measurement of the air across the FCU-T coil

hole on the latter and inserting the probe in that hole. The probes are inserted in a way that the orifices will be in parallel with the air flow. Each probe is connected to the low pressure transducer by a 1/4"OD copper pilot line having PVC end connections. The probes are capable of operating under a maximum pressure of 10 psig and a maximum temperature of 250°F (Mamac 1991).

The Mamac low pressure transducer is mounted on the instrumentation board and is capable of detecting less than 0.001" water column differential (WCD) pressure change. It has a pressure range of 0 to 0.50" WCD and can operate at pressure and temperature limits up to 10 psig and 105°F, respectively. This low pressure transducer is accurate to ± 1% of the full-scale and needs a DC power supply of 12-28 Volts to operate, while it sends direct output signals of 4-20 mA (Mamac 1990b). The output signals are received by the computer through the data acquisition system. The DC power supply is provided to this low pressure transducer from the same Hewlett-Packard DC power supply used for the other pressure transducers.

3.1.5. Refrigerant Mass Flow Rate Measurements

Refrigerant mass flow rates have been measured at three locations in the refrigeration/defrost system. As shown in Figure 3.16, the hot-gas and the defrost orifice meters (Items 32 and 33, respectively, in Figure 3.16) are used to measure the refrigerant vapor mass flow rates while the turbine flow meter (Item 30 in Figure 3.16) is used to measure the liquid refrigerant mass flow rate.

The hot-gas orifice meter (model number M1) is identical to the defrost orifice meter (model number M2), where both are manufactured in house. The two orifice

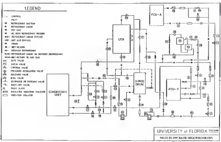

Figure 3.16 Locations of refrigerant mass flow rate measurements

meters were tested for their performance before their installation on the piping system. Results of the performance tests, and the equations derived to calculate the refrigerant vapor mass flow rate are discussed in Appendix E. A schematic describing the shape and dimensions of the orifice meters can be seen in Figure 3.17. Both meters are of the concentric type with sharp edges, and are employed with a D-and-D/2 taps. The inside diameter (D_1) of the pipe is 0.527", while the throat diameter (D_t) of the orifice is 0.2625". The ratio (β) of the orifice throat diameter to the pipe inside diameter is 0.5

The refrigerant vapor differential pressure across the hot gas orifice meter (Item 32 in Figure 3.16) is measured using an ultra low differential pressure transducer. This transducer is mounted on the instrumentation board and is connected to the taps of the hot-gas orifice meter through two 1/4"OD copper pilot lines. The differential pressure transducer is manufactured by Validyne Engineering Corporation (model number DP103 14-V-1-S-4-G) and is equipped with a replaceable sensing element (stainless steel diaphragm). It has a pressure range of 0 to 0.89" water column differential (WCD) and is accurate to ± 0.25% of the full-scale, while it can operate at a temperature limit up to 160°F (Validyne 1994).

A sine wave carrier demodulator is connected to the above differential pressure transducer through a 50-foot electrical cable. The demodulator is manufactured by Validyne Engineering Corporation (model number CD15-A-1-A-1) and is used to condition the output signals of the differential pressure transducer. The electrical specifications of the demodulator are 105-125 Volts, 60-400 Hz, and 5 Watts. The demodulator can operate at a temperature limit up to 185°F (Validyne 1988).

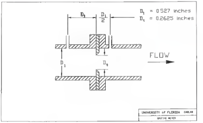

Figure 3.17 Schematic diagram of the orifice meter

The Validyne demodulator applies a sine wave excitation to the Validyne differential pressure transducer which causes the latter to send its AC output signals back to the demodulator. The demodulator receives these AC signals and amplifies, rectifies, and then filters them into output signals of ± DC voltages. This DC voltage represents the magnitude of the differential pressure across the hot-gas orifice meter, where the Validyne demodulator has an output DC voltage range of ± 10 Volts (Validyne 1988, 1993). The demodulator's DC output signals are received by the computer employing the data acquisition system.

The refrigerant vapor differential pressure across the defrost orifice meter (Item 33 in Figure 3.16) is measured using a CEC differential pressure transducer which is mounted on the instrumentation board and connected to the taps of the defrost orifice meter through two 1/4"OD copper pilot lines. This transducer (model number 4-351-0152) is an accurate strain gage type pressure transducer that has a pressure range of 0 to 20 psid. The transducer needs a DC power supply to operate, while it sends output signals to the computer through the data acquisition system.

The CEC differential pressure transducer is connected to a digital strain gage indicator through an electrical cable. This indicator is manufactured by Vishay Intertechnology, Inc. (model number V/E 20A) and is used to provide a DC power supply to the transducer. The digital strain gage indicator is also used to provide a numerical display of the stress applied on the strain gage. The electrical specifications of the digital strain gage indicator are: 105-130 Volts, 50-60 Hz, and 10 Watts.

The turbine flow meter (Item 30 in Figure 3.16) is manufactured by Signet Scientific Company (model number MK-525) and is used to measure the mass flow rate of the liquid refrigerant. It is a paddlewheel transducer mounted on a mini-tap fitting where the latter is constructed in house This mini-tap fitting is welded to a small 1 1/8"OD portion of the liquid refrigerant pipe, where the paddlewheel is housed The paddlewheel transducer has a stainless steel construction and is equipped with a sensor (model number MK-525-1) and a paddlewheel of four blades (Signet 1994)

The turbine flow meter is employed with a Signet analog flow meter (model number MK 584) which consists of two gages One of the gages has a flow rate range of 0 to 12 gpm, while the other has a flow rate range of 0 to 50 gpm (Signet 1994) A picture of the Signet analog flow meter is shown in Figure 3 18 The analog flow meter is externally powered with a Signet DC power supply (model number P30075) in order to operate the two gages

The paddlewheel transducer is installed in a way that allows the paddlewheel to be located at the center of the pipe This location will cause the transducer to sense the maximum local velocity of the liquid refrigerant. The maximum local velocity sensed by the transducer is about 25% higher than the local average velocity of the liquid refrigerant. As the liquid refrigerant flows through the pipe housing the paddlewheel, it causes the paddlewheel to rotate which causes the paddlewheel blades to cross the magnetic field of the coil in the transducer Each blade crossing of the magnetic field will induce an output AC voltage in the coil in the form of a sine wave. This wave is the output signal that will be sent to the computer through the data acquisition system, as well as the Signet analog flow meter (Signet 1994)

The frequency of the output signals (number of output signals per second) is directly proportional to the maximum local velocity of the liquid refrigerant This

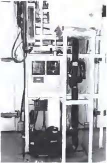

Figure 3.18 Signet analog flow meter

frequency is measured in Hertz and stored by the computer, while the calibration factor of this turbine flow meter is 15 Hz per foot per second. The equations derived to calculate the liquid refrigerant mass flow rate are discussed in Appendix F. This turbine flow meter has a flow rate range of 1 to 30 feet per second and is capable of operating under a maximum pressure of 1500 psig and a maximum temperature of 300°F (Signet 1994).

3.1.6. Humidity Measurements

The relative humidity (RH) of the air inside the freezer has been detected at two locations as shown in Figure 3.19. The first location (RH1) is upstream of the FCU/T, while the other (RH2) is downstream of the FCU/T blower. The relative humidity measurements were performed using a Mamac humidity transducer (model number HU-222-4-2-3-A) at each location. The two transducers are mounted on an instrumentation board outside the freezer while each transducer is connected to a remote probe hung inside the freezer at the position shown in Figure 3.19. These two remote probes serve as humidity sensors.

The two Mamac humidity transducers have a humidity range of 0 to 100% RH and are accurate to ± 2% of the full-scale. They need a DC power supply of 12-28 Volts to operate, while they send output signals of 4-20 mA. The output signals are received by the computer through the data acquisition system. DC power is provided to the humidity transducers from the same Hewlett-Packard DC power supply (model number HP-6202 4C) used for the pressure transducers.

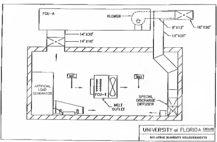
FCU–A
BLOWER
14"X30"
14"X10"
8"X12"
10"X20"
10"X20"
RH1
RH2
ARTIFICIAL LOAD GENERATOR
FCU–T
MELT OUTLET
SPECIAL DISCHARGE DIFFUSER
UNIVERSITY of FLORIDA CAD LAB
RELATIVE HUMIDITY MEASUREMENTS

Figure 3.19 Locations of relative humidity measurements

3.1.7. Electric Power Measurements

Electric power measurements have been conducted using five power transducers manufactured by Ohio Semitronics, Inc. where each transducer has been assigned to measure specific devices used in this project as shown in Table 3.4. Each power transducer measures the instantaneous electric power and the electric energy consumption of its assigned devices. The specifications of the power transducers are shown in Table 3.5 (Ohio 1992).

Every power transducer requires an AC power supply to operate, while it sends output signals of 4-20 mA (Ohio 1992). The 4-20 mA output signals are calibrated to the instantaneous electric power in kilowatts (kW) as shown in Table 3.5 and are received by the computer through the data acquisition system. The computer stores the measured values of the instantaneous electric power in kilowatts.

Each power transducer also sends output pulse signals of 5 Volts to the computer through the data acquisition system, where the number of pulses is counted and stored. This is done in order to measure the consumed electric energy by the assigned devices in Watt-hours. Each output pulse signal from power transducers PT1, PT2 and PT5 represents an electric energy consumption of one Watt-hour, while each output pulse signal from power transducers PT3 and PT4 represents an electric energy consumption of ten Watt-hours (Ohio 1992).

3.1.8. Electrical Wiring

A schematic diagram describing the electrical wiring is shown in Figure 3.20, while a summary description of the electrical wiring components can be seen in Table 3.6. The

Table 3.4. Power Transducers and the Devices They Measure

Transducer Number	Devices They Measure
PT1	1) FCU-T fan
PT2	1) Three heating elements of the water vapor generator (WVG) 2) Ceramic radiant heater
PT3	1) Six band heaters of the load compensation unit (LCU)
PT4	1) Electric duct heater of the artificial load generation system.
PT5	1) Two light fixtures hanged on the ceiling of the psychrometric freezer room 2) Direct-drive blower of the artificial load generation system 3) "Clean up" strip heater of the artificial load generation system. 4) Electric heating cable of the artificial load generation system. 5) Two heating cables on the FCU-T melt line.

Table 3.5 Specifications of the Power Transducers

Transducer Number	Model Number	Input Ranges		Phase & Frequency	Instantaneous Power Calibration	Output Signals for Energy Consumption
		Voltage (Volts)	Current (Amps)			
TT1	W-110E-T	0-300	0-20	Single & 50/60 Hz	4-20 mA = 0-4 kW	5 Volts Pulses *
TT2	W-020E-T	0-300	0-15	Single & 50/60 Hz	4-20 mA = 0-3 kW	5 Volts Pulses *
TT3	W-062E-T	0-300	0-100	Three & 50/60 Hz	4-20 mA = 0-40 kW	5 Volts Pulses **
TT4	W-062E-T	0-300	0-100	Three & 50/60 Hz	4-20 mA = 0-40 kW	5 Volts Pulses **
TT5	W-117E-T	0-150	0-20	Single & 50/60 Hz	4-20 mA = 0-2 kW	5 Volts Pulses *

* Each pulse represents an energy consumption of 1 Watt-hour.

** Each pulse represents an energy consumption of 10 Watt-hours.

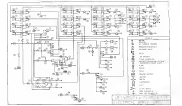

Figure 5.36 Schematic diagram of the electrical wiring

Table 3 6 Summary Description of the Electrical Wiring Components

Item	Manufacturer	Model Number	Description
1	Carling	N/A	Toggle Switch S1
2	Carling	N/A	Toggle Switch S2
3	Carling	N/A	Toggle Switch S3
4	Carling	N/A	Toggle Switch S4
5	Carling	N/A	Toggle Switch S5
6	Carling	N/A	Toggle Switch S6
7	Carling	N/A	Toggle Switch S7
8	Carling	N/A	Toggle Switch S8
9	Carling	N/A	Toggle Switch S9
10	Carling	N/A	Toggle Switch S10
11	Carling	N/A	Toggle Switch S11
12	Carling	N/A	Toggle Switch S12
13	Carling	N/A	Toggle Switch S13
14	Carling	N/A	Toggle Switch S14
15	Carling	N/A	Toggle Switch S15
16	Carling	N/A	Toggle Switch S16
17	Carling	N/A	Toggle Switch S17
18	ComputerBoards	SSR-OAC05	Computer Controlled Relay for S1
19	ComputerBoards	SSR-OAC05	Computer Controlled Relay for S2
20	ComputerBoards	SSR-OAC05	Computer Controlled Relay for S3
21	ComputerBoards	SSR-OAC05	Computer Controlled Relay for S4
22	ComputerBoards	SSR-OAC05	Computer Controlled Relay for S5
23	ComputerBoards	SSR-OAC05	Computer Controlled Relay for S6
24	ComputerBoards	SSR-OAC05	Computer Controlled Relay for S7
25	ComputerBoards	SSR-OAC05	Computer Controlled Relay for S8
26	ComputerBoards	SSR-OAC05	Computer Controlled Relay for S9
27	ComputerBoards	SSR-OAC05	Computer Controlled Relay for S10
28	ComputerBoards	SSR-OAC05	Computer Controlled Relay for S11
29	ComputerBoards	SSR-OAC05	Computer Controlled Relay for S12
30	ComputerBoards	SSR-OAC05	Computer Controlled Relay for S13
31	ComputerBoards	SSR-OAC05	Computer Controlled Relay for S14

Table 3.6 — continue

Item	Manufacturer	Model Number	Description
32	ComputerBoards	SSR-OAC05	Computer Controlled Relay for S15
33	ComputerBoards	SSR-OAC05	Computer Controlled Relay for S16
34	Potter & Brumfield	KRPA-11AG-120	Relay for S1
35	Potter & Brumfield	KRPA-11AG-120	Relay for S2
36	Potter & Brumfield	KRPA-11AG-120	Relay for S3
37	Potter & Brumfield	KRPA-11AG-120	Relay for S4
38	Potter & Brumfield	KRPA-11AG-120	Relay for S5
39	Potter & Brumfield	KRPA-11AG-120	Relay for S6
40	Potter & Brumfield	KRPA-11AG-120	Relay for S7
41	Potter & Brumfield	KRPA-11AG-120	Relay for S8
42	Potter & Brumfield	KRPA-11AG-120	Relay for S9
43	Potter & Brumfield	KRPA-11AG-120	Relay for S10
44	Potter & Brumfield	KRPA-11AG-120	Relay for S11
45	Potter & Brumfield	KRPA-11AG-120	Relay for S12
46	Potter & Brumfield	KRPA-11AG-120	Relay for S13
47	Potter & Brumfield	KRPA-11AG-120	Relay for S14
48	Potter & Brumfield	KRPA-11AG-120	Relay for S15
49	Potter & Brumfield	KRPA-11AG-120	Relay for S16
50	N/A	N/A	486DX Computer
51	Square D	J 353640	Main Disconnect for "A" Circuits
52	G.E.	NP 266211-A	Disconnect "A_1" for FCU-T Fan
53	Ohio Semitronics	W 110E-T	Power Transducer: PT1
54	Square D	8910-DPA13	Relay for FCU-T Fan
55	Colmac	4HP1	FCU-T Fan
56	G.E.	HP 266211-A	Disconnect "$A_{2,1}$" for FCU-A Blower
57	G.E.	NP 266211-A	Disconnect "$A_{2,2}$" for FCU-A Blower
58	N/A	N/A	Relay for FCU-A Blower
59	Dayton	5C198A	FCU-A Blower
60	Square D	B-40274-859-04	Disconnect "A_3" for Steam Generators
61	Ohio Semitronics	W 020E-T	Power Transducer: PT2
62	Square D	1020	Relay for WVG

Table 3 6 -- continue

Item	Manufacturer	Model Number	Description
63	HCR Inc	N/A	Water Vapor Generator (WVG)
64	Square D	1020	Relay for Ceramic Radiant Heater
65	Omega	CRFC-312/240-C	Ceramic Radiant Heater
66	Square D	A-40274-850-01	Disconnect "A_1" for LCU Band Heaters
67	Omega	SCR73Z-260-M	Rectifier for LCU Band Heaters
68	Ohio Semitronics	W 062E T	Power Transducer: PT3
69	Chromalox	HB 2030	LCU Band Heaters
70	G E	NP 266208	Main Disconnect for "B" Circuits
71	Square D	J 353642	Disconnect "B_1" for Compressor
72	Copeland	4DL3-1500-TSK	Compressor
73	Square D	B-40274-859 04	Disconnect "B_2" for Duct Heater
74	Omega	SCR73Z-230-M	Rectifier for Duct Heaters
75	Ohio Semitronics	W-062E-T	Power Transducer; PT4
76	Warren Tech	HO-10.00-16X16	Duct Heater
77	Square D	40262 621-04	Breaker in Panel C_2
78	N/A	N/A	Outlet
79	Ohio Semitronics	W 117E-T	Power Transducer; PT5
80	N/A	N/A	Switch
81	N/A	N/A	Light Fixture Inside the Freezer
82	N/A	N/A	Switch
83	N/A	N/A	Light Fixture Inside the Freezer
84	Potter & Brumfield	KRPA-11AG-120	Relay of the Artificial Load Generator
85	Dayton	5C093A	Artificial Load Generator Blower
86	Raychem	W51-12P	Artificial Load Generator Heat Cable
87	N/A	N/A	Artificial Load Generator Strip Heater
88	Easyheat	CAHB-03	Heat Cables on the FCU T Melt Line
89	N/A	N/A	Breaker in the Electrical Room
90	N/A	N/A	Switch
91	Allen Bradley	509 BOA	Relay
92	Micropump	1800	Oil Pump
93	Sporlan	LMC-PVE-5-1/2	Heater of the LMC Element

Table 3 6 -- continue

Item	Manufacturer	Model Number	Description
94	Alco	100RB2S3	Oil Return Solenoid Valve
95	N/A	N/A	Breaker in the Electrical Room
96	Allen Bradley	509-BOA	Relay
97	Viking	SG-40550	Liquid Refrigerant Pump
98	Validyne	CD15-A-1-A-1	Demodulator
99	Arlyne Scale Co	610L	Precision Digital Scale
100	Hewlett Packard	62024C	DC Power Supply
101	Sporlan	MB25S2	Main Liquid Line Solenoid Valve
102	Signet	P30075	DC Power Supply
103	Sporlan	E19S270	FCU A Liquid Line Solenoid Valve
104	Sporlan	B10S2	Main Hot-Gas Line Solenoid Valve
105	Sporlan	B10S2	Hot-Gas Bypass Solenoid Valve
106	Sporlan	E9S240	Liquid Bypass Solenoid Valve
107	LMI Milton Roy	A751-95T	Electronic Diaphragm Metering Pump
108	Dayton	4Z843B	Motors of the Dampers Linear Actuators
109	Raychem	W51-6P	Damper Frames Heating Cables
110	HPI	N/A	Defrosting Heater Elements
111	Sporlan	OE34S290	FCU-A Wet Return Stop Solenoid Valve
112	Magnatrol	18A43	FCU-A Melt Solenoid Valve
113	Sporlan	E19S270	FCU-T Liquid Line Solenoid Valve
114	McMaster-Carr	4738K43	Melt Drain Solenoid Valve
115	Sporlan	MB19S2	Hot Gas Defrost Solenoid Valve
116	Sporlan	OE34S290	FCU-T Wet Return Stop Solenoid Valve
117	Sporlan	B10S2	Defrost Refrigerant Solenoid Valve
118	Magnatrol	18A44	FCU-T Melt Solenoid Valve
119	N/A	N/A	Disconnect for the Relays Power
120	Chromalox	N/A	Heating Cables of the Freezer Doors
121	Sporlan	E5S130	Water Feed Solenoid Valve
122	Sporlan	E3S130	Water Feed Solenoid Valve
123	Demand Defrost	DCUS 100E	Defrost Control Unit

Carling toggle switches (Items 1 to 16 in Figure 3.20) used to operate the system are single pole double throw switches while the Potter and Brumfield relays assigned to them (Items 34 to 49 in Figure 3 20) are double pole double throw relays. A picture showing the control panel with the toggle switches and their relays mounted on the panel can be seen in Figure 3.21

The toggle switches have three positions (on, off and automatic), and are connected to the devices in a way that all the devices can be operated manually by the switches while some devices can be operated by the computer through the data acquisition system Each toggle switch is assigned to operate certain devices in this project, where the toggle switches and the devices they function are identified in Table 3 7 The toggle switch S17 (Item 17 in Figure 3.20) is not connected to a computer controlled relay, where its automatic position is also used as a manual position The toggle switch S17 is used to operate the two steam generators (the water vapor generator and the ceramic radiant heater; Items 63 and 65, respectively in Figure 3 20) with their assigned water feed solenoid valves, where each toggle switch position is connected to one steam generator and its water feed solenoid valve

As can be seen in Figure 3 20 there are four AC current sources that supply the system with the required electricity The major AC current source is the one that supplies electricity to the main disconnects of the "A" and "B" circuits (Items 51 and 70 respectively, in Figure 3 20) The "A" circuit begins from the main disconnect (Item 51 in Figure 3 20) and branches out through the "A_1", "$A_{2,3}$", "A_3", and "A_4" disconnects (Items 52, 56, 60, and 66, respectively, in Figure 3 20) The "B" circuit begins from the main

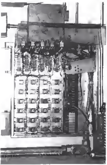

Figure 3 21 Control panel

Table 3.7 Functions of the Toggle Switches

Switch Number	Devices Operated by the Switch
S1	- Hewlett-Packard Power Supply - Validyne Demodulator - Heating Cables of the Freezer Doors - Precision Digital Scale - All Five Power Transducers
S2	- Main Liquid Line Solenoid Valve - Oil Return Solenoid Valve - Oil Pump - Heater of the LMC Element - Signet DC Power Supply
S3	- Artifical Load Generator Blower - Artifical Load Generator Heat Cable - Artifical Load Generator Strip Heater
S4	- FCU-A Liquid Line Solenoid Valve - FCU-A Blower
S5	- Compressor
S6	- Liquid Refrigerant Pump
S7	- Main Hot-Gas Line Solenoid Valve
S8	- Hot-Gas Bypass Solenoid Valve
S9	- Liquid Bypass Solenoid Valve
S10	- Electronic Diaphragm Metering Pump
S11	- FCU-A Wet Return Stop Solenoid Valve - Motors of the Dampers Linear Actuators - Damper Frames Heating Cables - Defrosting Heater Elements
S12	- FCU-A Melt Solenoid Valve
S13	- FCU-T Liquid Line Solenoid Valve
S14	- Melt Drain Solenoid Valve
S15	- Hot-Gas Defrost Solenoid Valve - FCU-T Wet Return Stop Solenoid Valve - Defrost Refrigerant Solenoid Valve
S16	- FCU-T Melt Solenoid Valve
S17	- Water-Vapor Generator (WVG) and its Water Feed Solenoid Valve - Ceramic Radient Heater and its Water Feed Solenoid Valve

disconnect (Item 70 in Figure 3.20) and branches through the "B_1" and "B_2" disconnects (Items 71, and 73 respectively in Figure 3.20)

Two of the remaining AC current sources supply the system with electricity from breakers (Items 89 and 95 in Figure 3.20) located in an electrical room near the laboratory where the facility is housed. The fourth AC current source is supplied from a breaker in a panel called "Panel C_6" (Item 77 in Figure 3.20) located inside the laboratory. There are two disconnect switches assigned for FCU-A (Items 56 and 57 in Figure 3.20). One of these switches is installed very close to the FCU-T for safety measures.

The Hewlett-Packard DC power supply (Item 100 in Figure 3.20) is the unit to supply DC power to all the Mamac transducers and the two Cole-Parmer pressure transducers, while the Signet DC power supply (Item 102 in Figure 3.20) is the unit to supply DC power to the Signet analog flow meter. The Validyne demodulator (Item 98 in Figure 3.20) is the charger and signal conditioner for the Validyne differential pressure transducer. The Vishay digital strain gage indicator used for the CEC differential pressure transducer is not shown in the electrical wiring diagram since it is connected to the electrical outlet (Item 78 in Figure 3.20)

The FCU-A blower, motors of the FCU-A dampers linear actuators, the dampers frames heating cables, and the defrosting heater elements (Items 59, 108, 109 and 110, respectively, in Figure 3.20) are all operated individually through the control panel located in the alcove of the FCU-A. This FCU-A control panel has six switches connected to it, where each switch is set to three different operating modes. The three modes are the on, off and the automatic mode of operation. The switches are connected to control the operations of the FCU-A blower, the FCU-A light fixture, the motors of the FCU-A dampers linear actuators, the FCU-A defrosting heater elements, the FCU-A electric heating cables and the FCU-A receptacles.

As can be seen in Table 3.7, the devices operated by toggle switch S11 are the FCU-A wet return stop solenoid valve the motors of the FCU-A dampers linear actuators, the FCU-A defrosting heater elements and the FCU-A electric heating cables. When toggle switch S11 is switched on, the FCU-A wet return stop solenoid valve is energized to close the motors of the FCU-A dampers linear actuators will close the dampers, the FCU-A defrosting heater elements are switched on while the FCU-A electric heating cables are switched off

3.2. Data Acquisition System

The data acquisition system used is capable of performing the test calculations instantaneously as the data are read and stored Based on these test calculations, the data acquisition system can be programmed to send feedback signals to the components of the refrigeration/defrost system in order to react accordingly While this data acquisition system is capable of recording data at a rate of 100 Hz, it was decided to average the readings over a 5-second interval for purposes of limiting the amount of data collected and in order to conserve disk space Thus every data point collected and plotted represents the average of 500 readings. The data acquisition system designed consists of a computer software, and data acquisition boards Detailed descriptions of these items follow

3.2.1. Computer

The computer employed has a 3486 system motherboard (serial number 092192) which features an Intel 486DX central processing unit with a speed of 50 MHz and an on board cache memory (RAM) of 256 kilobytes. The main memory (RAM) of this computer is 8 Megabytes. This high performance motherboard has six 16-bit slots for interface cards while one of these slots is a local bus slot for adapting a proper local bus device. An enhanced video graphic adapter (VGA) board is used on this motherboard local bus where the enhanced VGA board has a 1 Megabyte video memory (RAM) and supports a resolution of 1024 x 768 with both interlaced and non interlaced modes.

The computer has two floppy drives and one hard drive; a 1.2 Megabyte 5.25" and a 1.44 Megabyte 3.5" floppy drives, while the hard drive is 850 Megabyte. The hard drive is manufactured by Western Digital (model number WDAC2850-00F). These drives are installed in a full tower case that has a DC power supply of 230 Watts. This computer is employed with a multi-function controller IDS card (model number SAI2S7) that controls the hard drive. This card is installed on one of the motherboard's 16-bit slots. The card also controls the floppy drives, one game port, one parallel printer port, and two serial ports. One of the serial ports is connected to the computer mouse while the other is connected to the digital scale.

3.2.2. Software

The PC-based data acquisition and process control software called LABTECH CONTROL for Windows (version 5.1) was used in this research. This software is designed by Laboratory Technologies Corporation and is capable of monitoring and controlling the processes performed by the refrigeration/defrost system The software is programmed to read the signals received from the data acquisition boards and is capable of converting them to the appropriate engineering units and storing them in the hard drive. The software can use the data it gathers as feedback to control various devices during the operation of the refrigeration/defrost system

The software is provided with graphical interface called "ICONview" which is used to create the monitoring and controlling setup required by the project. The ICONview interface consists of different types of icons representing different types of measurements (i.e. temperature icons, pressure icons, power icons, etc.) Each icon provides a block for a single monitored variable and the parameters (i.e. sampling rate, engineering units, etc) needed to define the monitored variable are defined in that block. This software is capable of providing a maximum of 600 blocks (ComputerBoards 1994a) A picture showing computer monitoring of several different blocks is shown in Figure 3 22.

The software has the capability to perform calculations during the operation of the refrigeration/defrost system and benefit from the results of these calculations in controlling the various operations of the system The software provides the user with the capability to trigger any block, in order to check or change the parameters of the measured variable, while the system is in operation (LABTECH 1995)

3.2.3. Data Acquisition Boards

Several data acquisition boards manufactured by ComputerBoards, Inc. have been used in this project. A schematic describing the layout of the data acquisition boards with

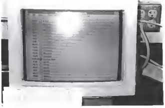

Figure 3.22 Computer monitoring of several different blocks

their input/output signals can be seen in Figure 3.23, while a summary description of the data acquisition boards can be seen in Table 3.8. The four data acquisition boards (Items 3, 4, 5 and 6 in Figure 3.23) are mounted on the remaining four 16-bit slots of the computer's motherboard.

The analog signals from the differential pressure, humidity, and pressure transducers and from the demand defrost control switch are all received by the analog input multiplexor (Item 1 in Figure 3.23) while all the thermocouple signals are received by the other analog input multiplexor (Item 2 in Figure 3.23). The two analog input multiplexors (model number CIO-EXP32) are identical and are used for signal conditioning and to expand the total number of analog input channels to the data acquisition boards. Each multiplexor is equipped with a temperature sensor on board for accurate thermocouple temperature measurements. The temperature sensors will measure the board temperature at the location of the board screw terminals and compensate its value from measurements of the thermocouple temperature (ComputerBoards 1992a, 1994a).

The analog signals leaving the first multiplexor (Item 1 in Figure 3.23) will be received by an analog-to-digital converter (model number CIO-DAS08) where the digital signals are then stored in the hard drive. This analog-to-digital converter (Item 3 in Figure 3.23) is employed with a 24-bit digital input/output connector which is used to send digital control signals to the solid state relays mounted on an interface rack (Item 7 in Figure 3.23) in order to operate the switches and devices of the refrigeration/defrost system (ComputerBoards 1992b; 1994a). The thermocouple analog signals leaving the second multiplexor (Item 2 in Figure 3.23) are received by an analog-to-digital converter (model

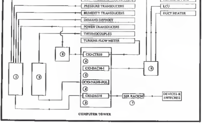

Figure 3 23 Schematic diagram of the data acquisition boards layout

Table 3.8 Summary Description of the Data Acquisition Boards

Item	Manufacturer	Model Number	Description
1	ComputerBoards, Inc	CIO-EXP32	32 Channel Analog Input Multiplexor
2	ComputerBoards, Inc	CIO-EXP32	32 Channel Analog Input Multiplexor
3	ComputerBoards, Inc	CIO-DAS08	8 Channel Analog/Digital Converter
4	ComputerBoards, Inc	CIO-DAS08-PGL	8 Channel Analog/Digital Converter With Programmable Gains
5	ComputerBoards, Inc	CIO-DAC08-I	8 Channel Digital/Analog Converter
6	ComputerBoards, Inc	CIO-CTR10	10 Channel Counter/Timer
7	ComputerBoards, Inc	SSR-RACK24	24 Channel Solid State Relay Mounting and Interface Rack
8	ComputerBoards, Inc	CIO-MINI37	Universal Screw Terminal
9	ComputerBoards, Inc	CIO-MINI37	Universal Screw Terminal

number CIO-DAS08 PGL) where the digital signals are then stored in the computer hard drive

The 24 solid state relay mounting and interface rack (model number SSR-RACK24) has 24 ComputerBoard solid state relays of three different types mounted on it. These relays consist of four input DC sensing relays (model number SSR-IDC05NP), four input AC sensing relays (model number SSR-IAC05) and 16 output AC switching relays (model number SSR-OAC05) The latter are the same 16 computer controlled relays for the control panel switches shown earlier in Section 3 1 8 (Items 18 to 33 in Figure 3.20 and Table 3 6). A picture of the Solid state relay mounting and interface rack located at the bottom of the control panel can be seen in Figure 3.24.

A digital-to-analog signal converter (model number CIO-DAC08-I) has been employed in the data acquisition system (Item 5 in Figure 3 23). This is used to convert the digital control signals sent by the computer to analog current output signals in the range of 4-20 mA (ComputerBoards 1993, 1994a) in order to control the water mass flow rate of the metering pump, the load of the load compensation unit (LCU) and the load of the electric duct heater of the artificial load generator These analog current output signals pass through a universal screw terminal (Item 9 in Figure 3.23, model number CIO-MINI37) before reaching the device needed to be controlled.

The output signals from the power transducers are of two types The first type are 4-20 mA analog output signals that are calibrated to measure the instantaneous electric power in kilowatts (kW), where these signals are received by the first analog input multiplexor (Item 1 in Figure 3 23) The second type are output pulse signals of 5 Volts to measure the consumed electric energy in Watt hours for specific devices, where these

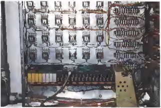

Figure 3.24 Solid state relay mounting and interface rack

pulses are received by a counter/timer board (Item 6 in Figure 3.23). The 5-volt output pulses pass through a universal screw terminal (Item 8 in Figure 3.23, model number CIO-MINI37) before being received by the counter/timer board (model number CIO-CTR10). The counter/timer board counts the number of pulses and then stores them in the computer hard drive.

The counter/timer board (Item 6 in Figure 3.23) is used for frequency and pulse measurements since it has event counting capability, where it can be programmed to perform these measurements (ComputerBoards 1994a, 1994b). The frequency of the output voltage signals from the turbine flow meter is also measured by the counter/timer board and then the measured frequency is stored in the computer hard drive.

All the 4-20 mA analog input signals received by the first analog input multiplexor (Item 1 in Figure 3.23) have been converted to proportional voltage signals in the range of 1-5 Volts. This conversion is done by placing a 250-ohm shunt resistor across every multiplexor terminal that receives a 4-20mA analog signal. A picture of the two analog input multiplexors can be seen in Figure 3.25, while the two universal screw terminals can also be seen in the figure to the right of the two analog input multiplexors.

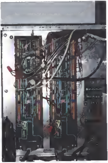

Figure 3.25 Analog input multiplexers

CHAPTER 4
TESTING PROCEDURES AND DATA REDUCTION

The purpose of this chapter is to provide a description of the testing procedures and the data reduction methodologies used to determine the heat loads due to coil hot-gas defrosting. The discussion of the testing procedures will include the initial positions of the system valves before starting up the system, the start up operating sequence to set the psychrometric freezer room to the desired testing conditions, the operating procedures of a complete refrigeration/hot-gas defrost cycle, and the shut down operating sequence.

The data reduction section will explain in detail the methodologies used in calculating the total refrigeration load rate, the average load sensible heat ratio, the defrost heat input, the defrost efficiency and some other important parameters that lead to the determination of the heat loads due to coil hot-gas defrosting. These calculations are performed for the refrigeration and hot-gas defrosting modes of the test fan-coil unit (FCU/T).

4.1. Testing Procedures

The testing procedures employed in this investigation are discussed in detail in Appendix G. These procedures will cover the initial positions of the system valves before starting up the system, the start up operating sequence to set the freezer to the desired testing conditions, the operating procedures of a complete refrigeration/hot-gas defrost cycle, and the shut down operating sequence.

4.2. Data Reduction

All the methodologies used to perform the calculations in this project are explained in detail in this section. These methodologies are employed for analyzing the refrigeration and defrosting modes of the test fan-coil unit (FCU-T). The total refrigeration load rate ($\dot{Q}_{total}$) is calculated considering the fact that there are four types of naturally occurring heat loads that contribute to it, the transmission load (sensible and latent) due to heat transfer through the freezer outer surfaces; internal load (sensible and latent) from the lights, motors, heaters and heating cables that reside inside the freezer; product load and the infiltration load due to the air exchange between the inside and outside of the freezer.

The product and infiltration loads do not apply in this project as there are no products kept inside the freezer and the freezer doors are kept closed during the refrigeratino and defrosting modes of FCU-T. The latent components of the transmission and internal loads are negligible and are not accounted for in the calculations. A fifth load, which is an artificial latent load, is also contributing to the value of the total refrigeration load rate. This artificial latent load is due to the steam injected inside the freezer which is provided by the water vapor generator (WVG) of the artificial load generation system.

The following procedure is used to calculate the total refrigeration load rate:

1. Calculate the sensible transmission heat gain through the front wall ($\dot{Q}_{fw}$) in Btu per hour using the following equation

$$Q_{fw} = U_{fw}\ A_{fw}\left(T_2 - T_1\right) \tag{4.1}$$

where

U_{fw} = Overall coefficient of heat transfer of the front wall (0.075 Btu/(hr-ft^2-°F))

A_{fw} = Outside area of the front wall (71.61 ft^2)

T_2 = Freezer outside air temperature (°F), which is the measurement of thermocouple TC20

T_1 = Freezer inside air temperature next to the front wall (°F), which is the measurement of thermocouple TC15

2- Calculate the sensible transmission heat gain through the other walls ($\dot{Q}_{ow}$) (the rear and side walls) in Btu per hour using the following equation.

$$Q_{ow} = U_{ow}\ A_{ow}\left(T_2 - T_1\right) \tag{4.2}$$

where

U_{ow} = Overall coefficient of heat transfer of the rear and side walls (0.039 Btu/(hr ft^2-°F))

A_{ow} = Outside area of the rear and side walls (271.47 ft^2)

T_1 = Freezer inside air temperature next to the right wall (°F), which is the measurement of thermocouple TC14

3- Calculate the sensible transmission heat gain through the ceiling ($\dot{Q}_{cl}$) in Btu per hour using the following equation

$$\dot{Q}_{cl} = U_{cl}\ A_{cl}\left(T_2 - T_1\right) \tag{4.3}$$

where

U_{cl} = Overall coefficient of heat transfer of the ceiling (0.028 Btu/(hr-ft^2-°F))

A_{cl} = Outside area of the ceiling (129.36 ft^2)

T_1 = Freezer inside air temperature next to the right wall (°F), which is the measurement of thermocouple TC14.

4. Calculate the sensible transmission heat gain through the two doors ($\dot{Q}_{dr}$) in Btu per hour using the following equation

$$\dot{Q}_{dr} = U_{dr}\ A_{dr} \left(T_2 - T_1\right) \tag{4.4}$$

where

U_{dr} = Overall coefficient of heat transfer of the doors (0.070 Btu/(hr-ft^2-°F))

A_{dr} = Outside area of the two doors (30.46 ft^2)

T_1 = Freezer inside air temperature next to the front wall (°F), which is the measurement of thermocouple TC15

5. Calculate the sensible transmission heat gain through the two windows ($\dot{Q}_{wn}$) in Btu per hour using the following equation

$$\dot{Q}_{wn} = U_{wn}\ A_{wn} \left(T_2 - T_1\right) \tag{4.5}$$

where

U_{wn} = Overall coefficient of heat transfer of the windows (0.51 Btu/(hr-ft^2-°F))

A_{wn} = Outside area of the two windows (2.34 ft^2)

T_1 = Freezer inside air temperature next to the front wall (°F) which is the measurement of thermocouple TC15

6- Calculate the total sensible transmission heat gain ($\dot{Q}_{st}$) in Btu per hour using the following equation:

$$\dot{Q}_{st} = \dot{Q}_{fw} + \dot{Q}_{ow} + \dot{Q}_{cl} + \dot{Q}_{dr} + \dot{Q}_{wn} \qquad (4.6)$$

7- Calculate the total sensible internal heat gain ($\dot{Q}_{si}$) in Btu per hour using the following equation.

$$\dot{Q}_{si} = \dot{Q}_{elec} + \dot{Q}_{light} + \dot{Q}_{fan} + \dot{Q}_{hl} + \dot{Q}_{sbo} + \dot{Q}_{ash} + \dot{Q}_{misc} \qquad (4.7)$$

where $\dot{Q}_{elec}$ $\dot{Q}_{light}$ $\dot{Q}_{fan}$, $\dot{Q}_{hl}$, $\dot{Q}_{sbo}$, $\dot{Q}_{ash}$ and $\dot{Q}_{misc}$ are the sensible internal heat gain components contributing to the total sensible internal heat gain as shown in Table 4.1

8- Calculate the total natural sensible heat gain ($\dot{Q}_{sn}$) in Btu per hour using the following equation

$$\dot{Q}_{sn} = \dot{Q}_{si} + \dot{Q}_{st} \qquad (4.8)$$

9- Calculate the average frost temperature ($T_{f\ avg}$) using the procedures outlined in Appendix H.

10- Calculate the total artificial latent heat gain ($\dot{Q}_{latent}$) in Btu per hour using the following equation

$$\dot{Q}_{latent} = \dot{m}_s \left(h_2 - h_1 \right) \qquad (4.9)$$

where

$\dot{m}_s$ = Mass flow rate of the steam injected inside the freezer during the FCU-T refrigeration mode (lbm/hr) This mass flow rate is equal to the adjustable water flow rate of the metering pump (Item 72 in Figure 2.23)

Table 4.1. Components Contributing to the Total Sensible Internal Heat Gain

Item	Component	Symbol	Heat Gain (Btu/h)
1	Two 16-foot heating cables of the freezer doors (3 Watt per foot each). It is assumed that 50% of their heat transfers to the inside of the freezer	Q_{dhc}	163.81
2	Four 60 Watt Fluorescent lamps	Q_{light}	819.05
3	1/4-hp FCU-T fan motor	Q_{fan}	1150 *
4	1/2-hp blower motor of the artifical load generation system	Q_{bl}	1900 *
5	12-foot heating cable of the artificial load generation system (5 Watt per foot)	Q_{dhc}	204.76
6	"clean-up" strip heater of the artificial load generation system (150 Watts)	Q_{ash}	511.91
7	Two FCU-T melt line heating cables (21 Watts each)	$\dot{Q}_{mhc}$	143.33

* (ASHRAE 1994)

h_2 = Enthalpy of steam, saturated vapor at the atmospheric pressure, where it is assumed that any deviation from the atmospheric pressure or any superheating may safely be ignored (Btu/lbm)

h_3 = Enthalpy of ice at the average frost temperature ($T_{f\ avg}$), where it is assumed that the deviation that will occur from the $T_{f\ avg}$ may be safely ignored (Btu/lbm)

11- Calculate the total refrigeration load rate ($\dot{Q}_{total}$) in Btu per hour using the following equation

$$\dot{Q}_{total} = \dot{Q}_{ss} + \dot{Q}_{latent} \tag{4.10}$$

The average load sensible heat ratio (LSHR) is one of the important variables that has been calculated in this project. It is calculated here for every FCU-T refrigeration mode in order to observe its behavior as the refrigeration/defrost cycles progress The following equation is used to calculate the average load sensible heat ratio (LSHR)

$$\mathrm{LSHR} = \frac{\dot{Q}_{ss}}{\dot{Q}_{total}} \tag{4.11}$$

In the field of industrial refrigeration, where the hot-gas is the major method of defrosting, it is known that the defrost heat input from the hot-gas will be utilized in three parts. Part of the defrost heat input will be used to melt the frost while the second part warms the metal of the coil and its contents, where this second part will be transferred to the refrigerant when the unit cooler switches from the hot-gas defrosting mode to the next refrigeration mode. The third part of the defrost heat input will transfer into the freezer space (Cole 1989, ASHRAE 1992b) The second and third parts represent the defrost heat load affecting the refrigeration system.

The concept of a defrost efficiency (η_D) has been used in this project to analyze the hot-gas defrost processes of the FCU-T. The defrost efficiency is defined as the ratio of the total heat required to melt the frost, including the sensible warming of the frost, to that of the total amount of defrost heat input including any refrigeration load effects (Kerschbaumer 1971).

The following procedure is used to calculate the defrost efficiency:

1- Calculate the total amount of defrost heat input (Q_{input}) in Btu using the following equation, where the defrost heat input is calculated in short time intervals and summed up over the entire time period of the FCU-T defrosting mode.

$$Q_{input} = \sum_{i=1}^{end} \left(\dot{m}_{v1} \left(h_2 - h_1 \right) \Delta t \right)_i \tag{4.12}$$

where

$\dot{m}_{v1}$ = Mass flow rate of the hot-gas (lbm/h) flowing through the hot-gas orifice meter (Item 32 in Figure 3.16), and is calculated using the procedure shown in Appendix E

h_2 = Enthalpy of the hot-gas entering the FCU-T drain pan (Btu/h) and is calculated at the pressure measurement of P4 and the temperature measurement of TC4

h_1 = Enthalpy of the defrost refrigerant leaving the FCU-T (Btu/h), and is calculated at the pressure measurement of P3 and the temperature measurement of TC6

Δt = Short time interval in hours over which the calculation is performed.

When calculating the enthalpy of the defrost refrigerant above (h_1), the defrost refrigerant might exist as a liquid-vapor mixture for some period of time during the hot gas defrosting mode. During that time, the quality (x) of the defrost refrigerant is calculated using the following equation

$$x = \frac{\dot{m}_{v2}}{\dot{m}_{v1}} \tag{4.13}$$

where

$\dot{m}_{v1}$ = Mass flow rate of the hot gas (lbm/h) as discussed in Equation (4.12), where it represents here the total mass flow rate of the defrost refrigerant leaving the FCU-T in an assumed steady state flow process

$\dot{m}_{v2}$ = Mass flow rate of the vapor part of the defrost refrigerant (lbm/h) flowing through the defrost orifice meter (Item 33 in Figure 3.16), and is calculated using the procedure shown in Appendix E.

2- Calculate the total heat required to melt the frost from the FCU-T (Q_{melt}) in Btu using the following equation:

$$Q_{melt} = m_{melt} \left(h_2 - h_1 \right) \tag{4.14}$$

where

m_{melt} = Mass of the melt collected (lbm)

h_2 = Enthalpy of liquid water at 36.5°F which is the approximate leaving melt temperature as detected by temperature measurements (Btu/lbm)

h_1 = Enthalpy of ice at the average frost temperature ($T_{f\ avg}$) which is the same $T_{f\ avg}$ value discussed before in Equation (4.9) (Btu/lbm).

3- Calculate the defrost efficiency (η_D) using the following equation

$$\eta_D = \frac{Q_{melt}}{Q_{input}} (100) \tag{4.15}$$

Determining the heat loads associated with coil defrosting is a major objective in this project. It has been mentioned before that the utilized second and third parts of the defrost heat input (the heat transferred with the refrigerant and the heat transferred into the freezer space respectively) represent the defrost heat loads affecting the refrigeration system. The defrost heat load rate ($\dot{Q}_{def}$) in Btu per hour during the FCU-T defrosting mode is calculated using the following equation

$$\dot{Q}_{def} = \frac{\left(Q_{input} - Q_{melt} \right)}{t_d} \tag{4.16}$$

where

t_d = Duration of the FCU-T hot gas defrosting mode (hours).

A new term called "Average Coil Performance Load Rate" is defined here for the purpose of a comparison analysis among the various FCU-T refrigeration/defrost cycles. The Average Coil Performance Load Rate (ACPLR) is defined as the ratio of the sum of the total refrigeration load and the defrost heat load in Btu to the total combined time in hours of the FCU-T refrigeration and defrosting modes. The following procedure is used to calculate the Average Coil Performance Load Rate:

1- Calculate the total refrigeration load (Q_{total}) in Btu using the following equation:

$$Q_{total} = \dot{Q}_{total}\ t_r \tag{4.17}$$

where

t_r = Duration of the FCU-T refrigeration mode (hours)

2 Calculate the defrost heat load (Q_{def}) in Btu using the following equation.

$$Q_{def} = \dot{Q}_{def} \; t_d \tag{4.18}$$

where

t_d = Duration of the FCU-T hot-gas defrosting mode (hours).

3 Calculate the total time duration (t_t) in hours for a complete FCU-T refrigeration and defrosting cycle using the following equation

$$t_t = t_r + t_d \tag{4.19}$$

4- Calculate the Average Coil Performance Load Rate (ACPLR) in Btu per hour using the following equation

$$\text{ACPLR} = \frac{(Q_{total} + Q_{def})}{t_t} \tag{4.20}$$

In many refrigeration systems the theoretical contribution of the fan and defrost heat load to the net refrigeration load exceeds 15% of the net refrigeration load (ASHRAE 1994), where the net refrigeration load equals the total refrigeration load less the fan heat. Considering that idea, the ratio of the fan and defrost heat loads to the net refrigeration load has been utilized here in this project for the comparison analysis among the various FCU-T refrigeration/defrost cycles, and is given the name "Fan-Defrost Contribution" (FDC).

The following procedure is used to calculate the Fan Defrost Contribution:

1- Calculate the fan heat (Q_{fan}) in Btu using the following equation.

$$Q_{fan} = \dot{Q}_{fan} \; t_r \tag{4.21}$$

where

$\dot{Q}_{fan}$ = Fan power (Btu/h)

t_r = Duration of the FCU-T refrigeration mode (hours).

2 Calculate the net refrigeration load (Q_{net}) in Btu using the following equation.

$$Q_{net} = Q_{total} - Q_{fan} \tag{4.22}$$

where

Q_{total} = Total refrigeration load calculated using Equation (4.17) (Btu)

3 Calculate the Fan-Defrost Contribution (FDC) using the following equation.

$$FDC = \frac{\left(Q_{fan} + Q_{def} \right)}{Q_{net}} (100) \tag{4.23}$$

where

Q_{def} = Defrost heat load calculated using Equation (4.18) (Btu).

CHAPTER 5
QUALIFICATIONS TESTS

In order for the designed system to perform the task of operating and collecting reliable data for one complete run of a specific value of coil entering air dry bulb temperature (EAT) in the range of 0°F to -20°F, several tests were performed to qualify the system for that purpose. One of these qualification tests was performed for a coil entering air dry bulb temperature (EAT) of 0°F, while limiting the run to a single FCU-T refrigeration/defrost cycle (one R/D cycle). This qualification test (EAT = 0°F) happens to be the one that had the approval from the ASHRAE personnel to proceed in performing the experimental program of this project.

The purpose of this chapter is to provide a time-dependent history of the variations of some key variables for the above mentioned qualification test of coil entering air dry bulb temperature (EAT) of 0°F. The refrigeration/defrost system is operated in this run such that a single FCU-T refrigeration/defrost cycle is performed. The frequencies and durations of the different modes in this run are shown in Table 5.1. The system is started by operating the FCU-A in its initial refrigeration mode until the testing conditions of the freezer are reached at which point the FCU-T refrigeration mode is activated while keeping the FCU-T entering air dry bulb temperature (EAT) constant at 0°F. The FCU-A electric defrosting mode is also activated right after the termination of the FCU-A initial refrigeration mode in order to remove, collect and weigh the FCU-A melt. This latter

Table 5.1 Frequency and Duration of the Different
Modes for the Run of (EAT = 0°F)

Mode	Starting Time	Terminating Time	Duration	
	(Seconds)	(Seconds)	(Seconds)	(Hours)
FCU-A Initial Refrigeration	00000	14585	14585	4.05
FCU-A Initial Electric Defrosting	14585	23835	9250	2.57
FCU-T Refrigeration	14585	35590	21005	5.83
FCU-T Hot-Gas Defrosting	35590	36815	1225	0.34
FCU-A Final Refrigeration	35590	38510	2920	0.81
FCU-A Final Electric Defrosting	38510	41570	3060	0.85

quantity represents the moisture removed from the freezer during the initial room conditioning period and which is deposited as frost on the FCU-A coil.

In this run, the demand defrost system was set to a frost thickness (S_f) of 0.117", where the FCU-T refrigeration mode was terminated when the frost accumulated on its coil reached that thickness. At that instance, the FCU-T hot-gas defrosting mode is activated in order to remove, collect and weigh the FCU-T melt.

Due to the FCU-T hot-gas defrost heat input, some of the FCU-T frost will escape as moisture in the freezer space. The FCU-A final refrigeration mode is activated at the same instant the FCU-T hot-gas defrosting mode is activated in order for the FCU-A to capture that moisture. The FCU-A will continue to operate in its final refrigeration mode in order to bring the freezer back to its initial testing conditions, at which point the FCU-A final electric defrosting mode is activated in order to remove, collect and weigh the FCU-A melt. The FCU-A melt collected this time represents the moisture-escape from the FCU-T due to the latter's hot-gas defrost heat input. The amount of melt of both FCU-A and FCU-T is shown in Table 5.2.

The behavior of some of the measured variables (refrigerant temperatures and pressures and air temperatures) versus time for this run, have been plotted for different operating modes. The FCU-A inlet and outlet refrigerant temperatures versus time in the initial and final FCU-A refrigeration modes are shown in Figures 5.1 and 5.2, respectively. In Figure 5.1, the refrigerant temperatures are shown to drop sharply from an initial refrigerant temperature of about 80°F to below than 10°F in about 2500 seconds, while then the same temperatures continued to drop at a much slower pace

Table 5.2. Mass of Melt Collected From Both Fan-Coil Units for the Run of (EAT = 0°F)

Mode	FCU-A Melt	FCU-T Melt
	(lbm)	(lbm)
FCU-A Initial Electric Defrosting	14.88	--
FCU-T Hot Gas Defrosting	--	3.92
FCU-A Final Electric Defrosting	4.37	--

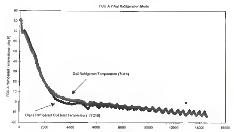

Figure 5 1 FCU A inlet and outlet refrigerant temperatures versus time during FCU A initial refrigeration mode for the run of (EAT = 0°F)

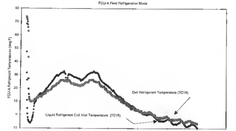

Figure 5.2. FCU-A inlet and outlet refrigerant temperatures versus time during FCU-A final refrigeration mode for the run of (EAT = 0°F)

A sudden drop in the FCU-A inlet and outlet refrigerant temperatures at the instant of starting the FCU-A final refrigeration mode can be seen in Figure 5.2, where the FCU-A refrigerant temperature was at a high value due to the FCU-A electric defrosting mode. After the sudden drop of the FCU-A inlet and outlet refrigerant temperatures, it is expected to see (Figure 5.2) the two temperatures rise for a short period of time and then drop gradually. This expected FCU-A refrigerant temperature rise is due to the fact that the FCU-T operation (in parallel with the FCU-A final refrigeration mode) is under the hot-gas defrosting mode which affects the FCU-A refrigerant temperatures. However, the two temperatures, as can be seen in Figure 5.2, continue to rise for a long period of time and the outlet refrigerant temperature is seen to be higher than the inlet refrigerant temperature. This unexpected behavior is due to the fact that the FCU-A dampers jammed for a few minutes and could not open, which in turn prevented the start of the FCU-A blower. This problem was solved at about 37500 seconds, where the FCU-A refrigerant temperatures are observed to drop gradually.

The air dry bulb temperatures across the freezer walls during the FCU-A initial and final refrigeration modes can be seen in Figures 5.3 and 5.4, respectively. As shown in Figure 5.4, the air temperatures inside the freezer rose until the time approached the 36800 second mark, at which point the inside air temperatures started to drop. This rise in the air temperatures is due to the FCU-T defrost heat input during the hot-gas defrosting mode.

For the FCU-T refrigeration mode the FCU-T inlet and outlet refrigerant temperatures, the air dry bulb temperatures across the freezer walls, the air dry-bulb temperatures across FCU-T and the temperature difference (TD) across FCU-T are all

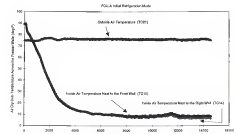

Figure 5.3 Air dry bulb temperatures across the freezer walls versus time during FCU-A initial refrigeration mode for the run of (EAT = 0°F)

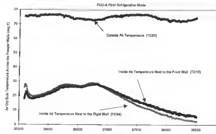

Figure 5.4. Air dry bulb temperatures across the freezer walls versus time during FCU-A final refrigeration mode for the run of (EAT = 0°F)

shown versus time in Figures 5.5, 5.6, 5.7 and 5.8, respectively. Here TD is the difference between the FCU-T coil entering air dry bulb temperature (EAT) and the coil refrigerant temperature (CRT) leaving the coil (Smith 1989).

Temperatures of the refrigerant entering and leaving the FCU-T pan, and also of the refrigerant entering and leaving the FCU-T coil versus time are shown in Figure 5.9 for the FCU-T hot-gas defrosting mode. In this figure, the hot-gas discharged from the compressor enters the FCU-T pan at a high temperature (TC4) in the range of 100 to 120°F, where it then decreases in its value as it leaves the FCU-T pan (TC5), since some of the refrigerant heat is lost to melt the frost accumulated in the FCU-T pan. The hot gas leaving the latter then enters the FCU-T coil at a lower value (TC3) due to the loss of heat when the hot gas mixes with the liquid refrigerant at and inside the FCU-T coil. The defrost refrigerant leaves the FCU-T coil at a lower value (TC6) due to the mixing with the liquid refrigerant inside the FCU-T and also due to the refrigerant heat lost to melt the frost accumulated on the FCU-T coil.

Some of the refrigerant pressures versus time are shown in Figure 5.10 for the entire time period of the run. It is interesting to observe the jump in the refrigerant pressures around the time of 35560 seconds. This is the time when the FCU-T hot-gas defrosting mode was in operation where the high jump in the hot-gas pressure upstream of the hot-gas orifice meter (P4 in Figure 5.10) identifies that mode. Another jump in the refrigerant pressures is observed around the time of 14585 seconds which is attributed to switching from FCU-A to FCU-T refrigeration modes.

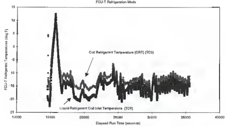

Figure 5.5 FCU-T inlet and outlet refrigerant temperatures versus time during FCU-T refrigeration mode for the run of (EAT = 0°F)

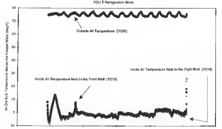

Figure 5 6. Air dry bulb temperatures across the freezer walls versus time during FCU-T refrigeration mode for the run of (EAT = 0°F)

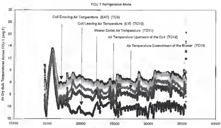

Figure 5.7 Air dry bulb temperatures across FCU T versus time during FCU-T refrigeration mode for the run of (EAT = 0°F)

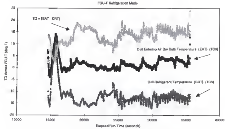

Figure 5 8 TD across FCU-T versus time during FCU T refrigeration mode for the run of (EAT = 0°F)

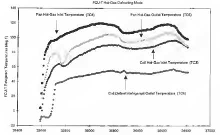

Figure 5.9 FCU-T inlet and outlet refrigerant temperatures versus time during FCU-T hot-gas defrosting mode for the run of (EAT = 0°F)

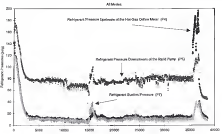

Figure 5.10 Refrigerant pressures versus time for the run of (EAT = 0°F)

As part of the visualization study in this project, a picture of the FCU-T coil right after the termination of the hot-gas defrosting mode is shown in Figure 5 11 while a closer view of the same coil is shown in Figure 5 12.

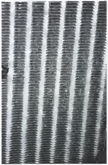

Figure 5.11 FCU-T coil after the hot-gas defrosting mode has been completed for the run of (EAT = 0°F)

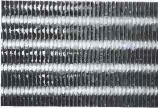

Figure 5.12. A close-up of the FCU-T coil after the hot-gas defrosting mode has been completed for the run of (EAT = 0°F)

CHAPTER 6
REFRIGERATION/DEFROST CYCLE DYNAMICS

The purpose of this chapter is to provide a time-dependent history of the variations of some key variables during the complete refrigeration/defrost (R/D) cycle. The dynamics of the refrigeration/defrost cycle has been examined for two test fan-coil unit (FCU-T) entering air dry bulb temperatures (EAT) of -8 and -13°F. In order to simulate the actual performance of freezer coils during the R/D cycle, three complete consecutive cycles (three R/D cycles) are considered at the above two FCU-T entering air dry bulb temperatures. The intent is to provide an insight into how a refrigeration system behaves during the complete refrigeration/defrost cycle using the hot gas refrigerant defrost method.

6.1. Case of Entering Air Temperature of -8°F

The refrigeration/defrost system is operated in this run such that three FCU-T refrigeration/defrost cycles are performed. The frequencies and durations of the different modes in this run are shown in Table 6.1. The system is started by operating the FCU-A in its initial refrigeration mode until the testing conditions of the freezer are reached, at which point the FCU-T refrigeration mode No. 1 is activated while keeping the FCU-T entering air dry bulb temperature (EAT) constant at -8°F. The FCU-A electric defrosting mode No. 1 is also activated right after the termination of the FCU-A initial refrigeration

Table 6.1 Frequency and Duration of the Different Modes for the Run of (EAT = -8°F)

Mode	Starting Time	Terminating Time	Duration	
	(Seconds)	(Seconds)	(Seconds)	(Hours)
FCU A Initial Refrigeration	0000	6705	6705	1 86
FCU A Initial Electric Defrosting	6705	9705	3000	0 83
FCU T Refrigeration No. 1	6705	10385	3680	1 02
FCU T Hot-Gas Defrosting No 1	10385	10860	475	0 13
FCU A Refrigeration No 1	10385	14745	4360	1.21
FCU A Electric Defrosting No 1	14745	17235	2490	0 69
FCU T Refrigeration No. 2	14745	17325	2580	0 72
FCU T Hot-Gas Defrosting No. 2	17325	17765	440	0 12
FCU A Refrigeration No 2	17325	21005	3680	1 02
FCU A Electric Defrosting No. 2	21005	23285	2280	0.63
FCU T Refrigeration No. 3	21005	23510	2505	0 70
FCU-T Hot-Gas Defrosting No. 3	23510	23860	350	0 10
FCU A Refrigeration No 3	23510	25760	2250	0.63
FCU-A Electric Defrosting No. 3	25760	29000	3240	0 90

mode in order to remove, collect and weigh the FCU-A melt. This latter quantity represents the moisture removed from the freezer during the initial room conditioning period and which is deposited as frost on the FCU-A coil.

In this run, the demand defrost system was set to a frost thickness (S_f) of 0.079", where the FCU-T refrigeration mode No. 1 was terminated when the frost accumulated on its coil reached that thickness. At that instance, the FCU-T hot-gas defrosting mode No. 1 is activated in order to remove, collect and weigh the FCU-T melt. The mass of this FCU-T melt (m_{melt}) is used in calculating the total heat required to melt the FCU-T frost during the FCU-T hot gas defrosting mode No. 1 as described in Chapter 4.

Due to the FCU-T hot-gas defrost heat input, some of the FCU-T frost will escape as moisture in the freezer space. The FCU-A refrigeration mode No. 1 is activated at the same instant the FCU-T hot-gas defrosting mode No. 1 is activated in order for the FCU-A to capture that moisture. The FCU-A will continue to operate in its refrigeration mode No. 1 in order to bring the freezer back to its initial testing conditions, at which point the FCU-A electric defrosting mode No. 1 is activated in order to remove, collect and weigh the FCU-A melt. The FCU-A melt collected this time represents the moisture-escape from the FCU-T during the FCU-T hot-gas defrosting mode No. 1 due to the FCU-T hot gas defrost heat input.

As can be seen in Table 6.1, the FCU-T refrigeration mode No. 2 is activated at the same instant the FCU-A electric defrosting mode No. 1 is activated in order for the refrigeration/defrost system to continue activating two more complete refrigeration/defrost cycles. In the other two cycles, the demand defrost system setting was kept unchanged at a frost thickness (S_f) of 0.079"

The amount of melt of both FCU-A and FCU-T for all the three cycles is shown in Table 6.2. The amount of both FCU-A and FCU-T melts collected in the second and third complete cycles can be seen to continuously decrease. While the absolute amount decreased for both quantities, the relative amount of the FCU-A melt continued to be far more significant than the FCU-T melt collected.

The behavior of some of the measured variables (refrigerant temperatures and pressures and air temperatures) versus time for this run, have been plotted for different operating modes. The FCU-A inlet and outlet refrigerant temperatures versus time in the initial and the other three FCU-A refrigeration modes are shown in Figures 6.1 through 6.4. In Figure 6.1, the refrigerant temperatures during the initial FCU-A refrigeration mode are shown to drop sharply from an initial refrigerant temperature of about 65°F to 10°F in about 1500 seconds, while then the same temperatures continued to drop at a much slower pace.

A sudden drop in the FCU-A inlet and outlet refrigerant temperatures at the instant of starting the three FCU-A refrigeration modes can be seen in Figures 6.2 through 6.4, where the FCU-A refrigerant temperature was at a high value due to the FCU-A electric defrosting modes. After the sudden drop of the FCU-A inlet and outlet refrigerant temperatures, the two temperatures are shown to rise for a short period of time and then drop gradually in all of the three figures. This behavior is due to the fact that the FCU-T operation (in parallel with FCU-A refrigeration modes) is under the hot-gas defrosting mode which affects the FCU-A refrigerant temperatures.

The air dry bulb temperatures across the freezer walls during the initial and the other three FCU-A refrigeration modes can be seen in Figures 6.5 through 6.8,

Table 6.2 Mass of Melt Collected From Both Fan-Coil Units for the Run of (EAT = -8°F)

Mode	FCU-A Melt	FCU-T * Melt
	(lbm)	(lbm)
FCU-A Initial Electric Defrosting	5.14	--
FCU-T Hot Gas Defrosting No. 1	--	0.20
FCU-A Electric Defrosting No. 1	3.38	--
FCU-T Hot-Gas Defrosting No. 2	--	0.15
FCU-A Electric Defrosting No. 2	3.00	--
FCU-T Hot-Gas Defrosting No. 3	--	0.07
FCU-A Electric Defrosting No. 3	2.42	--

* The mass of FCU-T melt is used for the value of (m_{melt}) in Equation (4.14)

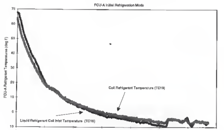

Figure 6.1 FCU A inlet and outlet refrigerant temperatures versus time during FCU-A initial refrigeration mode for the run of (EAT = -8°F)

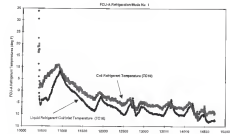

Figure 6.2. FCU-A inlet and outlet refrigerant temperatures versus time during FCU-A refrigeration mode No 1 for the run of (EAT = -8°F)

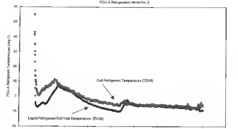

Figure 6 3 FCU-A inlet and outlet refrigerant temperatures versus time during FCU-A refrigeration mode No 2 for the run of (EAT = 8°F)

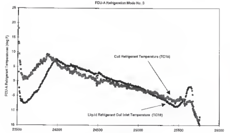

Figure 6.4. FCU-A inlet and outlet refrigerant temperatures versus time during FCU-A refrigeration mode No. 3 (for the run of (EAT = -8°F)

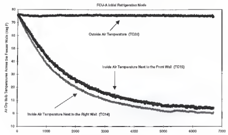

Figure 6.5 Air dry bulb temperatures across the freezer walls versus time during FCU A initial refrigeration mode for the run of (EAT = 8°F)

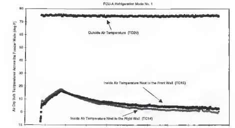

Figure 5.6 Air dry bulb temperatures across the freezer walls versus time during FCU-A refrigeration mode No. 1 for the run of (EAT = -8°F)

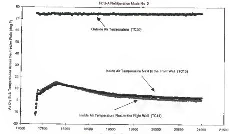

Figure 6.7 Air dry bulb temperatures across the freezer walls versus time during FCU-A refrigeration mode No. 2 for the run of (EAT = -8°F)

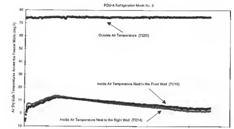

Figure 6.8 Air dry bulb temperatures across the freezer walls versus time during FCU-A refrigeration mode No. 3 for the run of (EAT = 8°F)

respectively. In all the FCU-A refrigeration modes other than the initial mode, as shown in Figures 6.6 through 6.8 the air temperatures inside the freezer rise for a short period of time and then drop. This rise in the air temperatures is due to the FCU-T defrost heat input during the hot-gas defrosting modes.

For all the FCU-T refrigeration modes, the FCU-T inlet and outlet refrigerant temperatures versus time are shown in Figures 6.9 through 6.11. The air dry bulb temperatures across the freezer walls versus time are shown in Figures 6.12 through 6.14, while the air dry bulb temperatures across FCU-T versus time are shown in Figures 6.15 through 6.17. The TD across FCU-T versus time is shown in Figures 6.18 through 6.20.

Temperatures of the refrigerant entering and leaving the FCU-T pan, and also of the refrigerant entering and leaving the FCU-T coil versus time, are shown in Figures 6.21 through 6.23 for the three FCU-T hot-gas defrosting modes. In these figures, the hot-gas discharged from the compressor enters the FCU-T pan at a high temperature (TC4) of about 160°F where it then decreases in its value as it leaves the FCU-T pan (TC5), since some of the refrigerant heat is lost to melt the frost accumulated in the FCU-T pan. The hot-gas leaving the latter then enters the FCU-T coil at a lower value (TC3) due to the loss of heat when the hot gas mixes with the liquid refrigerant at and inside the FCU-T coil. The defrost refrigerant leaves the FCU-T coil at a lower value (TC6) due to the mixing with the liquid refrigerant inside the FCU-T and also due to the refrigerant heat lost to melt the frost accumulated on the FCU-T coil.

Some of the refrigerant pressures versus time are shown in Figure 6.24 for the entire time period of this run. It is interesting to observe the jumps in the refrigerant pressures around the times of 10385, 17325 and 23510 seconds. These are the times

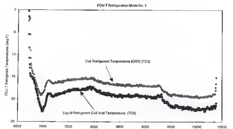

Figure 6.9 FCU-T inlet and outlet refrigerant temperatures versus time during FCU-T refrigeration mode No. 1 for the run of (EAT = -8°F)

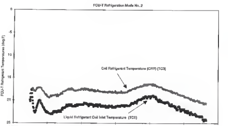

Figure 6.10 FCU-T inlet and outlet refrigerant temperatures versus time during FCU-T refrigeration mode No. 2 for the run of (EAT = 8°F)

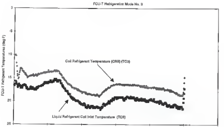

Figure 6.11 FCU-T inlet and outlet refrigerant temperatures versus time during FCU-T refrigeration mode No. 3 for the run of (EAT = -8°F)

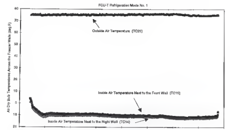

Figure 6.12 Air dry bulb temperatures across the freezer walls versus time during FCU-T refrigeration mode No. 1 for the run of (EAT = 8°F)

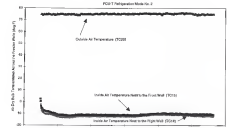

Figure 6.13 Air dry bulb temperatures across the freezer walls versus time during FCU-T refrigeration mode No. 2 for the run of (EAT = -8°F)

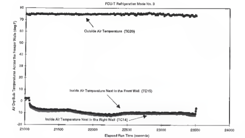

Figure 6.14. Air dry bulb temperatures across the freezer walls versus time during FCU-T refrigeration mode No. 3 for the run of (EAT = -8°F)

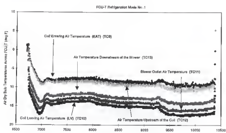

Figure 6.15 Air dry bulb temperatures across FCU-T versus time during FCU-T refrigeration mode No. 1 for the run of (EAT = -8°F)

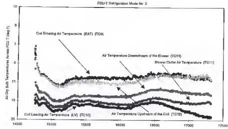

Figure 6.16. Air dry bulb temperatures across FCU-T versus time during FCU-T refrigeration mode No. 2 for the run of (EAT = -8°F)

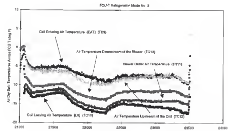

Figure 6 17 Air dry bulb temperatures across FCU-T versus time during FCU-T refrigeration mode No 3 for the run of (EAT = -8°F)

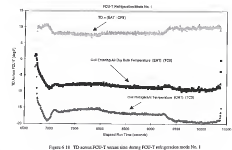

Figure 6 18 TD across FCU-T versus time during FCU-T refrigeration mode No. 1 for the run of (EAT = -8°F)

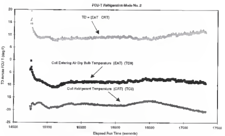

Figure 6.19 TD across FCU-T versus time during FCU-T refrigeration mode No 2 for the run of (EAT = -8°F)

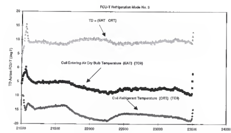

Figure 6.20 TD across FCU-T versus time during FCU-T refrigeration mode No. 3 for the run of (EAT = -8°F)

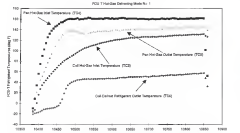

Figure 6.21 FCU-T inlet and outlet refrigerant temperatures versus time during FCU-T hot gas defrosting mode No 1 for the run of (EAT = -8°F)

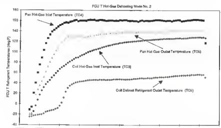

Figure 6.22. FCU T inlet and outlet refrigerant temperatures versus time during FCU T hot gas defrosting mode No. 2 for the run of (EAT = -8°F)

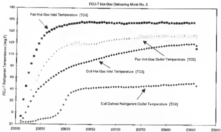

Figure 6 23. FCU-T inlet and outlet refrigerant temperatures versus time during FCU-T hot-gas defrosting mode No 3 for the run of (EAT = -8°F)

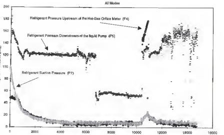

Figure 6.24 Refrigerant pressures versus time for the run of (EAT = -8°F)

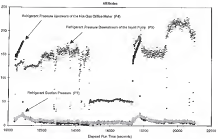

Figure 6.24 -- continued

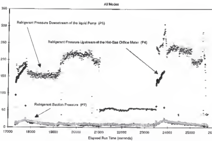

Figure 6.24 -- continued

when the FCU-T hot-gas defrosting modes were in operation, where the high jumps in the hot-gas pressure upstream of the hot-gas orifice meter (P4 in Figure 6.24) identify these modes. Figure 6.24 also shows the pressure of the liquid refrigerant downstream of the liquid pump. While the liquid pressure downstream of the pump (P5 in Figure 6.24) was continuously monitored during all runs, its value did not affect any calculations performed in this investigation. Recording this pressure was performed for the sole purpose of monitoring the operation of the system. The drops in the liquid refrigerant pressure downstream of the liquid pump observed in Figure 6.24 around the times of 6705, 14745 and 21005 seconds are attributed to switching from FCU-A to FCU-T refrigeration modes.

6.2. Case of Entering Air Temperature of -13°F

The refrigeration/defrost system is operated in this run in the same manner as the previous run, where three FCU-T refrigeration/defrost cycles are performed. In this run, the FCU-T entering air dry bulb temperature (EAT) is kept constant at -13°F while the demand defrost system was set to a frost thickness (S_f) of 0.079" during all the FCU-T refrigeration modes. The frequencies and durations of the different modes in this run are shown in Table 6.3.

The amount of melt of both FCU-A and FCU-T for all the three cycles is shown in Table 6.4. The amount of both FCU-A and FCU-T melts collected in the second and third complete refrigeration/defrost cycles can be seen to continuously decrease. While the absolute amount decreased for both quantities, the relative amount of the FCU-A melt continued to be far more significant than the FCU-T melt collected.

Table 6.3 Frequency and Duration of the Different
Modes for the Run of (EAT = -13°F)

Mode	Starting Time	Terminating Time	Duration	
	(Seconds)	(Seconds)	(Seconds)	(Hours)
FCU A Initial Refrigeration	00000	15855	15855	4.40
FCU A Initial Electric Defrosting	15855	21330	5475	1.52
FCU T Refrigeration No 1	15855	34475	18620	5.17
FCU T Hot-Gas Defrosting No. 1	34475	34950	475	0.13
FCU A Refrigeration No 1	34475	40770	6295	1.75
FCU A Electric Defrosting No 1	40770	46350	5580	1.55
FCU T Refrigeration No 2	40770	51870	11100	3.08
FCU T Hot-Gas Defrosting No. 2	51870	52360	490	0.14
FCU A Refrigeration No 2	51870	57410	5540	1.54
FCU A Electric Defrosting No. 2	57410	60170	2760	0.77
FCU T Refrigeration No 3	57410	61585	4175	1.16
FCU T Hot Gas Defrosting No. 3	61585	61985	400	0.11
FCU-A Refrigeration No 3	61585	66295	4710	1.31
FCU-A Electric Defrosting No 3	66295	70555	4260	1.18

Table 6.4 Mass of Melt Collected From Both Fan-Coil Units for the Run of (EAT = -13°F)

Mode	FCU-A Melt (lbm)	FCU-T * Melt (lbm)
FCU-A Initial Electric Defrosting	9.34	--
FCU-T Hot-Gas Defrosting No. 1	--	0.21
FCU-A Electric Defrosting No. 1	6.30	--
FCU-T Hot-Gas Defrosting No. 2	--	0.02
FCU-A Electric Defrosting No. 2	5.20	--
FCU-T Hot-Gas Defrosting No. 3	--	0.01
FCU-A Electric Defrosting No. 3	4.99	--

* The mass of FCU-T melt is used for the value of (m_{melt}) in Equation (4.14)

The behavior of some of the measured variables (refrigerant temperatures and pressures and air temperatures) versus time for this run, have been illustrated for different operating modes The FCU-A inlet and outlet refrigerant temperatures versus time in the initial and the other three FCU-A refrigeration modes are shown in Figures 6.25 through 6.28. In Figure 6.25, the refrigerant temperatures during the initial FCU-A refrigeration mode are shown to behave in the same manner shown in Figure 6.1 for the initial FCU-A refrigeration mode of the previous run where the refrigerant temperatures drop sharply for a short period of time and then drop gradually later on In the same figure (Figure 6.25), the refrigerant temperatures are seen to fluctuate abnormally between 7500 and 11500 seconds where the system has tripped three times in that period of time and was allowed to resume its operation a few seconds after each trip

A sudden drop in the FCU-A inlet and outlet refrigerant temperatures at the instant of starting the three FCU-A refrigeration modes can be seen in Figures 6.26 through 6.28, where the FCU-A refrigerant temperature was at a high value due to the FCU-A electric defrosting modes After the sudden drop of the FCU-A inlet and outlet refrigerant temperatures, the two temperatures are shown to rise for a short period of time and then drop gradually in all three figures This behavior is due to the fact that the FCU-T operation (in parallel with FCU-A refrigeration modes) is under the hot-gas defrosting mode which affects the FCU-A refrigerant temperatures.

The air dry bulb temperatures across the freezer walls during the initial and the other three FCU-A refrigeration modes can be seen in Figures 6.29 through 6.32, respectively The effect of the system's three trips on the air temperatures across the freezer walls during the initial FCU-A refrigeration mode can be seen in Figure 6.29 In

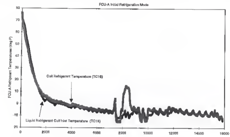

Figure 6.25. FCU-A inlet and outlet refrigerant temperatures versus time during FCU-A initial refrigeration mode for the run of (EAT = 13°F)

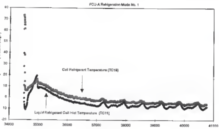

Figure 6 26 FCU A inlet and outlet refrigerant temperatures versus time during FCU A refrigeration mode No 1 for the run of (EAT = -13°F)

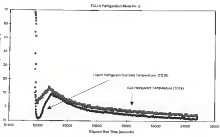

Figure 6.27 FCU A inlet and outlet refrigerant temperatures versus time during FCU-A refrigeration mode No 2 for the run of (EAT = -13°F)

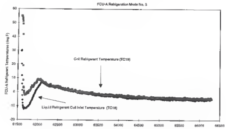

Figure 6.28 FCU-A inlet and outlet refrigerant temperatures versus time during FCU-A refrigeration mode No. 3 for the run of (EAT = -13°F)

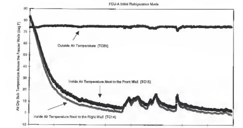

Figure 6.29 Air dry bulb temperatures across the freezer walls versus time during FCU-A initial refrigeration mode for the run of (EAT = -13°F)

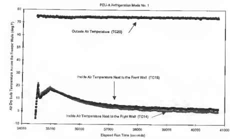

Figure 6.30. Air dry bulb temperatures across the freezer walls versus time during FCU-A refrigeration mode No. 1 for the run of (EAT = -13°F)

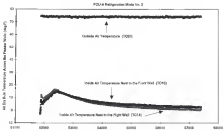

Figure 6.31 Air dry bulb temperatures across the freezer walls versus time during FCU-A refrigeration mode No. 2 for the run of (EAT = -13°F)

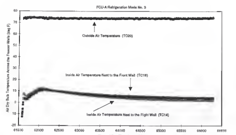

Figure 6 32 Air dry bulb temperatures across the freezer walls versus time during FCU-A refrigeration mode No 3 for the run of (EAT = -13°F) all the FCU-A refrigeration modes other than the initial mode, as shown in Figures 6.30 through 6.32, the air temperatures inside the freezer rose for a short period of time and then dropped. This rise in air temperatures is due to the FCU-T defrost heat input during the hot-gas defrosting modes.

For all the FCU-T refrigeration modes, the FCU-T inlet and outlet refrigerant temperatures versus time are shown in Figures 6.33 through 6.35. The air dry bulb temperatures across the freezer walls versus time are shown in Figures 6.36 through 6.38 while the air dry bulb temperatures across FCU-T versus time are shown in Figures 6.39 through 6.41. The TD across FCU-T versus time is shown in Figures 6.42 through 6.44.

The temperatures of the refrigerant entering and leaving the FCU-T pan, and also of the refrigerant entering and leaving the FCU-T coil versus time, are shown in Figures 6.45 through 6.47 for the three FCU-T hot-gas defrosting modes. In these three figures, the hot gas discharged from the compressor enters the FCU-T pan at a high temperature (TC4) of about 140°F, where it then decreases in its value as it leaves the FCU-T pan (TC5), since some of the refrigerant heat is lost to melt the frost accumulated in the FCU-T pan. The hot-gas leaving the FCU-T pan then enters the FCU-T coil at a lower value (TC3) due to the loss of heat when the hot-gas mixes with the liquid refrigerant at and inside the FCU-T coil. The defrost refrigerant leaves the FCU-T coil at a lower value (TC6) due to the mixing with the liquid refrigerant inside the FCU-T and also due to the refrigerant heat lost to melt the frost accumulated on the FCU-T coil.

Some of the refrigerant pressures versus time are shown in Figure 6.48 for the entire time period of this run. Again one can observe the jumps in the refrigerant pressures around the times of 34475, 51870 and 61585 seconds. These are the times

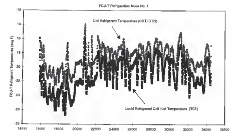

Figure 6.33 FCU-T inlet and outlet refrigerant temperatures versus time during FCU-T refrigeration mode No. 1 for the run of (EAT = -13°F)

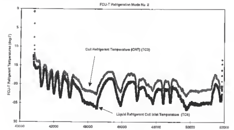

Figure 6.34. FCU-T inlet and outlet refrigerant temperatures versus time during FCU-T refrigeration mode No 2 for the run of (EAT = 13°F)

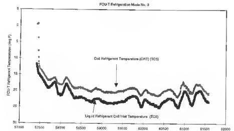

Figure 6.35 FCU-T inlet and outlet refrigerant temperatures versus time during FCU-T refrigeration mode No 3 for the run of (EAT = -13°F)

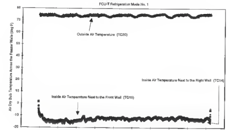

Figure 6.36 Air dry bulb temperatures across the freezer walls versus time during FCU-T refrigeration mode No. 1 for the run of (EAT = -13°F)

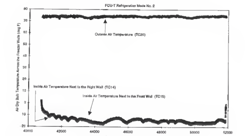

Figure 6.37 Air dry bulb temperatures across the freezer walls versus time during FCU-T refrigeration mode No. 2 for the run of (EAT = -13°F)

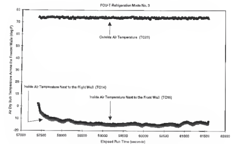

Figure 6.38. Air dry bulb temperatures across the freezer walls versus time during FCU-T refrigeration mode No. 3 for the run of (EAT = -13°F)

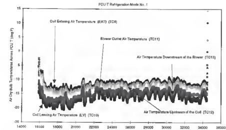

Figure 6.39 Air dry bulb temperatures across FCU-T versus time during FCU-T refrigeration mode No. 1 for the run of (EAT = -13°F)

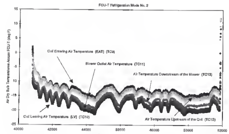

Figure 6.40 Air dry bulb temperatures across FCU-T versus time during FCU-T refrigeration mode No. 2 for the run of (EAT = 13°F)

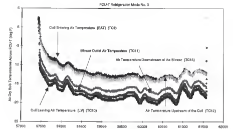

Figure 6.41 Air dry bulb temperatures across FCU-T versus time during FCU-T refrigeration mode No. 3 for the run of (EAT = -13°F)

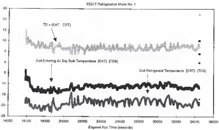

Figure 6.42. TD across FCU-T versus time during FCU-T refrigeration mode No. 1 for the run of (EAT = -13°F)

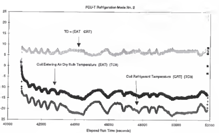

Figure 6.43. TD across FCU-T versus time during FCU-T refrigeration mode No. 2
for the run of (EAT = -13°F)

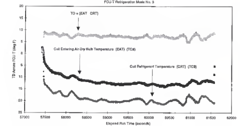

Figure 6 44 TD across FCU-T versus time during FCU-T refrigeration mode No 3 for the run of (EAT = -13°F)

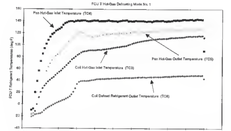

Figure 6.45 FCU-T inlet and outlet refrigerant temperatures versus time during FCU-T hot gas defrosting mode No. 1 for the run of (EAT = -13°F)

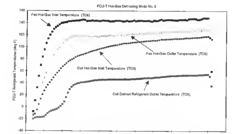

Figure 6.46 FCU-T inlet and outlet refrigerant temperatures versus time during FCU-T hot-gas defrosting mode No. 2 for the run of (EAT = -13°F)

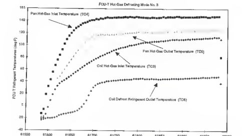

Figure 6.47 FCU-T inlet and outlet refrigerant temperatures versus time during FCU-T hot gas defrosting mode No. 3 for the run of (EAT = -13°F)

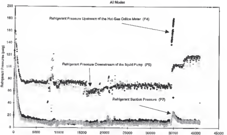

Figure 6.48 Refrigerant pressures versus time for the run of (EAT = -13°F)

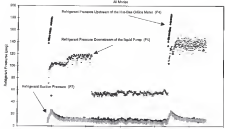

Figure 6.48 -- continued

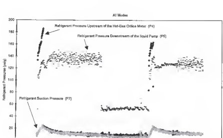

Figure 6 48 -- continued

when the FCU-T hot gas defrosting modes were in operation, where the high jumps in the hot-gas pressure upstream of the hot gas orifice meter (P4 in Figure 6.48) identify these modes. Figure 6.48 also shows the pressure of the liquid refrigerant downstream of the liquid pump (P5), where the drops in its value around the times of 15855, 40770 and 57410 seconds are attributed to switching from FCU-A to FCU-T refrigeration modes.

CHAPTER 7
ANALYSIS OF LOADS

This chapter provides load analysis for cases having FCU-T entering air dry bulb temperatures (EAT) of -8 and -13°F. These are the same two cases discussed in the previous chapter. All the methodologies used to perform load calculations were described in Chapter 4. The load analysis covers the total refrigeration load rats, average load sensible heat ratio, defrost heat input, defrost efficiency, and other relevant parameters that lead to the determination of the heat loads due to coil hot-gas defrosting. The intent is to provide some insight into the energy penalty associated with defrosting finned-tube freezer coils using the hot-gas refrigerant method.

7.1. Case of Entering Air Temperature of -8°F

Using the procedures described in Appendix H, the average frost temperature ($T_{f\ avg}$) for this case was calculated to be (-18.56°F). The variation of the total sensible transmission heat gain and its components with time during the three FCU-T refrigeration modes is shown in Figures 7.1 through 7.3. As can be seen, the highest sensible transmission heat gain component is through the three walls of the freezer other than the front wall while the smallest component is through the freezer windows. The variation of the total natural sensible heat gain and its components with time during the three FCU-T refrigeration modes is shown in Figures 7.4 through 7.6, while the calculated average

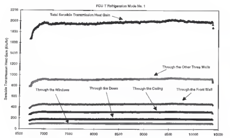

Figure 7 1 Total sensible transmission heat gain and components versus time during FCU T refrigeration mode No 1 for the run of (EAT = -8°F)

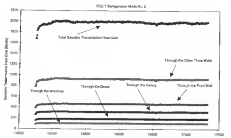

Figure 7.2. Total sensible transmission heat gain and components versus time during FCU T refrigeration mode No. 2 for the run of (EAT = 8°F)

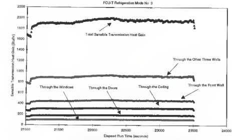

Figure 7 3 Total sensible transmission heat gain and components versus time during FCU T refrigeration mode No. 3 for the run of (EAT = 8°F)

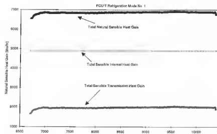

Figure 7.4 Total natural sensible heat gain and components versus time during FCU/T refrigeration mode No. 1 for the run of (EAT = -8°F)

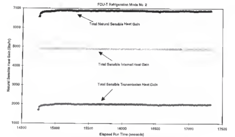

Figure 7.5 Total natural sensible heat gain and components versus time during FCU-T refrigeration mode No. 2 for the run of (EAT = -8°F)

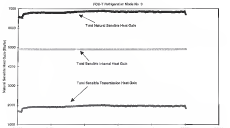

Figure 7 6 Total natural sensible heat gain and components versus time during FCU-T refrigeration mode No 3 for the run of (EAT = 8°F) values of the loads over their FCU-T refrigeration modes are shown in Table 7 1 along with the total artificial latent heat gain, the total refrigeration load rate and the average load sensible heat ratio (LSHR)

The total sensible transmission and the total natural sensible heat gains are shown to be almost constant in Table 7 1 for the three FCU-T refrigeration modes. The total artificial latent heat gain for the FCU-T refrigeration mode No 2 is shown in Table 7 1 to be about twice that of the FCU-T refrigeration mode No 1, and the same as that of the FCU-T refrigeration mode No 3. This is caused by increasing the steam injection rate inside the freezer in the FCU-T refrigeration mode No. 2 to values larger than that of the FCU-T refrigeration mode No 1, and keeping it constant throughout the duration of the FCU-T refrigeration mode No 3 This is done to experiment with the effect of varying the total artificial latent heat gain on the total refrigeration load rate and the average load sensible heat ratio (LSHR)

The total refrigeration load rate is shown in Table 7 1 to increase for the FCU-T refrigeration mode No 2 to values larger than those for the FCU-T refrigeration mode No 1 while the LSHR is shown to decrease for the FCU-T refrigeration mode No 2 to values below those for the FCU-T refrigeration mode No 1 These two quantities are shown in Table 7 1 to be almost the same for the second and third FCU-T refrigeration modes Having the average load sensible heat ratios (LSHR) constant for the second and third FCU-T refrigeration modes demonstrates the capability of the refrigeration/defrost system to perform at a constant LSHR.

For the three FCU-T hot gas defrosting modes, the defrost heat input, the heat required to melt FCU-T frost, the defrost heat load rate and the defrost efficiency are

Table 7.1. Total Refrigeration Load Rate with Components and the Average Load Sensible Heat Ratio for the Run of (EAT = 8°F)

Quantity	Mode			Units	Remarks
	FCU-T Refrigeration No. 1	FCU-T Refrigeration No. 2	FCU-T Refrigeration No. 3		
Total Sensible Transmission Heat Gain ($\dot{Q}_{st}$)	1973.75	1983.81	1938.12	Btu/h	Equ. (4.6)
Total Sensible Internal Heat Gain ($\dot{Q}_{si}$)	4892.86	4892.86	4892.86	Btu/h	Equ. (4.7)
Total Natural Sensible Heat Gain ($\dot{Q}_{sn}$)	6866.61	6876.67	6830.98	Btu/h	Equ. (4.8)
Total Artificial Latent Heat Gain ($\dot{Q}_{latent}$)	686.41	1294.13	1294.13	Btu/h	Equ. (4.9)
Total Refrigeration Load Rate ($\dot{Q}_{total}$)	7553.02	8170.80	8125.11	Btu/h	Equ. (4.10)
Average Load Sensible Heat Ratio (LSHR)	0.91	0.84	0.84	--	Equ. (4.11)

calculated and are shown in Table 7.2. The low values calculated for the defrost efficiencies indicate that most of the defrost heat input during the FCU-T hot gas defrosting modes has apparently affected badly the refrigeration load in a form of an extra defrost heat load. The Average Coil Performance Load Rate (ACPLR) and the Fan-Defrost Contribution (FDC) for the three FCU-T refrigeration/defrost cycles are calculated and are shown in Table 7.3. Fan Defrost Contributions of 20.92, 21.26 and 20.57%, respectively, for the three cycles are acceptable values considering that in many refrigeration systems the theoretical contribution of the fan and defrost heat loads exceeds 15% of the net refrigeration load (ASHRAE 1994).

7.2. Case of Entering Air Temperature of -13°F

Again, using the procedures described in Appendix H, the average frost temperature ($T_{f\ avg}$) for this case was calculated to be (-20.32°F). The variation of the total sensible transmission heat gain and its components with time during the three FCU-T refrigeration modes is shown in Figures 7.7 through 7.9. As can be seen, the highest sensible transmission heat gain component is through the three walls of the freezer other than the front wall, while the smallest component is through the freezer windows. The variation of the total natural sensible heat gain and its components with time during the three FCU-T refrigeration modes is shown in Figures 7.10 through 7.12, while the calculated average values of the loads over their FCU-T refrigeration modes are shown in Table 7.4 along with the total artificial latent heat gain, the total refrigeration load rate and the average load sensible heat ratio (LSHR). As can be seen in Figures 7.10 through 7.12 and in Table 7.4, the total sensible internal heat gain is less than that of the previous run

Table 7.2 Defrost Heat Input, Heat Required to Melt FCU-T Frost, Defrost Heat Load Rate and Defrost Efficiency for the Run of (EAT = -8°F)

Quantity	Mode			Units	Remarks
	FCU-T Hot-Gas Defrosting No. 1	FCU-T Hot Gas Defrosting No. 2	FCU-T Hot-Gas Defrosting No. 3		
Defrost Heat Input (Q_{input})	292.81	272.69	211.15	Btu	Equ. (4.12)
Heat Required to Melt FCU-T Frost (Q_{melt})	34.41	25.80	12.04	Btu	Equ. (4.14)
Duration of Hot Gas Defrosting Mode (t_d)	0.13	0.12	0.10	Hours	Table 6.1
Defrost Heat Load Rate ($\dot{Q}_{df}$)	1987.69	2057.42	1991.10	Btu/h	Equ. (4.16)
Defrost Efficiency (η_D)	11.75	9.46	5.70	%	Equ. (4.15)

Table 7.3 Average Coil Performance Load Rate and Fan-Defrost Contribution for the Run of (EAT = -8°F)

Quantity	Cycle			Units	Remarks
	FCU-T Refrig./ Defrost No. 1	FCU-T Refrig./ Defrost No. 2	FCU-T Refrig./ Defrost No. 3		
Duration of Refrigeration Mode (t_r)	1.02	0.72	0.70	Hours	Table 6.1
Duration of Hot Gas Defrosting Mode (t_d)	0.13	0.12	0.10	Hours	Table 6.1
Total Time Duration of FCU-T Refrigeration/Defrost Cycle (t_t)	1.15	0.84	0.80	Hours	Equ. (4.19)
Average Coil Performance Load Rate (ACPLR)	6923.90	7297.46	7358.36	Btu/h	Equ. (4.20)
Fan Defrost Contribution (FDC)	21.92	21.26	20.57	%	Equ. (4.23)

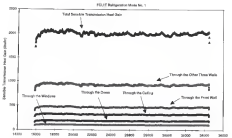

Figure 7.7 Total sensible transmission heat gain and components versus time during FCU T refrigeration mode No. 1 for the run of (**EAT = -13°F**)

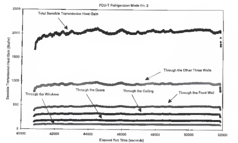

Figure 7.8 Total sensible transmission heat gain and components versus time during FCU-T refrigeration mode No. 2 for the run of (EAT = 13°F)

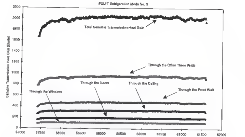

Figure 7.9 Total sensible transmission heat gain and components versus time during FCU-T refrigeration mode No. 3 for the run of (EAT = -13°F)

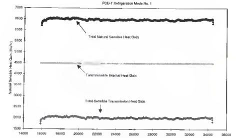

Figure 7.10 Total natural sensible heat gain and components versus time during FCU-T refrigeration mode No. 1 for the run of (EAT = -13°F)

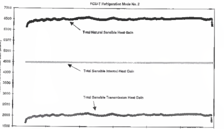

Figure 7.11 Total natural sensible heat gain and components versus time during FCU-T refrigeration mode No. 2 for the run of (EAT = -13°F)

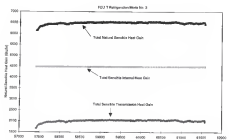

Figure 7 12 Total natural sensible heat gain and components versus time during FCU T refrigeration mode No. 3 for the run of (EAT = -13°F)

Table 7.4 Total Refrigeration Load Rate with Components and the Average Load Sensible Heat Ratio for the Run of (EAT = -13°F)

Quantity	Mode			Units	Remarks
	FCU-T Refrigeration No. 1	FCU-T Refrigeration No. 2	FCU-T Refrigeration No. 3		
Total Sensible Transmission Heat Gain ($\dot{Q}_{st}$)	2008.30	2037.09	2013.07	Btu/h	Equ. (4.6)
Total Sensible Internal Heat Gain ($\dot{Q}_{si}$) *	4483.33	4483.33	4483.33	Btu/h	Equ. (4.7)
Total Natural Sensible Heat Gain ($\dot{Q}_{sn}$)	6491.63	6520.42	6496.40	Btu/h	Equ. (4.8)
Total Artificial Latent Heat Gain ($\dot{Q}_{latent}$)	136.69	242.96	439.95	Btu/h	Eqn. (4.9)
Total Refrigeration Load Rate ($\dot{Q}_{total}$)	6628.32	6763.38	6936.35	Btu/h	Equ. (4.10)
Average Load Sensible Heat Ratio (LSHR)	0.98	0.96	0.94	--	Equ. (4.11)

* The total sensible internal heat gain here is less than that of the previous run (EAT = -8°F) because two of the four fluorescent lamps inside the freezer were not turned on

(EAT = 8°F) because two of the four fluorescent lamps inside the freezer were not turned on.

Similar to the previous case, the total sensible transmission and the total natural sensible heat gains are shown to be almost constant in Table 7.4 for the three FCU-T refrigeration modes. The total artificial latent heat gain for the FCU-T refrigeration modes is shown in Table 7.4 to increase in value in every refrigeration/defrost cycle. The lowest artifical latent heat gain is shown to be at the FCU-T refrigeration mode No. 1, while the highest is at the FCU-T refrigeration mode No. 3. This is caused by increasing the steam injection rate inside the freezer for each FCU-T refrigeration mode. This is done to experiment with the effect of varying the total artificial latent heat gain on the total refrigeration load rate and the average load sensible heat ratio (LSHR). The total refrigeration load rate and the average load sensible heat ratio (LSHR) are shown in Table 7.4, to increase and decrease respectively with the increase of the total artifical latent heat gain for the FCU-T refrigeration modes.

For the three FCU-T hot gas defrosting modes, the defrost heat input, the heat required to melt FCU-T frost, the defrost heat load rate, and the defrost efficiency are calculated and are shown in Table 7.5. The low values calculated for the defrost efficiencies indicate that most of the defrost heat input during the FCU-T hot-gas defrosting modes has affected badly the refrigeration load in a form of an extra defrost heat load. The Average Coil Performance Load Rate (ACPLR) and the Fan-Defrost Contribution (FDC) for the three FCU-T refrigeration/defrost cycles are calculated and are shown in Table 7.6. Fan Defrost Contributions of 21.90, 22.23 and 23.50% respectively for the three cycles are acceptable values considering that in many refrigeration systems

Table 7.5 Defrost Heat Input, Heat Required to Melt FCU-T Frost, Defrost Heat Load Rate and Defrost Efficiency for the Run of (EAT = -13°F)

Quantity	Mode			Units	Remarks
	FCU-T Hot-Gas Defrosting No. 1	FCU-T Hot-Gas Defrosting No. 2	FCU-T Hot Gas Defrosting No. 3		
Defrost Heat Input (Q_{input})	293.13	305.24	245.05	Btu	Equ. (4.12)
Heat Required to Melt FCU-T Frost (Q_{melt})	36.29	3.46	1.73	Btu	Equ. (4.14)
Duration of Hot Gas Defrosting Mode (t_d)	0.13	0.14	0.11	Hours	Table 6.3
Defrost Heat Load Rate ($\dot{Q}_{def}$)	1975.69	2155.57	2212.00	Btu/h	Equ. (4.16)
Defrost Efficiency (η_D)	12.38	1.13	0.71	%	Equ. (4.15)

Table 7.6. Average Coil Performance Load Rate and Fan-Defrost Contribution for the Run of (EAT = -13°F)

Quantity	Cycle			Units	Remarks
	FCU-T Refrig./ Defrost No. 1	FCU-T Refrig./ Defrost No. 2	FCU-T Refrig./ Defrost No. 3		
Duration of Refrigeration Mode (t_r)	5.17	3.08	1.16	Hours	Table 6.3
Duration of Hot Gas Defrosting Mode (t_d)	0.13	0.14	0.11	Hours	Table 6.3
Total Time Duration of FCU-T Refrigeration/Defrost Cycle (t_t)	5.30	3.22	1.27	Hours	Equ. (4.19)
Average Coil Performance Load Rate (ACPLR)	6514.20	6563.04	6527.15	Btu/h	Equ. (4.20)
Fan Defrost Contribution (FDC)	21.90	22.23	23.50	%	Equ. (4.23)

the theoretical contribution of the fan and defrost heat loads exceeds 15% of the net refrigeration load (ASHRAE 1994)

CHAPTER 8
A PARAMETRIC STUDY OF HOT-GAS DEFROSTING OF A CYLINDRICAL COIL COOLER

The experimental work conducted in this research has documented the energy penalty associated with using hot-gas defrosting in industrial freezers. This penalty is realized by the large amount of the defrost heat input being transferred to the refrigerated space due to the evaporation of melt and sublimation of frost (latent heat) as compared with the smaller amount that is utilized to melt the frost. Part of this penalty is also attributed to the residual heat that goes into the refrigerant during the defrosting process. This heat has to be extracted from the system during the refrigeration portion of the R/D cycle.

The purpose of this chapter is to describe a mathematical model for predicting the evaporation and sublimation rates on a frosted cylindrical cooler during hot-gas defrosting. The frosted cylindrical cooler is to model a single nonfinned tube in the first row of the coil employed in the experimental investigation. This model is to provide some insight into the hot-gas defrosting processes performed in this project and which are typically found in the operation of true-to-life industrial freezers.

8.1. Introduction

The hot-gas defrosting processes utilized in industrial freezers represent a type of transient heat transfer problems described in the literature as phase change or moving boundary problems and sometimes as Stefan problems (Ozisik 1994). In this process, the homogeneous ice goes through three different forms of phase transformations. A solid-to-liquid phase change occurs when the frost is transformed into melt, at the same time a solid-to-gas phase change occurs when the frost is sublimated into water vapor and finally a liquid-to-gas phase change occurs when the melt itself is evaporated into water vapor. Some of these processes may take place simultaneously. In this model all three processes in question are assumed to take place at the same time.

Mathematical modeling of phase change problems is a difficult and challenging task as the literature indicates. This difficulty is attributed to the fact that these problems are nonlinear where the location of the phase change interface is not known *a priori* and therefore becomes a part of the solution to the problem (Ozisik 1993, 1994). Due to this difficulty, there are very few exact analytical solutions available, while the majority of the solutions in the literature are of the approximate numerical and experimental types (Alexiades and Solomon 1993, Ozisik 1994). Several comprehensive reviews of available solutions to phase change problems can be found in Boley (1963), Bankoff (1964), Muehlbauer and Sunderland (1965) and Mori and Araki (1976).

The phase change problem to be modeled in this chapter is for a hot-gas defrosting process of a frosted cylindrical coil cooler having the frost initially at a uniform subfreezing temperature (T_f). A hot gas defrost heat input rate ($\dot{Q}_{input}$) which is to be applied from the inside of the cooler is assumed to be increasing with time such that a constant heat flux ($\overline{Q}_{input}$) representing the hot-gas defrost heat input is applied at the phase change interface. The model is only valid for a short period of time representing the duration of the defrosting process as the cooler experiences an increasing defrost heat input rate and in turn the cooler's wall temperature would have to be an increasing function of time which is consistent with the thermal transient experienced by the flow in the cooler The frost is assumed to be represented by a homogenous semi-infinite medium where the heat flux would cause the temperature of the frost to rise as the heat penetrates the frost region. When the temperature of the frost layer touching the wall of the cooler rises to the water triple point temperature (T_{tp}) the phase change processes will be initiated and the phase change interface will begin to move outward relative to the cooler outer surface. The frost will start to melt and sublimate at the water triple point temperature The bulk of the melt itself is assumed to be removed from the cooler by a special mechanism while a thin film of it will be evaporating at the water triple point temperature

Lunardini (1981) reported that there are no exact general solutions for phase change problems in cylindrical coordinates. Meanwhile, an approximate analytical method called "the heat-balance integral technique" has been employed to solve the model presented in this chapter This technique dates back to von Karman and Pohlhausen when analyzing the boundary layer problem in fluid mechanics (Schlichting 1979) The technique was then introduced by Goodman (1958, 1960) in his attempts to solving the melting problem of a slab

The heat-balance integral technique has been employed by several investigators in their studies to solve phase change problems in cylindrical coordinates. The list includes Lardner and Pohle (1961) Lunardini (1980) and Lunardini and Varotta (1981)

8.2. Model Development

The hot-gas defrosting process modeled in this section is divided into two stages. The pre-melting stage, in which the temperature of the frost layer touching the wall of the cooler rises to the water triple point temperature (T_{tp}), and the melting stage itself, where the melting process and the other assumed phase change processes (evaporation and sublimation) will occur. The pre-melting stage is a very fast stage (in the order of 10^{-3} seconds) where it is assumed that the defrost heat input rate inside the cooler is constant, as compared with the increasing defrost heat input rate assumed in the melting stage. The above assumptions will lead to the fact that, in this model, the defrost heat input flux ($\overline{Q}_{input}$) is always constant at the inner boundary of the frost layer. It is also assumed in this model that the thermal properties of the frost are constant in spite of the fact that their values have been calculated using established empirical formulas.

8.2.1. Pre-Melting Stage

Consider a frosted cylindrical coil cooler of an outside radius (R_b), where the frost is represented by a homogenous semi-infinite medium bounded from the inside by the cooler's outer surface. A schematic drawing describing this process can be seen in Figure 8.1. The frost is initially at a uniform subfreezing temperature (T_f) and is subjected to a constant defrost heat input flux ($\overline{Q}_{input}$) at the boundary $r = R_b$ at time $t = 0$. The governing equation with the initial and boundary conditions representing the case are as follows

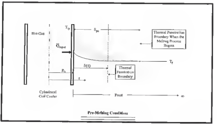

Figure 8.1 Pre melting stage

$$\frac{1}{r}\frac{\partial}{\partial r}\left(r\frac{\partial T_s}{\partial r}\right)=\frac{1}{\alpha_s}\frac{\partial T_s}{\partial t} \tag{8.1}$$

$$T_s(r,0)=T_f \tag{8.2}$$

$$K_s\frac{\partial T_s(R_b,t)}{\partial r}=-\overline{Q}_{input} \tag{8.3}$$

where the subscript "s" denotes the solid (frost) layer, and "α_s" and "K_s" are the thermal diffusivity and thermal conducuvity of the frost, respectively

The thermal conductivity of the frost is calculated using the formula (Zakrzewski 1984)

$$K_s = 2.85(\rho_s)^2\,10^{-6} \tag{8.4}$$

where (K_s) is in W/m-K and the frost density (ρ_s) is in kg/m^3 The frost density is calculated using the formula.

$$\rho_s = 650\exp(0.277\,T_s) \tag{8.5}$$

where (ρ_s) is in kg/m^3, and the temperature (T_s) in °C is the average of the frost subfreezing temperature (T_f) and the water triple point temperature (T_{tp}). This frost density formula was developed by O Neal (1982) from experimental data generated by Hayashi et al. (1977)

The thermal diffusivity of the frost is calculated using the formula.

$$\alpha_s = \frac{K_s}{\rho_s C_s} \tag{8.6}$$

where (C_s) is the specific heat of the frost and is calculated by the formula (Alexiades and Solomon 1993)

$$C_s = 7.16\,(10)^{-3}\,(T_s + 273.16) + 0.138 \tag{8.7}$$

where (C_s) is in kJ/kg K, and the temperature (T_s) is in °C and is the same as the temperature used in the frost density equation above

Since the defrost heat input flux ($\overline{Q}_{input}$) will cause the temperature of the frost to rise as the heat penetrates the frost region, a quantity is defined as the thermal penetration depth ($\delta(t)$) in order to represent the distance between the cooler surface and the farthest location in the frost region that has been affected by the heat. In other words, the concept of the thermal penetration depth is analogous to the boundary layer thickness concept in fluid mechanics (Goodman 1964) This means that the frost temperature beyond the thermal penetration depth is still at the subfreezing uniform temperature (T_f). Therefore, at the thermal penetration boundary as can be seen in Figure 8.1 the following boundary conditions exist.

$$T_s(R_b + \delta, t) = T_f \tag{8.8}$$

$$\frac{\partial T_s(R_b + \delta, t)}{\partial r} = 0 \tag{8.9}$$

Figure 8.1 shows the temperature profiles as the temperature of the frost layer touching the wall of the cooler rises to the water triple point temperature (T_{tp}), at which time the thermal penetration depth is equal to (δ_{pc}) where the phase change processes will be initiated and the subscript "pc" refers to "phase change." In what follows are the mathematical steps leading to the formulas for calculating the penetration depth (δ_{pc}) and the time of its occurrence (t_{pc}) using the heat balance integral technique.

To simplify the algebra, the temperature of the frost (T_s) has been scaled by subtracting from it the value of the frost's initial uniform subfreezing temperature (T_f) as follows.

$$\bar{T}_s(r,t) = T_s(r,t) - T_f \tag{8.10}$$

where, when this equation is substituted for the value of (T_s) in Equations 8.1, 8.2, 8.3, 8.8 and 8.9 the following five equations evolve, respectively:

$$\frac{1}{r}\frac{\partial}{\partial r}\left(r\frac{\partial \bar{T}_s}{\partial r}\right) = \frac{1}{\alpha_s}\frac{\partial \bar{T}_s}{\partial t} \tag{8.11}$$

$$\bar{T}_s(r,0) = 0 \tag{8.12}$$

$$K_s\frac{\partial \bar{T}_s(R_b,t)}{\partial r} = -\bar{Q}_{input} \tag{8.13}$$

$$\bar{T}_s(R_b+\delta,t) = 0 \tag{8.14}$$

$$\frac{\partial \bar{T}_s(R_b+\delta,t)}{\partial r} = 0 \tag{8.15}$$

Applying the heat balance integral method, the governing equation [Equation (8.11)] is integrated from (R_b) to $(R_b+\delta)$ with respect to (r) as shown below

$$\int_{R_b}^{R_b+\delta} \alpha_s\frac{\partial}{\partial r}\left[r\left(\frac{\partial \bar{T}_s}{\partial r}\right)\right]dr = \int_{R_b}^{R_b+\delta} r\,\frac{\partial \bar{T}_s}{\partial r}\,dr \tag{8.16}$$

as the main concept for this integration is to average, approximately, the second order temperature differential term between the limits (R_b) and $(R_b+\delta)$. This step will simplify the solution by reducing the order of the governing equation to a first order differential equation

The left hand side of Equation (8 16) is integrated to become

$$\int_{R_b}^{R_b+\delta} \alpha_s \frac{\partial}{\partial r}\left[r\left(\frac{\partial \bar{T}_s}{\partial r}\right)\right] dr = \alpha_s\left[(R_b+\delta)\left(\frac{\partial \bar{T}_s(R_b+\delta,t)}{\partial r}\right) - R_b\left(\frac{\partial \bar{T}_s(R_b,t)}{\partial r}\right)\right] \tag{8 17}$$

where, when the boundary condition of Equation (8 15) is substituted into Equation (8 17) the following equation evolves.

$$\int_{R_b}^{R_b+\delta} \alpha_s \frac{\partial}{\partial r}\left[r\left(\frac{\partial \bar{T}_s}{\partial r}\right)\right] dr = -\,\alpha_s\, R_b\left(\frac{\partial \bar{T}_s(R_b,t)}{\partial r}\right) \tag{8 18}$$

Defining the following term for the convenience of the analyses

$$\theta(r,t) = \int_{R_b}^{R_b+\delta} f(r,t)\, dr \tag{8.19}$$

where

$$f(r,t) = r\,\bar{T}_s(r,t) \tag{8.20}$$

with the Leibnitz's integral formula for a general function $F(r,t)$ is stated as (Arpaci 1966):

$$\frac{d}{dt}\int_{a(t)}^{b(t)} F(r,t)\,dr = F(b,t)\frac{db}{dt} - F(a,t)\frac{da}{dt} + \int_{a(t)}^{b(t)} \frac{\partial F(r,t)}{\partial t}\, dr \tag{8.21}$$

and when the function $f(r,t)$ in Equation (8 20) is substituted into Equation (8 21), the following equation evolves

$$\frac{d}{dt}\int_{a(t)}^{b(t)} r\,\bar{T}_s(r,t)\,dr = b\,\bar{T}_s(b,t)\frac{db}{dt} - a\,\bar{T}_s(a,t)\frac{da}{dt} + \int_{a(t)}^{b(t)} r\,\frac{\partial \bar{T}_s(r,t)}{\partial r}\, dr \tag{8 22}$$

Applying Equation (8.22) to the right hand side of Equation (8.16) will produce the following equation:

$$\int_{R_b}^{R_b+\delta} r\,\frac{\partial \overline{T}_s(r,t)}{\partial t}\,dr = \frac{d}{dt}\left[\int_{R_b}^{R_b+\delta} r\,\overline{T}_s(r,t)\,dr\right] + R_b\,\overline{T}_s(R_b,t)\,\frac{dR_b}{dt} - (R_b+\delta)\,\overline{T}_s(R_b+\delta,t)\,\frac{d(R_b+\delta)}{dt} \tag{8.23}$$

where, when the boundary condition of Equation (8.14) is substituted into Equation (8.23), and the second term in the right hand side of Equation (8.23) is dropped due to the derivative term of a constant (R_b), the following equation results:

$$\int_{R_b}^{R_b+\delta} r\,\frac{\partial \overline{T}_s(r,t)}{\partial t}\,dr = \frac{d}{dt}\int_{R_b}^{R_b+\delta} r\,\overline{T}_s(r,t)\,dr \tag{8.24}$$

When Equations (8.18) and (8.24) are substituted into Equation (8.16), the following equation evolves:

$$\frac{d}{dt}\int_{R_b}^{R_b+\delta} r\,\overline{T}_s(r,t)\,dr = -\,\alpha_s\,R_b\left(\frac{\partial \overline{T}_s(R_b,t)}{\partial r}\right) \tag{8.25}$$

and when Equations (8.19) and (8.20) are substituted into Equation (8.25), the following equation is produced

$$\frac{d\theta}{dt} = -\,\alpha_s\,R_b\left(\frac{\partial \overline{T}_s(R_b,t)}{\partial r}\right) \tag{8.26}$$

A temperature profile is assumed for the frost in the pre-melting stage as follows.

$$\overline{T}_s(r,t) = \frac{\left(\dfrac{-\overline{Q}_{input}\,R_b}{K_s}\right)\left[\dfrac{(\delta+R_b)-r}{R_b}\right]^2}{\left(\dfrac{\delta}{R_b}\right)\left[2\ln\left(\dfrac{\delta+R_b}{R_b}\right)+\left(\dfrac{\delta}{R_b}\right)\right]}\,\ln\left(\frac{r}{\delta+R_b}\right) \tag{8.27}$$

where this profile has been tested by Lardner and Pohle (1961) to produce good results. The profile is a combination of a logarithmic term in (r) and a polynomial in (r) which is what is required to solve a cylindrical coordinate problem using the heat-balance integral method. This profile is found to satisfy the boundary conditions of this stage of the problem (Equations 8.13 to 8.15)

The derivative of the temperature profile of Equation (8.27) with respect to (r) is calculated at the outer surface of the cooler ($r = R_b$), and is found to be

$$\frac{\partial \overline{T}_s (R_b, t)}{\partial r} = \frac{-\overline{Q}_{input}}{K_s} \tag{8.28}$$

and when this equation is substituted into Equation (8.26), the following equation results

$$\frac{d\theta}{dt} = \frac{\alpha_s \, R_b \, \overline{Q}_{input}}{K_s} \tag{8.29}$$

When the temperature profile of Equation (8.27) is substituted into Equation (8.20), and then the result is substituted into Equation (8.19) to derive an equation for the defined variable (θ (r, t)), the following equation evolves

$$\theta (r,t) = \left[\frac{\left(\frac{-\overline{Q}_{input}}{K_s \, R_b} \right)}{\left(\frac{\delta}{R_b} \right) \left[2 \ln \left(\frac{\delta + R_b}{R_b} \right) + \left(\frac{\delta}{R_b} \right) \right]} \right] \left[A_1(t) + A_2(t) + A_3(t) \right] \tag{8.30}$$

where

$$A_1(t) = -\frac{13}{144} (\delta + R_b)^4 - \frac{72}{144} R_b^2 (\delta + R_b)^2 \ln \left(\frac{R_b}{\delta + R_b} \right) + \frac{9}{144} R_b^4 \tag{8.31}$$

$$A_2(t) = +\frac{36}{144} R_b^2 (\delta + R_b)^2 - \frac{36}{144} R_b^4 \ln\left(\frac{R_b}{\delta + R_b}\right) \tag{8.32}$$

$$A_3(t) = -\frac{32}{144} R_b^3 (\delta + R_b) + \frac{96}{144} R_b^3 (\delta + R_b) \ln\left(\frac{R_b}{\delta + R_b}\right) \tag{8.33}$$

Taking the derivative of Equation (8 30) and substituting the result into Equation (8 29) and then simplifying, an equation for the time (t) in terms of the thermal penetration depth ($\delta(t)$) will result as follows

$$t = \left[\frac{R_b^2}{\alpha_s}\right]\left[\frac{-72\,\eta^2 \ln\eta + 96\,\eta \ln\eta - 36 \ln\eta + 13\,\eta^4 - 36\,\eta^2 + 32\,\eta - 9}{144\,(\eta - 1)\,(2 \ln\eta + \eta - 1)}\right] \tag{8 34}$$

where

$$\eta(t) = 1 + \frac{\delta(t)}{R_b} \tag{8.35}$$

which is the same equation derived by Lardner and Pohle (1961) in their research

When the temperature profile of Equation (8.27) is substituted into Equation (8 10), and the resulting equation is solved for the temperature at the outer surface of the cooler ($r = R_b$) the result is found to be

$$T_s(R_b, t) = T_f + \frac{\left(\frac{-\overline{Q}_{input}\ \delta}{K_s}\right)}{\left[2 \ln\left(\frac{\delta + R_b}{R_b}\right) + \left(\frac{\delta}{R_b}\right)\right]} \ln\left(\frac{R_b}{\delta + R_b}\right) \tag{8 36}$$

When the temperature of the frost layer touching the wall of the cooler rises to the water triple point temperature (T_{tp}), the thermal penetration depth at that time (δ_{pe}) can be calculated by iteration from Equation (8.36) by substituting the value of (T_{tp}) for the term $T_s(R_b, t)$, and simplifying the form of the equation. This yields

$$\delta_{pc} = \frac{(T_{tp} - T_f)\left[2 \ln\left(\frac{\delta_{pc} + R_b}{R_b}\right) + \left(\frac{\delta_{pc}}{R_b}\right)\right]\left[\frac{-K_s}{\overline{Q}_{input}}\right]}{\ln\left(\frac{R_b}{\delta_{pc} + R_b}\right)} \tag{8.37}$$

Equation (8.37) is to be solved by iteration for the value of (δ_{pc}), where at that depth the melting process will begin along with the other phase change processes (evaporation and sublimation). The time required for the frost layer touching the wall of the cooler to reach the water triple point temperature (t_{pc}) can be calculated by substituting the value of (δ_{pc}) into Equation (8.35) and substituting the result into Equation (8.34)

8.2.2. Melting Stage

The melting process along with the other phase change processes (evaporation and sublimation) and a convection heat transfer process will be initiated at this stage. The frost will start to melt and sublimate at the water triple point temperature. The bulk of the melt itself is assumed to be removed from the cooler by a special mechanism while a thin film of it will be evaporating at the water triple point temperature. A schematic drawing describing this process can be seen in Figure 8.2 where the phase change interface (also called "the frost-melt-air interface"), will begin to move outward relative to the cooler outer surface

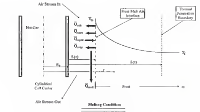

Figure 8.2. Melting stage

Since the defrost heat input flux ($\overline{Q}_{input}$) will cause the frost melt-air interface to move outward relative to the cooler outer surface, a quantity ($S(t)$) is defined to represent the distance between the cooler outer surface and the phase change interface (as can be seen in Figure 8.2). As the phase change processes progress, part of the defrost heat input flux will still continue to penetrate through the frost.

The governing equation with the boundary conditions representing this stage are as follows

$$\frac{1}{r}\frac{\partial}{\partial r}\left(r\frac{\partial T_s}{\partial r}\right)=\frac{1}{\alpha_s}\frac{\partial T_s}{\partial t} \tag{8.38}$$

$$T_s(R_b+S,t)=T_{sp} \tag{8.39}$$

$$T_s(R_b+\delta,t)=T_f \tag{8.40}$$

$$\frac{\partial T_s(R_b+\delta,t)}{\partial r}=0 \tag{8.41}$$

$$\overline{Q}_{input}-\overline{Q}_{conv}-\overline{Q}_{sub}-\overline{Q}_{evap}+K_s\frac{\partial T_s(R_b+S,t)}{\partial r}=\rho_s L_{melt}\frac{dS}{dt} \tag{8.42}$$

while the conditions of the thermal penetration depth and the distance of the phase change interface from the cooler outer surface are as follows.

$$\delta(t=t_{pc})=\delta_{pc} \tag{8.43}$$

$$S(t=t_{pc})=0 \tag{8.44}$$

The thermal properties of the frost in this stage are calculated in the same manner employed for the pre-melting stage, while the latent heat of fusion (L_{melt}) is assumed to be equal to 143.33 Btu/lbm of water. To simplify the analysis of this stage, the convection, sublimation, and evaporation heat fluxes ($\overline{Q}_{conv}$, $\overline{Q}_{sub}$, and $\overline{Q}_{evap}$, respectively) are all assumed to be constant. As can be seen in Equation (8.42), which represents the boundary condition at the frost-melt-air interface, the melting process has been assumed to be the main mechanism during the interface. In other words, the melt interface has been assumed to coincide with both the evaporation interface and the sublimation interface.

As was reported in the experimental part of this investigation, the convection heat flux ($\overline{Q}_{conv}$) is due to the forced convection heat transfer between the frost-melt-air interface at the triple point temperature (T_{tp}) and the air stream inside the freezer due to the operation of the FCU-A blower during that time. The air stream velocity in front of the first row of the coil has been observed experimentally to be equal to 5.5 ft/sec while the air stream temperature (T_{∞}) is assumed to be constant and is equal to the freezer temperature during the refrigeration mode before switching to the hot-gas defrosting mode.

The convection heat flux ($\overline{Q}_{conv}$) is calculated using the formula.

$$\overline{Q}_{conv} = h_{conv} (T_{tp} - T_{\infty}) \tag{8.45}$$

where (h_{conv}) is the film convection heat transfer coefficient, and is calculated using the empirical correlation due to Hilbert (1933)

$$h_{conv} = 0.683\ (Re_D)^{0.466}\ Pr^{1/3}\ (\frac{K_a}{D_b}) \tag{8.46}$$

This is a widely used correlation (Incropera and Dewitt 1996) where (Pr) is the Prandtl number of the air stream and (D_b) is assumed to be equal to the outside diameter of the cooler.

The Reynolds number (Re_D) of the air stream is calculated using the following formula,

$$Re_D = \frac{V_\infty D_h}{\nu_a} \tag{8.47}$$

where (V_∞) is the air stream velocity and (ν_a) is the kinematic viscosity of the air. All the air properties employed in Equations (8.46) and (8.47) are to be evaluated at the film temperature (T_{film}) which is the average of the air stream temperature (T_∞) and the water triple point temperature (T_{tp}).

The evaporation heat flux ($\overline{Q}_{evap}$) is calculated using the formula,

$$\overline{Q}_{evap} = h_D L_{evap} \left[W_m \left(P_{sv,m}, T_{tp} \right) - W_\infty \left(50\% \, RH, T_\infty \right) \right] \tag{8.48}$$

where (L_{evap}) is the latent heat of evaporation and is assumed to equal 1075.15 Btu/lbm of water. The term (W_m) is the humidity ratio of the saturated moist air over the melt at the frost-melt-air interface. This quantity (W_m) is evaluated at the water vapor saturation pressure over the melt ($P_{sv,m}$) and the water triple point temperature(T_{tp}).

The water vapor saturation pressure over the melt ($P_{sv,m}$) is calculated in psia using the formula (Hyland and Wexler 1983, Olivieri et al. 1996)

$$\ln\left(P_{sv,m}\right) = \sum_{i=-1}^{3} g_i \left(T + 459.69 \right)^i + g_4 \ln\left(T + 459.69 \right) \tag{8.49}$$

where the constants are

$$g_{-1} = -1.044039708 \times 10^4$$

$$g_0 = -1.12946495635 \times 10^1$$

$g_1 = -2.7022355 \times 10^{-2}$

$g_2 = 1.28903604938 \times 10^{-5}$

$g_3 = -2.478068072 \times 10^{-9}$

$g_4 = 6.5459673$

and the temperature substituted in the above formula [Equation (8.49)] is the water triple point temperature which must be in °F

The humidity ratio of the saturated moist air over the melt (W_{sm}) is calculated using the common formula for the humidity ratio of saturated moist air (Wang 1993)

$$W(P_{sv}, T) = 0.62198 \frac{P_{sv}}{P_{atm} - P_{sv}} \tag{8.50}$$

by substituting the value of ($P_{sv,m}$) for the variable (P_{sv}) where (P_{atm}) is the air atmospheric pressure, and is assumed to equal 14.697 psia.

The term (W_∞) in Equation (8.48) is the humidity ratio of the air stream which is evaluated at the temperature (T_∞) and is assumed to be at 50% relative humidity. The quantity (W_∞) is evaluated from the tables of moist air properties or the psychrometric chart. The term (h_D) in Equation (8.48) is the convection mass transfer coefficient and is related to the convection heat transfer coefficient by the Lewis analogy as follows (Padki et al. 1989, Threlkeld 1970).

$$h_D = \frac{h_{conv}}{C_{pm} \, (Le)^{2/3}} \tag{8.51}$$

where (C_{pm}) is the specific heat of moist air and is assumed to be equal to 0 243 Btu/lbm -°F of dry air (Wang 1993), while (Le) is the Lewis number for air and water vapor mixtures, and is assumed to be equal to 0.845 (ASHRAE 1993)

The sublimation heat flux $(\overline{Q}_{sub})$ is calculated using the formula

$$\overline{Q}_{sub} = h_D\, L_{sub} \left[W_f \left(P_{sv,f}\ T_{tp} \right) - W_\infty \left(50\%\, RH\ ,\ T_\infty \right) \right] \tag{8 52}$$

where (L_{sub}) is the latent heat of sublimation and is assumed to equal 1218 42 Btu/lbm of water The term (W_f) is the humidity ratio of the saturated moist air over the frost at the frost-melt-air interface This quantity (W_f) is evaluated at the water vapor saturation pressure over the frost $(P_{sv,f})$ and the water triple point temperature (T_{tp}).

The water vapor saturation pressure over the frost $(P_{sv,f})$ is calculated in psia using the formula (Hyland and Wexler 1983, Olivieri et al. 1996)

$$\ln\left(P_{sv\,f}\right) = \sum_{i=0}^{5} m_i \left(T + 459.69 \right)^{i-1} + m_6 \ln\left(T + 459\,69 \right) \tag{8.53}$$

where the constants are,

$$m_0 = -1.021416462 \times 10^{4}$$

$$m_1 = -4\,89324277179$$

$$m_2 = -5.3765794445 \times 10^{-3}$$

$$m_3 = 1.92023768519 \times 10^{-7}$$

$$m_4 = 3.55758316187 \times 10^{-10}$$

$m_5 = -9.03446883097 \times 10^{-14}$

$m_6 = 0.41635019 \times 10^{1}$

and the temperature substituted in the above formula [Equation (8.53)] is the water triple point temperature, which must be substituted in °F

The humidity ratio of the saturated moist air over the frost ($\mathbf{W}_f$) is calculated using Equation (8.50) by substituting the value of ($P_{sv,f}$) for the variable (P_{sv}), while the terms ($\mathbf{W}_\infty$) and (h_D) in Equation (8.52) are exactly the same terms shown previously in Equation (8.48).

Scaling the temperature of the frost (T_s) by subtracting from it the value of the water triple point temperature ($\mathbf{T}_{tp}$) will simplify the algebra in this melting stage where the scaling equation is as follows.

$$\bar{\mathbf{T}}_s(r,t) = T_s(r,t) - \mathbf{T}_{tp} \tag{8.54}$$

where, when this equation is substituted for the value of ($\mathbf{T}_s$) in Equations 8.38 to 8.42, the following five equations evolve respectively

$$\frac{1}{r}\frac{\partial}{\partial r}\left(r\frac{\partial \bar{T}_s}{\partial r}\right) = \frac{1}{\alpha_s}\frac{\partial \bar{T}_s}{\partial t} \tag{8.55}$$

$$\bar{\mathbf{T}}_s(R_b + S, t) = 0 \tag{8.56}$$

$$\bar{T}_s(R_b + \delta, t) = T_f - T_{tp} = \Delta\mathbf{T} \tag{8.57}$$

$$\frac{\partial \bar{\mathbf{T}}_s(R_b + \delta, t)}{\partial r} = 0 \tag{8.58}$$

$$\overline{Q}_{input} - \overline{Q}_{conv} - \overline{Q}_{sub} - \overline{Q}_{evap} + K_s \frac{\partial \hat{T}_s (R_b + S, t)}{\partial r} = \rho_s L_{melt} \frac{dS}{dt} \tag{8.59}$$

Collecting the constant heat flux terms in one term called the net heat flux term ($\overline{Q}_{net}$) as follows.

$$\overline{Q}_{net} = \overline{Q}_{input} - \overline{Q}_{conv} - \overline{Q}_{sub} - \overline{Q}_{evap} \tag{8.60}$$

will simplify the algebra, where Equation (8.59) will then have less terms as follows

$$\overline{Q}_{net} + K_s \frac{\partial \hat{T}_s (R_b + S, t)}{\partial r} = \rho_s L_{melt} \frac{dS}{dt} \tag{8.61}$$

Applying the heat-balance integral method, the governing equation [Equation (8.55)] is integrated from $(R_b + S)$ to $(R_b + \delta)$ with respect to (r) as shown below

$$\int_{R_b + S}^{R_b + \delta} \alpha_s \frac{\partial}{\partial r} \left[r \left(\frac{\partial \hat{T}_s}{\partial r} \right) \right] dr = \int_{R_b + S}^{R_b + \delta} r \frac{\partial \hat{T}_s}{\partial t} \, dr \tag{8.62}$$

The left hand side of Equation (8.62) is integrated to become

$$\begin{aligned} &\int_{R_b + S}^{R_b + \delta} \alpha_s \frac{\partial}{\partial r} \left[r \left(\frac{\partial \hat{T}_s}{\partial r} \right) \right] dr = \\ &\qquad \alpha_s \left[(R_b + \delta) \left(\frac{\partial \hat{T}_s (R_b + \delta, t)}{\partial r} \right) - (R_b + S) \left(\frac{\partial \bar{T}_s (R_b + S, t)}{\partial r} \right) \right] \end{aligned} \tag{8.63}$$

where, when the boundary condition of Equation (8.58) is substituted into Equation (8.63), the following equation evolves

$$\int_{R_b + S}^{R_b + \delta} \alpha_s \frac{\partial}{\partial r} \left[r \left(\frac{\partial \hat{T}_s}{\partial r} \right) \right] dr = - \alpha_s (R_b + S) \left(\frac{\partial \bar{T}_s (R_b + S, t)}{\partial r} \right) \tag{8.64}$$

Defining the following term for the convenience of the analysis

$$\theta_1(r,t) = \int_{R_b+S}^{R_b+\delta} f_1(r,t)\,dr \tag{8.65}$$

where

$$f_1(r,t) = r\,\bar{T}_s(r,t) \tag{8.66}$$

and when the function $f_1(r,t)$ in Equation (8.66) is substituted into the Leibnitz's integral formula [Equation (8.21)], the following equation evolves

$$\frac{d}{dt}\int_{a(t)}^{b(t)} r\bar{T}_s(r,t)\,dr = b\,\bar{T}_s(b,t)\frac{db}{dt} - a\,\bar{T}_s(a,t)\frac{da}{dt} + \int_{a(t)}^{b(t)} r\,\frac{\partial\bar{T}_s(r,t)}{\partial t}\,dr \tag{8.67}$$

Applying Equation (8.67) to the right hand side of Equation (8.62), will produce the following equation.

$$\int_{R_b+S}^{R_b+\delta} r\,\frac{\partial\hat{T}_s(r,t)}{\partial t}\,dr = \frac{d}{dt}\left[\int_{R_b+S}^{R_b+\delta} r\,\bar{T}_s(r,t)\,dr\right] + (R_b+S)\,\bar{T}_s(R_b+S,t)\frac{d(R_b+S)}{dt} - (R_b+\delta)\,\hat{T}_s(R_b+\delta,t)\frac{d(R_b+\delta)}{dt} \tag{8.68}$$

where when the boundary conditions of Equations (8.56) and (8.57) are substituted into Equation (8.68), and dropping the terms in the right hand side of Equation (8.68) which correspond to the derivatives of a constant (R_b), the following equation results.

$$\int_{R_b+S}^{R_b+\delta} r\,\frac{\partial\hat{T}_s(r,t)}{\partial t}\,dr = \frac{d}{dt}\left[\int_{R_b+S}^{R_b+\delta} r\,\bar{T}_s(r,t)\,dr\right] - (R_b+\delta)\,\Delta T\,\frac{d\delta}{dt} \tag{8.69}$$

When Equations (8.64) and (8.69) are substituted into Equation (8.62), the following equation evolves:

$$\frac{d}{dt}\left[\int_{R_b+S}^{R_b+\delta} r\,\bar{T}_s(r,t)\,dr\right]-(R_b+\delta)\,\Delta T\,\frac{d\delta}{dt}=-\,\alpha_s\,(R_b+S)\left(\frac{\partial \bar{T}_s(R_b+S,t)}{\partial r}\right) \tag{8.70}$$

and when Equations (8.61), (8.65) and (8.66) are substituted into Equation (8.70), the following equation is produced

$$\frac{d\theta_1}{dt}-(R_b+\delta)\,\Delta T\,\frac{d\delta}{dt}+\frac{\alpha_s\,\rho_s\,L_{melt}}{K_s}\,(R_b+S)\,\frac{dS}{dt}=\frac{\alpha_s\,\overline{Q}_{net}}{K_s}\,(R_b+S) \tag{8.71}$$

A temperature profile is assumed for the frost in the melting stage as follows.

$$\bar{T}_s(r,t)=\left(a_0+a_1 r\right)\,\ln\left(\frac{r}{R_b+S}\right) \tag{8.72}$$

and is substituted into Equations 8.56 to 8.58 in order to evaluate the coefficients of the polynomial of Equation (8.72). These coefficients are given below

$$a_0=\frac{\Delta T}{\ln\left(\frac{R_b+\delta}{R_b+S}\right)+\left[\ln\left(\frac{R_b+\delta}{R_b+S}\right)\right]^2} \tag{8.73}$$

$$a_1=\frac{-\,\Delta T}{(R_b+\delta)\left[\ln\left(\frac{R_b+\delta}{R_b+S}\right)\right]^2} \tag{8.74}$$

When the temperature profile of Equation (8.72) is substituted into Equation (8.66), and then the result is substituted into Equation (8.65) to derive an equation for the defined variable $(\theta_1(r,t))$, the following equation evolves.

$$\theta_1(r,t)=\frac{\frac{1}{4}\Delta T\,(R_b+S)^2}{\ln\left(\frac{R_b+\delta}{R_b+S}\right)}+\frac{1}{2}\Delta T\,(R_b+\delta)^2-\frac{\frac{1}{12}\Delta T\,(R_b+\delta)^2}{\ln\left(\frac{R_b+\delta}{R_b+S}\right)}$$

$$+\frac{\frac{1}{4}\Delta T\,(R_b+S)^2}{\left[\ln\left(\frac{R_b+\delta}{R_b+S}\right)\right]^2}-\frac{\frac{5}{36}\Delta T\,(R_b+\delta)^2}{\left[\ln\left(\frac{R_b+\delta}{R_b+S}\right)\right]^2}-\frac{\frac{1}{9}\Delta T\,(R_b+S)^3}{(R_b+\delta)\left[\ln\left(\frac{R_b+\delta}{R_b+S}\right)\right]^2} \qquad (8.75)$$

To simplify the analysis, it is assumed that the ratio inside the logarithmic term in Equation (8.75) is a constant ($\bar{b}$) as follows

$$\frac{R_b+\delta}{R_b+S}=\bar{b} \qquad (8.76)$$

where this assumption implies that the ratio of the thermal penetration depth radius to the radius of the phase change interface is constant. The above assumption has been employed by Khakimov (1957), Lunardini (1980, 1981) and Gupta (1973). Khakimov (1957) has found experimentally that this ratio for constant temperature applications to be in the range of 4.5 - 5.5, but he recommended the value of 4.5 and used it in his model on freezing outside cylinders. Lunardini (1980, 1981) on the other hand suggested that this assumption is not valid for cylindrical systems, but argued that it does simplify the analysis and produce reasonable solutions nevertheless. Lunardini (1980, 1981) used this assumption for his model on thawing outside cylinders. Gupta (1973) applied this assumption to his model on spheres and cylinders using a value of 4.5 for the constant, and was able to produce meaningful results. In this model, it will be assumed that this constant is equal to 4.5.

Substituting Equation (8.76) into Equation (8.75) results in the following equation

$$\theta_1\ (r,t) = (R_b + S)^2\ B\ \Delta T \tag{8.77}$$

where

$$B = \frac{1}{4\ \ln \bar{b}} + \frac{\bar{b}^2}{2} - \frac{\bar{b}^2}{12\ \ln \bar{b}} + \frac{1}{4\left[\ln \bar{b}\right]^2} - \frac{5\ \bar{b}^2}{36\ \left[\ln \bar{b}\right]^2} - \frac{1}{9\ \bar{b}\ \left[\ln \bar{b}\right]^2} \tag{8.78}$$

and when taking the derivative of Equation (8.77) with respect to (t), the following equation results

$$\frac{d\theta_1}{dt} = 2\ B\ \Delta T\ (R_b + S)\ \frac{dS}{dt} \tag{8.79}$$

Taking the derivative of Equation (8.76) with respect to (t), will result in the following equation

$$\frac{d\bar{\delta}}{dt} = \bar{b}\ \frac{dS}{dt} \tag{8.80}$$

and when Equations (8.76), (8.79) and (8.80) are substituted into Equation (8.71), an equation describing the time rate of change of the location of the phase change interface evolves

$$\frac{dS}{dt} = \frac{\left(\dfrac{\alpha_s\ \overline{Q}_{net}}{K_s}\right)}{\left(2\ B\ \Delta T - \bar{b}^2\ \Delta T + \dfrac{\alpha_s\ \rho_s\ L_{melt}}{K_s}\right)} \tag{8.81}$$

Integrating Equation (8.81) between the limits (S = 0 at t = t_{pc}) and (S(t) at t) yields the following result.

$$S(t) = \frac{\left(\frac{\alpha_s \overline{Q}_{net}}{K_s}\right)(t - t_{pc})}{\left(2 B \Delta T - \hat{b}^2 \Delta T + \frac{\alpha_s \rho_s L_{melt}}{K_s}\right)} \tag{8.82}$$

which is an important equation for the location of the phase change interface in terms of time

From Equations (8.81) and (8.82), the rates of evaporation, sublimation and melting can be calculated as functions of time as follows.

$$Q_{evap}(t) = \overline{Q}_{evap}\, 2\pi\lambda\, S(t) \tag{8.83}$$

$$Q_{sub}(t) = \overline{Q}_{sub}\, 2\pi\lambda\, S(t) \tag{8.84}$$

$$Q_{melt}(t) = (\rho_s L_{melt} \frac{dS}{dt})\, 2\pi\lambda\, S(t) \tag{8.85}$$

where (λ) represents the length of the cooler coil.

Assuming the initial frost thickness on the cooler to be defined as (S_i), then the frost thickness at any instant of time ($S_f(t)$) during the hot-gas defrosting process is calculated as follows:

$$S_f(t) = S_i - S(t) \tag{8.86}$$

8.3. Results and Discussion

The model described above has been tested for three different cases. The first case is for testing the effects of changing the defrost heat input flux on the sublimation, evaporation and melting heat rates along with the frost thickness while keeping the other parameters fixed. The effects of the defrost heat input flux has been tested for three different values as can be seen in Figures 8 3 to 8 6, where the values of the other constant parameters are also shown.

As can be seen, it is clear that the duration of the hot-gas defrosting mode decreases while increasing the defrost heat input flux. The sublimation, evaporation and melting heat rates are all shown to increase with time where the sublimation heat rate is higher than the evaporation heat rate while the latter is higher than the melting heat rate. This observation is shown to be in agreement with what has been observed in the experimental investigation. Part of the rationale for the increasing rates is the fact that the defrost heat input rate itself is an increasing function of time as was reported earlier in this chapter Again, this trend will hold true for relatively short time periods which represent the duration of the defrosting phase.

The margin between the melting heat rate and the other two heat rates (sublimation and evaporation) is shown to decrease with the increase of the defrost heat input flux. The sublimation heat rate is shown to be the same at the termination of the of the hot-gas defrosting process regardless of the defrost heat flux value This observation can also be seen for the evaporation heat rate, but for the melting process, the melting heat rate at the termination of the hot-gas defrosting process is shown to increase with increasing the defrost heat input flux. In the case of the sublimation and evaporation processes, the above observation is attributed to the fact that the sublimation and evaporation heat fluxes are assumed constants in this model. In Figure 8 6, the frost thickness is shown to decrease faster while increasing the defrost heat input flux

The second case tested pertains to the effects of changing the tube diameter on the sublimation, evaporation and melting heat rates along with the frost thickness while

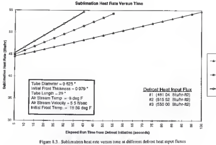

Figure 8.3 Sublimation heat rate versus time at different defrost heat input fluxes

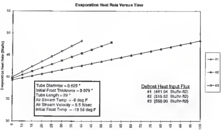

Figure 8.4 Evaporation heat rate versus time at different defrost heat input fluxes

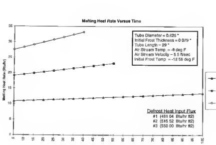

Figure 8.5 Melting heat rate versus time at different defrost heat input fluxes

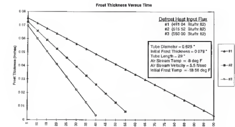

Figure 9 6 Frost thickness versus time at different defrost heat input fluxes keeping the other parameters constant. The effect of the tube diameter has been tested for three different values as can be seen in Figures 8.7 to 8.10 where the values of the other parameters are also shown.

As can be seen, it is clear that the duration of the hot-gas defrosting mode decreases while increasing the tube diameter. The sublimation, evaporation and melting heat rates are all shown to increase with time. Again, this can be partially attributed to the increasing defrost heat input rate. The sublimation heat rate is higher than the evaporation heat rate, while the latter is higher than the melting heat rate except for the third tube diameter where the melting heat rate is higher than the evaporation heat rate. This observation implies that at higher tube diameters, the melting heat rate closes its margins with the other heat rate processes and might even pass them.

The heat transfer rates for the three different modes are shown to increase with increasing tube diameter at the termination of the hot-gas defrosting process. In Figure 8.10, the frost thickness is shown to decrease faster as the tube diameter is increased.

The last case tested pertains to the effects of changing the initial frost thickness on the sublimation, evaporation and melting heat rates along with the frost thickness while keeping the other parameters constant. The effects of changing the initial frost thickness have been tested for three different values as can be seen in Figures 8.11 and 8.12, where the values of the other parameters are also shown.

As can be seen, it is clear that the duration of the hot-gas defrosting mode increases while increasing the initial frost thickness, which is quite logical. The sublimation, evaporation and melting heat rates are all shown to increase with time where the sublimation heat rate is higher than the evaporation heat rate while the latter is higher

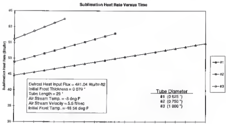

Figure 8 7. Sublimation heat rate versus time at different tube diameters

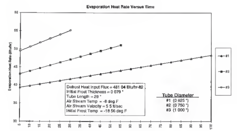

Figure 8 8 Evaporation heat rate versus time at different tube diameters

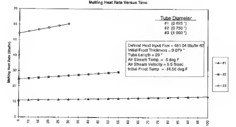

Figure 8.9 Melting heat rate versus time at different tube diameters

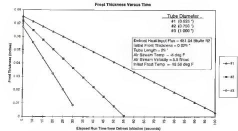

Figure 8.10 Frost thickness versus time at different tube diameters

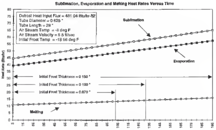

Figure 8 11 Sublimation, evaporation and melting heat rates versus time at different initial frost thicknesses

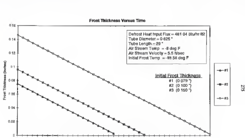

Figure 8.12. Frost thickness versus time at different initial frost thicknesses

than the melting heat rate. This observation is shown to be in agreement with what has been observed in the experimental investigation. In Figure 8.12 the frost thickness is shown to decrease faster while decreasing the initial frost thickness.

8.4. Conclusions

The model developed in this chapter provides interesting qualitative and quantitative trends during the hot-gas defrosting process on a cylindrical coil cooler. The model predicts the duration of the hot-gas defrosting process to decrease with increasing the defrost heat input flux, increasing the tube diameter, and decreasing the initial frost thickness.

The model shows that the evaporation heat rate is always lower than the sublimation heat rate, while the margin between the melting heat rate and the other two modes closes as the defrost heat input flux increases, and as the tube diameter increases.

The frost thickness is shown to decrease faster as the defrost heat input flux increases, the tube diameter increases and as the initial frost thickness decreases.

CHAPTER 9
VISUALIZATION STUDY

The purpose of this chapter is to provide a qualitative assessment of psychrometric processes typically found in industrial freezers. The discussion will include some background information pertaining to psychrometrics in the frost zone and visualization of the frost formation process under different freezer conditions

9.1. Psychrometrics in the Frost Zone

Wile (1944) was probably the first person to investigate psychrometry in the frost zone Wile observed that significant difficulties exist in measuring temperature and humidity at freezer temperatures He noted, for example, that if the wick of a wet bulb thermometer is wetted with subcooled water and calculations are based on ice, large errors may result. Wile also observed that at low air velocities, the psychrometer tends to overpredict the relative humidity while the reverse is true at high air velocities. Difficulties in measuring air relative humidity at low dry bulb temperatures (less than 0°F) can be exemplified by noting the very narrow band in the subsaturated zone of the psychrometric chart shown in Figure 9 1.

One of the major issues associated with industrial freezers is that of infiltration/exfiltration between the cold and dry freezer air and the warmer and more humid surrounding ambient air Figure 9 2 illustrates the frequently encountered

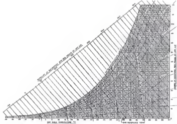

Figure 9.1. Psychrometric chart

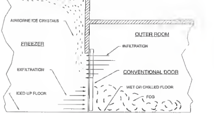

Figure 9 2. Encountered conditions at a typical freezer due to infiltration/exfiltration problems (HCR 1995a) conditions of airborne ice crystals, ordinary fog, ice-up freezer floors and seriously chilled outer room floors found in a typical freezer where infiltration/exfiltration problems exist. These conditions can also be seen in Figures 9.3 and 9.4 which represent an actual industrial freezer that has experienced these problems. Figure 9.3 illustrates fog formation outside freezer entrances and haze (frozen fog particles) flowing inward at freezer entrances (HCR 1995b). Figure 9.4 on the other hand, illustrates snow-like frost accumulations found on coils located near freezer doorways.

A typical infiltration/exfiltration air mixing process across a true-to-life freezer doorway is represented graphically on the psychrometric chart in Figure 9.5. In this figure, the cold and dry freezer air at -10°F (Point F) is shown to mix with the warmer and more humid outer room air at 40°F (Point O). The air path O-F representing the air-mixing process is shown to cross the saturation line and invade the supersaturated zone. The invasion of the supersaturated zone above the water freezing temperature (32°F) in Figure 9.5 represents the fog formation process in the outer room, while the invasion below the water freezing temperature represents the haze formation process inside the freezer (HCR 1995a).

One of the objectives of the research program upon which this dissertation partly reports was to present a qualitative assessment of the different psychrometric processes typically encountered in true-to-life industrial freezers. The following section describes results of a visualization study which was conducted to achieve the aforementioned objective.

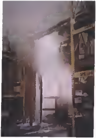

Figure 9.3 Fog and haze formation at an actual freezer entrance (HCR 1995b)

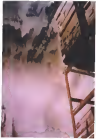

Figure 9.4 Snow-like frost accumulations on an actual freezer coil (courtesy of HCR, Inc.)

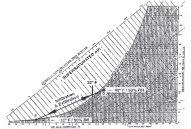

Figure 9.5 Infiltration/exfiltration air path typically encountered at actual freezer doorways (HCR 1995a)

9.2. Visualizations of Frost Formation

A visualization study of the frost formation process on the FCU-T coil has been conducted in this project. The study was to visualize the development of the frost formation on the FCU-T coil as the moist air conditions inside the psychrometric freezer room changed from subsaturated to supersaturated conditions and then restored back to subsaturated conditions. This experiment was performed by operating the FCU-T under its refrigeration mode while continuously injecting steam inside the psychrometric freezer room. The steam injected was produced by the water-vapor generator (WVG).

In this experiment, there was no need to initially operate the FCU-A to bring the FCU-T coil entering air dry bulb temperature to a low value. The operation of the FCU-T under the refrigeration mode started at the initial existing FCU-T coil entering air dry bulb temperature which was 83°F when this experiment was conducted. The steam injection started at the same time.

9.2.1. Subsaturated Conditions

The starting of the FCU-T refrigeration mode and the steam injection process occurred while moist air conditions inside the freezer were subsaturated. The FCU-T coil refrigerant temperature started to drop immediately, while at the same time, the FCU-T coil entering air dry bulb temperature dropped. After about 35 minutes the color of the FCU-T finned tubes turned white which marked the started of frost formation on the FCU-T coil.

The frost formation process under subsaturated conditions is a transformation process of water vapor into frost bypassing the liquid phase. The formation of frost on the

FCU-T coil continued in the form of ice-like frost (ASHRAE 1992b, Smith 1989) where a picture of the FCU-T coil with frost thickness (S_f) of 0.031" can be seen in Figure 9.6. Another picture showing the development of frost formation is shown in Figure 9.7, where the frost thickness is 0.069"

9.2.2. Transition from Subsaturated to Supersaturated Conditions

As the injection of steam inside the psychrometric freezer room continued, the frost thickness continued to grow on the FCU-T coil. It was observed that fog (water droplets suspended in the air) started to form inside the psychrometric freezer room when the frost thickness approached 0.107", while the FCU-T coil entering air dry bulb temperature (EAT) was above the water freezing temperature. The fog formation marked the transition of the moist air conditions from subsaturated to supersaturated. A picture of the FCU-T coil with frost thickness of 0.107" can be seen in Figure 9.8, while a picture showing the fog formation at that thickness is shown in Figure 9.9

9.2.3. Supersaturated Conditions

The frost and fog formation continued to occur during supersaturated conditions of the moist air while steam was being injected inside the freezer. The frost formation process under these conditions is thought to be a combination of two processes: a deposition process in which the water vapor in the air transforms to frost on the finned tubes, and a solidification process in which water droplets in the air transforms to ice on the finned tubes.

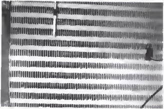

Figure 9.6 Frost formation on the FCU-T coil ($S_f = 0.031''$)

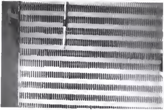

Figure 9.7 Frost formation on the FCU-T coil ($S_f = 0.069''$)

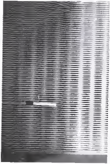

Figure 9.8 Frost formation on the FCU-T coil ($S_f = 0.107''$)

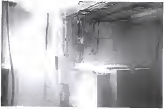

Figure 9.9 Fog formation at $S_f = 0.107''$

As the FCU-T refrigeration cycle continued to cool the freezer under supersaturated conditions, it was observed at a later time that haze (airborne ice crystals) started to form inside the room, while the FCU-T coil entering air dry bulb temperature (EAT) was below the water freezing temperature. These airborne ice crystals are thought to be developed by the freezing of some of the water droplets suspended in the air. A picture of the FCU-T coil under these conditions with a frost thickness of 0.146" can be seen in Figure 9.10. Another picture showing the development of frost formation under the same conditions is shown in Figure 9.11 with a frost thickness of 0.184", while a picture showing haze formation (airborne ice crystals) at that thickness ($S_f = 0.184"$) is shown in Figure 9.12.

Airborne ice crystals were observed to precipitate on the FCU-T finned tubes forming snow-like frost (ASHRAE 1992b, Smith 1989), which is of a different nature than the ice-like frost. The snow-like frost formation process under supersaturated conditions is thought to be a combination of three processes: a deposition process in which water vapor in the air transforms to frost on the finned tubes, a solidification process in which water droplets in the air transforms to ice on the finned tubes, and a solid to solid transformation in which the airborne ice crystals precipitate on the FCU-T finned tubes forming snow-like frost.

After frost formation has reached a thickness of 0.184", the amount of steam injected inside the freezer has been increased heavily in order to put the latter under severe supersaturated conditions. More haze formation has been visualized to occur, while the air circulated in fast movement inside the room. Two pictures of haze formation can be seen in Figures 9.13 and 9.14. The second picture (Figure 9.14) was taken a few seconds

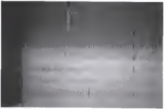

Figure 9.10 Frost formation on the FCU-T coil ($S_f = 0.146''$)

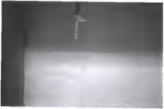

Figure 9 11 Frost formation on the FCU-T coil ($S_f = 0\ 184"$)

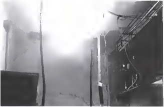

Figure 9.12. Airborne ice crystals at $S_f = 0.184$"

Figure 9 13 Haze formation

Figure 9 14 Haze formation -- a few seconds later after the first picture (Figure 9.13), as can be seen by the more intense haze covering the view of the duct opening in Figure 9.14.

As the heavy steam injection inside the room continued, more and more haze was observed to occur. Two pictures of haze formation under severe supersaturated conditions can be seen in Figures 9.15 and 9.16 for the location under the duct opening. The second picture (Figure 9.16) gives a close-up view. A picture of the FCU-T while being clogged by the unfavorable snow like frost under severe supersaturated conditions can be seen in Figure 9.17. The term "unfavorable" refers to the effects of this frost on the coil performance as it reduces the coil heat transfer rate (ASHRAE 1992b; Smith 1989). A picture of the FCU-T fan outlet being clogged under severe supersaturated conditions can be seen in Figure 9.18.

9.2.4. Transition from Supersaturated to Subsaturated Conditions

While moist air inside the freezer is still under severe supersaturated conditions, the steam injection process and the FCU-T refrigeration mode have both been terminated at the same time. Soon after the termination, the frost accumulated on the FCU-T finned tubes was observed to undergo a sublimation process (a solid to vapor transformation) where the frost on the finned tubes transforms to water vapor. This sublimation process marked the transition of moist air conditions from supersaturated to subsaturated. A picture of the FCU-T while the frost is sublimating can be seen in Figure 9.19.

When moist air conditions have been restored back to the subsaturated conditions, the remaining frost on the FCU-T finned tubes started to melt. A picture of the FCU-T

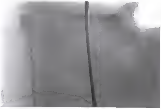

Figure 9.15 Supersaturated conditions

Figure 9 16 A close-up view of supersaturated conditions

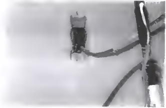

Figure 9.17 Unfavorable frost formation under severe supersaturated conditions

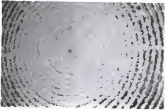

Figure 9.18 Clogging of FCU-T fan outlet under severe supersaturated conditions

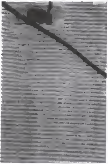

Figure 9.19 Frost sublimating

frost melting after subsaturated conditions have been restored can be seen in Figure 9.20, while a picture of the frosted FCU-T under these conditions is shown in Figure 9.21

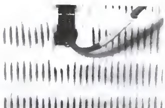

Figure 9.20 Frost melting after subsaturated conditions have been restored

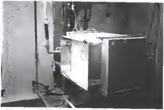

Figure 9.21 Frosted FCU-T after subsaturated conditions have been restored

CHAPTER 10
CONCLUSIONS AND RECOMMENDATIONS

10.1. Conclusions

Visualization studies of the frost and fog formation as moist air conditions inside the freezer changed from subsaturated to supersaturated indicated that the frost formed is ice-like. The fog (liquid water droplets suspended in air) would start to form while the test fan-coil unit (FCU-T) coil entering air dry bulb temperature (EAT) is above the freezing temperature of water. Fog formation marked the transition of moist air conditions from subsaturated to supersaturated.

Haze (airborne ice crystals) formation under supersaturated conditions inside the freezer was observed to occur while the FCU-T coil entering air dry bulb temperature (EAT) was below the freezing temperature of water. During supersaturated conditions airborne ice crystals were visualized and were observed to precipitate on the FCU-T tubes as snow-like frost. This frost was observed to clog the coil and reduce the coil thermal performance. Hence the term "unfavorable frost" was used to define snow-like frost as compared with the more favorable ice-like frost.

The frost sublimation observed at the termination of the steam injection process and the FCU-T refrigeration mode marked the transition of moist air conditions from supersaturated to subsaturated. This sublimation process was thought to occur when the air inside the freezer was starved for moisture. The sublimation of frost into the freezer was observed to continue until an equilibrium state has been reached at which point the frost stopped subliming and started to melt.

During the hot-gas defrosting mode, this investigation revealed that a major part of the frost accumulated on the coil escapes as moisture inside the freezer, while a smaller part of the frost removed from the coil collects as melt. The moisture escaped was shown to be an underestimated latent load component imposed on the refrigeration system. This observation held true regardless of the coil inlet conditions and despite the fact that the rate of both evaporation and sublimation on the coil surface was artificially enhanced by the convection currents created by the auxiliary fan-coil unit (FCU-A). This fan-coil unit was forced to operate during the defrosting phase of the test fan-coil unit (FCU-T) in order to help capture the moisture generated by defrosting the latter. While this is the usual practice in real life refrigeration applications, the rate of both evaporation and sublimation from FCU-T may have been slightly overpredicted due to the smaller freezer room size relative to that of the coil. However, the amount of both the moisture escaped and the melt collected in the second and third cycles of the complete refrigeration/defrost run continuously decreased. While the absolute amount decreased for both quantities, the relative amount of the moisture escaped continued to be far more significant than the melt collected.

Based on the testing results obtained for several coil entering air dry bulb temperatures (EAT), the investigation revealed that the defrost heat load's 15% rule of thumb is sufficiently accurate for purposes of industrial freezers design. The accuracy of this rule of thumb deteriorates in cases involving higher latent loads.

The analytical model developed in this study indicated that the duration of the hot gas defrosting process will decrease with increasing the defrost heat input flux, increasing the tube diameter, and decreasing the initial frost thickness. The model also showed the frost thickness to decrease faster as the defrost heat input flux increases the tube diameter increases, and as the initial frost thickness decreases.

10.2. Recommendations

Results of this project have brought about several important matters that deserve further extensive investigations. The refrigeration/defrost system built for this phase of the project is capable of handling these investigations with minor modifications to the system. These investigations should provide the refrigeration industry with an extensive body of original data pertaining to the heat loads associated with hot gas defrosting of freezer coils as well as an insightful understanding of the psychrometrics of freezer air-cooling processes under frosting conditions.

Future investigations should focus on providing a clear understanding of the role played by the moisture escaped during coil defrosting inside the freezer and the latent load associated with it. It is believed that the lack of information regarding the amount of this latent load and the associated increase in the rate of frost formation during the FCU-T refrigeration segment of the refrigeration/defrost cycle is a major reason why the present practices of refrigeration load calculations sometimes give unsatisfactory results when used by the industry Future needed investigations are described below

1- Tests performed in this project were intended to determine the heat loads due to coil defrosting using the hot gas method for a fan-coil unit having a face velocity of 750 feet per minute Tests were performed for a fan-coil unit with entering air dry bulb temperatures (EAT) of -8°F and 13°F at several load sensible heat ratios. One possible investigation is to repeat these tests for several other face velocities. 250, 500 750 1000, 1250, and 1500 feet per minute This should provide insight into the effects the fan-coil unit face velocity would have on the coil defrosting loads.

2- Another possible investigation is to repeat the above (Item 1) while setting the defrost initiation to the following thicknesses: 0.079", 0.117", 0.127", 0.146" and 0.165" This is believed to provide insight in choosing the optimum defrost initiation conditions that minimize the latent load during the defrosting process.

3 A third possible investigation is to repeat the above (Items 1 and 2) for fan-coil units of 8, 10 and 12 rows, as this is potentially capable of providing a large body of data which can be used for selecting the best conditions for a specific coil design from a defrosting load point of view

4- In this project, termination of the defrosting processes (electric and hot-gas) was based on visual observations. Defrosting in both cases was terminated when the frost has been physically removed and the tubes have been dried out. An investigation of the above three items while keeping electric defrosting terminated by visual observations and specifying a duration time for the hot-gas defrosting mode should provide insight into the best way to terminate hot gas defrosting This type of investigation can be performed for hot-gas defrosting durations of 5, 10, 15, 20, 25 30, 35 40, and 45 minutes. The defrosting efficiency (η_D) should be computed in all cases tested.

5- The relationship among the latent load inside the freezer, the frost thickness, the fan-coil unit entering air dry bulb temperature (EAT), time, and the load sensible heat ratio during the fan-coil unit refrigeration mode should also be investigated. This should provide an insight into the frosting processes and can produce correlations among the aforementioned variables. The system built in this project is capable of handling this type of investigation as the latent load can be provided by the water-vapor generator.

6- An investigation of the air movement around liquid overfeed fan-coil units during hot-gas defrosting is needed as this is believed to provide a better understanding of moisture movement in the freezer during hot-gas defrosting.

While resolving the above issues is of major importance in order to be able to properly quantify the heat loads associated with coil defrosting using the hot-gas method, it is important to emphasize that these issues cannot be all addressed in one research project. The author thus believes that these proposed investigations should be prioritized in accordance with their relevance to the issues facing the refrigeration industry today

APPENDIX A
DESCRIPTION OF THE CONDENSING UNIT

A schematic describing the system layout of the condensing unit can be seen in Figure A.1, while a summary description of associated auxiliaries can be seen in Table A.1. The unit is equipped with a high efficiency Krack condenser (model A), with a coil of staggered copper tubes arranged in three rows, in order to provide a large heat transfer area, where the tubes have 3/8" outside diameter. The refrigerant in the condenser coil is air-cooled by three fans installed on the top of the condenser. Each fan has a diameter of 24" and a speed of 1140 RPM and is operated by a 1/2-hp Franklin motor (Krack 1992b).

The system shown in Figure A.1 was modified by incorporating two Sporlan crankcase pressure regulating valves (model numbers CRO-10-0/60 and CROT-10-0/60), connected in parallel on the suction line downstream of the suction accumulator (Items 3 and 4 in Figure A.1). The two valves are hermetic (Sporlan 1989) and are identical except for the fact that one of them (Item 4) has a pressure tap on its inlet side. A crankcase pressure regulating valve is sensitive only to its outlet pressure (also called compressor crankcase or suction pressure). The valve throttles to open as its outlet pressure drops below a preset maximum crankcase pressure value and throttles to close as its outlet pressure rises toward the preset value. The valve will be fully closed when the outlet pressure is equal to or higher than the preset maximum crankcase pressure value (Sporlan

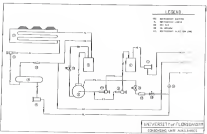

Figure A.1 Schematic diagram of the condensing unit with auxiliary components

Table A.1 Summary Description of the Condensing Unit Auxiliaries

Item	Manufacturer	Model Number	Description
1	SPORLAN	RSF-4817-T	Replaceable Suction Filter
2	REFRIGERATION RESEARCH	3639	Suction Accumulator
3	SPORLAN	CRO 10-0/60	Crankcase Pressure Regulating Valve # 1
4	SPORLAN	CROT 10-0/60	Crankcase Pressure Regulating Valve # 2
5	COPELAND	4DL3 1500-TSK	Compressor
6	AC&R	S-5690	Oil Separator
7	KRACK	A	Condenser
8	SPORLAN	OR1-6-65/225 H	Head Pressure Control Valve # 1
9	KRACK	E150732	Liquid Receiver
10	SPORLAN	C-967-M-G	Replaceable Core Filter-Drier
11	SPORLAN	SA-17S	Moisture and Liquid Indicator
12	SPORLAN	ORD-4-20	Head Pressure Control Valve # 2
13	ALCO	202CB-1/8B-1/16T	Oil Return Solenoid Valve
14	SUPERIOR	586W-8ST	Ball Valve
15	SPORLAN	C-163-S	Sealed Filter Drier
16	PARKER	H23TR	Injection Solenoid Valve

1994a). Therefore, its function is not to hold a constant crankcase pressure, but to limit a maximum crankcase pressure from occurring (Tomczyk 1996a).

Each of the two crankcase pressure regulating valves is employed with an inlet strainer and each has a pressure adjusting spring to preset a maximum crankcase pressure value, where the pressure adjustment ranges from 0 to 60 psig. Since during and after the defrosting mode and also after a normal shut down period the evaporator pressure will be high, it was found necessary to modify the system in order to protect the compressor motor from overloading by limiting the suction pressure (Sporlan 1994a). This action also contributes to relieving the excessive stress on the compressor (Tomczyk 1996a). These valves were set at 30 psig which helped control the amperage on the compressor motor.

The Krack liquid receiver (model number E150732) has a large storage capacity capable of storing up to 192 pounds of R-22 (Item 9 in Figure A.1), where the receiver length is 72" and its outside diameter is 10-3/4" (Krack 1992b). This receiver is a flow-thru type receiver in which the liquid refrigerant enters and leaves from tangential connections located at its bottom. This feature in the receiver will allow liquid subcooling to be maintained (Krack 1992a). The suction accumulator (Item 2 in Figure A.1) is manufactured by Refrigeration Research, Inc. (model number 3639) and its function is to protect the compressor from any sudden return of liquid refrigerant, where the latter is held inside the suction accumulator, and is then metered back to the compressor through a metering orifice. The suction accumulator has a height of 20" and an outside diameter of 8-5/8" (Refrigeration Research 1996).

An oil separator (Item 6 in Figure A.1) manufactured by AC&R (model number S-5690) is located in the condensing unit downstream of the compressor. This oil separator has a height of 15 5/8" and an outside diameter of 6", while the inlet and outlet refrigerant connections are employed with fine mesh screens (AC&R 2-025-001). An AC&R heat band (model number S9112) is fixed within 1 1/2" from the bottom of the oil separator. This heat band is six inches in diameter and works at 50 Watts and 220 Volts. It will be in operation at all times whether the system is in operation or not, in order to prevent the refrigerant gas from migrating and condensing inside the oil separator (AC&R 2 025-012).

A normally-closed solenoid valve manufactured by Alco Controls (model number 202CB-1/8B 1/16T) is located on the oil return line between the oil separator and the compressor crankcase (Item 13 in Figure A.1). This is a direct acting two-way valve that is to be energized by the compressor oil level float switch when the crankcase oil level drops. This will cause the oil to flow from the oil separator into the compressor crankcase.

The condensing unit is employed with two Sporlan head pressure control valves (model numbers ORI-6-65/225-H and ORD-4-20) which will maintain a constant receiver pressure in order for the unit to operate reliably under different ambient temperatures (Items 8 and 12 in Figure A.1). The two valves are hermetic (Sporlan 1990a) and are equipped with inlet strainers, while only one of them (Item 8) is an adjustable control valve (Sporlan 1986). The latter valve is sensitive only to its inlet pressure (condenser pressure) and is located between the condenser and the receiver. This valve throttles to close as its inlet pressure drops toward a preset minimum receiver pressure value, and throttles to open as its inlet pressure rises above the preset value. It will be fully closed when the condenser pressure is equal to or lower than the preset minimum receiver pressure value. The adjustable control valve has a pressure adjusting spring to preset a minimum receiver pressure value where the pressure adjustment ranges from 65 to 225 psig (Sporlan 1986).

The other head pressure control valve (Item 12 in Figure A.1) is a non-adjustable control valve that is located in a hot gas line bypassing the condenser and extending into the receiver. This control valve is sensitive to the pressure differential across it (the difference in pressure between the condenser and the receiver). The manufacturer differential pressure setting for this valve is 20 psi, where the valve starts throttling to open at this value and will be fully open when the differential pressure reaches 30 psi (Sporlan 1986). When the adjustable head pressure control valve restricts the flow of liquid refrigerant from the condenser to the receiver, a pressure differential is created across the adjustable valve, and when this differential pressure reaches 20 psi, the non-adjustable head pressure control valve starts to open and bypasses hot gas to the receiver. Since the refrigeration system utilizes hot-gas for coil defrosting and for compressor capacity control, it is important for the condensing unit to have a good head pressure to operate properly during different ambient temperatures.

In order to protect the condensing unit lines and auxiliaries from dirt, moisture, acids, sludges and varnish, the unit is employed with Sporlan replaceable suction filter (model number RSF-4817-T), Sporlan sealed filter-drier (model number C-163-S), Sporlan replaceable core type filter-drier (model number C-967-M-G), and Sporlan moisture and liquid indicator (model number SA 17S). These components serve as a guarding mechanism to the refrigeration system.

The Copeland compressor (model number 4DL3-1500-TSK) represents the heart of the condensing unit (Item 5 in Figure A.1). It is a 15-hp compressor that has four cylinders. The compressor is employed with overload protection suction and discharge service valves, a manual reset oil pressure safety switch, and high/low pressure control (Krack 1992a 1992b). The compressor crankcase includes an oil level sight glass and a Copeland crankcase heater (model number 518-0002-02) that works at 100 Watts and 240 Volts. This heater serves to prevent the refrigerant from condensing inside the crankcase.

The Parker injection solenoid valve (model number H23TR) installed on the refrigerant injection line (Item 16 in Figure A.1) is part of a demand cooling system employed by Copeland on all their compressors using R-502 in order for these compressors to be able to operate using R-22, as an alternative to R-502, for low temperature applications (Copeland 1990a; 1990b). The demand cooling system was employed considering the fact that R-502 is being phased out due to its high ozone depletion potential (ODP), and the fact that R-22 can create some problems in low temperature applications, where under some conditions, the temperature of R-22 at the internal discharge of the compressor exceeds the safe temperature limit required for the stability of the refrigeration oil (Copeland 1990b). A Superior ball valve (model number 586W-8ST) is located on the refrigeration injection line upstream of the injection solenoid valve. This valve (Item 14 in Figure A.1) is used to adjust the amount of the liquid refrigerant required by the demand cooling system.

The demand cooling system diagram is shown in Figure A.2, where it consists of a control module, a temperature sensor and an injection solenoid valve. The temperature sensor senses the internal discharge temperature of the compressor and sends an input signal to the control module. The control module checks this input signal and compares it to a preset internal discharge critical temperature (292°F). If the input signal is found to

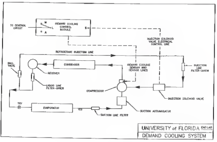
TO CONTROL CIRCUIT
M
L
A
DEMAND COOLING CONTROL MODULE
S
INJECTION SOLENOID VALVE ELECTRICAL CONTROL LINE
REFRIGERANT INJECTION LINE
BALL VALVE
CONDENSER
RECEIVER
LIQUID LINE FILTER-DRIER
DEMAND COOLING SENSOR AND SENSOR LINES
INJECTION LINE FILTER-DRIER
COMPRESSOR
INJECTION SOLENOID VALVE
TXV
EVAPORATOR
SUCTION LINE FILTER
SUCTION ACCUMULATOR
UNIVERSITY of FLORIDA CAD LAB
DEMAND COOLING SYSTEM

Figure A.2. Demand cooling system diagram

be higher than the preset critical temperature (292°F), the control module will send an output signal to energize the injection solenoid valve to open and meter the flow of refrigerant from the receiver to the suction cavity of the compressor in order to cool the suction gas. This injection process will continue until the internal discharge temperature of the compressor reaches (282°F), at which point the control module sends an output signal to de-energize the injection solenoid valve. The control module has another function to perform if the input signal from the temperature sensor is found to be higher than a preset maximum temperature (310°F). The control module will energize its normally closed alarm relay contact and turns the compressor off where the relay can be reset manually (Copeland 1990a, 1990b).

APPENDIX B
DESCRIPTION OF THE PIPING SYSTEM

The layout of the piping system is described here with reference to Figure 2.10 and Table 2.1 in Chapter 2. When the refrigeration/defrost system is in operation, the liquid refrigerant flows from the condensing unit receiver into the 1-1/8"OD main liquid line through the main liquid line solenoid valve (Item 18 in Figure 2.10). This Sporlan valve (model number MB25S2) is a normally-closed solenoid valve that is energized to open for the liquid refrigerant to flow into the piping system. This valve plays a major role in the control of the system pump down process during which time the valve is de-energized to close such that the system refrigerant is pumped into the receiver. This process is important since it will prevent high suction pressure during system startup which in turn will prevent overloading the compressor motor.

The liquid refrigerant then flows through a schrader valve, a full view flow meter and the surge drum liquid level control valve (Items 48, 28 and 14, respectively, in Figure 2.10) before entering the surge drum. The surge drum is a pressure vessel that serves as liquid refrigerant storage and as a liquid-vapor separator (Stoecker 1988). The schrader valve is used as a gage port to read the pressure of the main liquid line and is also used to charge and discharge refrigerant from the system (Pita 1991 Whitman and Johnson 1991).

The indicating type full view flow meter (Item 28 in Figure 2.10) is manufactured by Brooks Instrument (model number 1114CJ36CSAAA) and has a metal reading scale with a range of 0.13 to 1.3 gpm. This scale is 250 millimeter in length and is especially calibrated for liquid refrigerant R-22. The full-view flow meter is designed to operate for pressures and temperatures up to 300 psig and 250°F, respectively (Brooks 1991). The full-view flow meter was helpful in this research by being able to identify the condition of the refrigerant coming from the condensing unit receiver.

The surge drum liquid level control valve (Item 14 in Figure 2.10) is manufactured by Sporlan valve company (model number LMC-PVE-5-1/2) and is used to maintain the liquid level inside the surge drum at the desired static level, where the valve is employed with an adjusting stem and spring assembly for that purpose (Sporlan 1990b). This control valve is a standard Sporlan thermostatic expansion valve (type F) which is employed with a Level Master Control (LMC) element. The latter is an insert type sensing bulb incorporating a low wattage heater. The insert sensing bulb has a volatile fluid within it, called a thermostatic charge, which is responsive to the external heat applied on the insert sensing bulb. The heater of the LMC element operates at 120 Volts and has a power of 15 Watts (Sporlan 1990b). The control valve is an externally equalized valve (Sporlan 1981) where a 3/8"OD copper external equalizer connects the valve to the suction line as shown in Figure 2.10.

The operating mechanism of the surge drum liquid level control valve is based on three forces associated with three pressures acting on the valve's diaphragm. The spring and equalizer pressures act underneath the diaphragm in order to close the valve. The spring pressure is the adjustable pressure by the stem and spring assembly, while the equalizer pressure is the suction pressure. The third acting pressure is the insert bulb pressure acting on the top of the diaphragm in order to open the valve, where this pressure is a function of the thermostatic charge temperature. When the valve is in operation, the opening pressure must equal the closing pressure in order to maintain the liquid level inside the surge drum at the desired static level (Sporlan 1990b, 1993b)

The insert sensing bulb is installed inside the surge drum at the position of the desired static liquid level, and is connected to the valve by a 10-foot standard capillary tube of 1/8"OD When the liquid level at the insert sensing bulb drops, the heat provided by the heater increases the thermostatic charge pressure within the bulb which causes the valve to open and the liquid refrigerant to flow inside the surge drum in order to fill the latter to the desired static liquid level again On the other hand, when the liquid level at the insert sensing bulb rises, the heat provided by the heater is balanced by the transfer of heat from the bulb to the liquid refrigerant which decreases the thermostatic charge pressure and causes the valve either to modulate or shuts off depending on how high the rise of the liquid level was The heater must be on as long as the system is in operation and turned off otherwise since this will prolong the life of the thermostatic switch employed with the heater assembly This switch protects the LMC element against excessive heat (Sporlan 1990b).

The surge drum liquid level control valve is employed with a permanent coarse mesh strainer disc in its inlet connection (Sporlan 1981) This strainer is useful in protecting the valve by preventing scale particles, solder and other fine obstacles from entering the valve, otherwise these particles will damage the valve by affecting its modulating ability (Sporlan 1990c)

A Viking liquid refrigerant pump (model number SG-40550) is used to pump liquid refrigerant from the surge drum to any of the two fan-coil units when that unit is operating under the refrigeration mode The liquid refrigerant flows in a 7/8"OD copper tube and passes through the surge drum liquid line isolation valve, the liquid refrigerant pump, a turbine flow meter and a shut off valve (Items 39 52, 30 and 50 respectively, in Figure 2.10) before branching to the fan-coil unit which is operating under the refrigeration mode The Superior surge drum liquid line isolation valve (model number 587WA-14ST) is a ball valve (Item 39) used to isolate the surge drum when service and maintenance are needed for the piping system. It is also used to adjust the flow of the liquid refrigerant.

The liquid refrigerant pump (Item 52) has a bypass line with a Superior hand operated throttling valve (model number 255A-8S) that is used to adjust the liquid refrigerant flow rate through the liquid pump and to protect the liquid pump motor from overloading (Item 47 in Figure 2.10) The shut-off valve (Item 50) is manufactured by Parker Hannifin Corporation (model number QL171R-14-14), and is used to isolate the main liquid refrigerant line from the liquid line branches of the two fan-coil units when service and maintenance are needed. The shut-off valve has a service port that is designed for schrader type ports to be used to charge and discharge refrigerant from the system.

The turbine flow meter (Item 30) is manufactured by Signet Scientific Company (model number MK-525) and is used to measure the mass flow rate of the liquid refrigerant. Its flow sensor is a paddlewheel transducer that is interfaced with a computer to read and store the transducer output. The flow meter is also equipped with a Signet analog flow meter (model number MK-584) The paddlewheel transducer is mounted on a mini-tap fitting constructed in house This mini-tap fitting is welded to the liquid refrigerant pipe, where the paddlewheel is housed

After passing the shut-off valve, the liquid refrigerant will flow through the liquid refrigerant branch of the fan coil unit that is operating under the refrigeration mode. If the FCU-T is operating under the refrigeration mode, then the FCU-T liquid line solenoid valve (Item 2 in Figure 2.10) is energized to open allowing the liquid refrigerant to flow and pass through the FCU-T liquid line check valve and a hand operated throttling valve (Items 25 and 3, respectively, in Figure 2.10). The liquid refrigerant then enters the FCU-T and leaves as wet return, where then the latter flows in a 1-1/8"OD copper tube and passes through the FCU-T wet return stop solenoid valve, which is a normally-opened solenoid valve, and the FCU-T wet return check valve (Items 15 and 19, respectively, in Figure 2.10) before it connects to the 1-3/8"OD main wet return line.

During this refrigeration mode of the FCU-T, the FCU-A liquid line solenoid valve (Item 4 in Figure 2.10) is de-energized to close since at that time the FCU-A is either unloaded or operating under the electric defrosting mode. This de-energizing process of the FCU-A liquid line solenoid valve (Item 4) is important to prevent the liquid refrigerant from entering the FCU-A and also to allow the liquid refrigerant to flow from the main liquid refrigerant line into the liquid refrigerant branch to FCU-T.

When the FCU-A is operating under the refrigeration mode, the FCU-A liquid line solenoid valve (Item 4 in Figure 2.10) is energized to open allowing the liquid refrigerant to flow and pass through the FCU-A liquid line check valve and a hand operated throttling valve (Items 1 and 5, respectively, in Figure 2.10). The liquid refrigerant then enters the FCU-A and leaves as wet return, where then, the latter flows in a 1-1/8"OD copper tube and passes through FCU-A wet return check valve as well as the FCU-A wet return stop solenoid valve which is a normally-opened valve (Items 26 and 38 respectively, in Figure 2.10), before it connects to the 1-3/8 'OD main wet return line.

During this refrigeration mode of the FCU-A, the FCU-T liquid line solenoid valve (Item 2 in Figure 2.10) is de-energized to close since at that instant the FCU-T is either unloaded or operating under the hot-gas defrosting mode. This de-energizing process of the FCU-T liquid line solenoid valve (Item 2) is important to prevent the liquid refrigerant from entering the FCU-T and also to allow the liquid refrigerant to flow from the main liquid refrigerant line into the liquid refrigerant branch to the FCU-A.

The FCU-T liquid line solenoid valve is identical to the FCU-A liquid line solenoid valve (Items 2 and 4, respectively, in Figure 2.10) and are both manufactured by Sporlan Valve Company (model number E19S270). They are normally-closed solenoid valves. Each of the two valves is energized to open when its fan-coil unit is operating under the refrigeration mode, and de-energized to close when its fan-coil unit is unloaded or operating under the defrosting mode.

The FCU-T liquid line check valve is identical to the FCU-A liquid line check valve (Items 25 and 1, respectively, in Figure 2.10) and are manufactured by Superior valve company (model number 805C-14S). These check valves are used in the system in order to prevent backflow of refrigerant to the main liquid refrigerant line. The two hand operated throttling valves (Items 3 and 5 in Figure 2.10) are also identical and are manufactured by Superior valve company (model number 257B-14S). Each of the two valves is used to adjust the flow of the liquid refrigerant into the fan-coil unit it serves in order to have a proper overfeed recirculation in the respective fan-coil unit.

The FCU T wet return stop solenoid valve is identical to that of the FCU-A (Items 15 and 38, respectively, in Figure 2.10) and are both manufactured by Sporlan Valve Company (model number OE34S290) They are normally-opened solenoid valves. Each of the two valves is energized to close when its fan-coil unit is operating under the defrosting mode, and de-energized to open when its fan-coil unit is unloaded or operating under the refrigeration mode. The FCU T wet return check valve is identical to that of the FCU-A (Items 19 and 26, respectively, in Figure 2 10) and are manufactured by Superior valve company (model number 806C 11S). These valves are used in the system in order to prevent backflow of wet return to the fan-coil units

The refrigeration mode of the FCU-A is terminated by de-energizing the FCU-A liquid line solenoid valve to close and also energizing the FCU-A wet return stop solenoid valve to close (Items 4 and 38 respectively in Figure 2.10) After closing the valves, the electric defrosting mode of the FCU-A is initiated which increases the pressure and temperature of the refrigerant inside the FCU-A finned tubes. This increase in pressure will force the heated refrigerant to leave the FCU-A and flow through the FCU-A wet return check valve and the FCU A heated refrigerant strainer (Items 26 and 37, respectively, in Figure 2.10)

The heated refrigerant will not be able to flow through the FCU-A heated refrigerant pressure regulator (Item 36 in Figure 2.10) unless the pressure of the heated refrigerant reaches 70 psig This is an inlet pressure regulator which has a preset inlet pressure value of 70 psig. The heated refrigerant pressure regulator starts to open at that pressure value and modulates the heated refrigerant flow to the 1 3/8"OD main wet return line. The FCU A heated refrigerant pressure regulator closes when the pressure of the heated refrigerant at its inlet drops below 70 psig. This pressurizing process is needed to hold the heated refrigerant inside the FCU A finned tubes for a suitable period of time in order to confirm and speed the removal of all the frost accumulated on the finned tubes and also to dry out the finned tubes.

The FCU-A heated refrigerant pressure regulator and strainer (Items 36 and 37, respectively, in Figure 2.10) are manufactured by Refrigerating Specialties Divison of the Parker Hannifin Corporation (model numbers A4AK and RSF-SIZE-1", respectively). The strainer is close coupled with the pressure regulator, and has a 60 mesh stainless steel screen capable of collecting very small particles of diameter sizes up to six thousands of an inch. This strainer is used in the system to protect the pressure regulator from dirt and foreign materials which might damage the pressure regulator. The strainer is designed to operate at pressures up to 300 psig and has a 3/8" FPT drain connection to be used for refrigerant draining when strainer maintenance is needed (Refrigerating Specialties 1991a).

The FCU-A heated refrigerant pressure regulator (Item 36 in Figure 2.10) is a heavy duty pilot operated inlet pressure regulator with a size 3/4" port. The regulator has an iron alloy body with stainless steel diaphragm and a chrome plated pilot seat. This regulator is designed to operate at pressures up to 300 psig and a temperature range of -50°F to 220°F. The regulator starts to open on the rise of the inlet pressure above the preset value of 70 psig and modulate the flow of the heated refrigerant such that the inlet pressure stays constant. The regulator will be fully open when the pressure drop across the regulator reaches a value of 2 psig. The preset value of the inlet pressure can be adjusted to any other needed value in the range of 0 to 150 psig by rotating the adjusting stem of the inlet pressure regulator to the new desired preset pressure value (Refrigerating Specialties 1991b)

The refrigeration mode of the FCU-T is terminated by de-energizing the FCU-T liquid line solenoid valve to close and also energizing the FCU-T wet return stop solenoid valve to close (Items 2 and 15, respectively, in Figure 2 10) After the closing of these valves, the hot-gas defrosting mode of the FCU-T is initiated by having the hot-gas flow from the condensing unit in a 3/4"OD copper tube and pass through the main hot-gas line solenoid valve which is energized to open, the piercing valve, the hot-gas defrost solenoid valve which is energized to open, a hand operated throttling valve and the hot-gas orifice meter (Items 7, 54, 31, 8 and 32, respectively, in Figure 2.10) before entering the FCU-T drain pan.

The main hot-gas line solenoid valve (Item 7 in Figure 2.10) is manufactured by Sporlan Valve Company (model number B10S2) It is a normally-closed solenoid valve that is energized to open for the hot-gas to flow into the hot-gas bypass line. This valve is kept energized during all the refrigeration/defrost cycles in order to have hot-gas access to the hot-gas bypass line, where the latter and the components installed on it play an important role in the compressor capacity control system as described in Section 2.1 4.6 This valve plays a major role in the control of the pump down process, at which time the valve is de energized to close such that the system refrigerant is pumped into the receiver

The piercing valve (Item 54 in Figure 2.10) is manufactured by Watsco Components, Inc (model number WAT-B1-10S) and is used to gain access to the hot-gas line in order to charge and discharge refrigerant from the system This valve is also used as a gage port to read the pressure of the main hot gas line (Althouse et al 1988) The hot gas defrost solenoid valve (Item 31 in Figure 2 10) is manufactured by Sporlan Valve Company (model number MB19S2) It is a normally-closed valve that is energized to open only when the FCU-T is operating under the hot-gas defrosting mode.

The hand operated throttling valve (Item 8 in Figure 2 10) is manufactured by Superior valve company (model number 216-10ST) and is used to adjust the flow of the hot-gas into the FCU-T The hot-gas orifice meter (Item 32 in Figure 2 10) is manufactured in house (model M1) and is used to measure the mass flow rate of the hot-gas

After passing the hot-gas orifice meter the hot-gas enters the FCU-T drain pan and flows through the six copper tube passes at the bottom of the drain pan in order to remove the frost accumulated in the latter The hot-gas then leaves the FCU-T drain pan and passes through the hot-gas line check valve (Item 35 in Figure 2.10) on its way to the FCU-T wet return line This valve is manufactured by Watsco Components Inc., (model number MS-10) and has a copper body with a built in stainless steel strainer The valve is used in order to prevent backflow of refrigerant into the hot-gas line when the FCU-T is unloaded or is operating under the refrigeration mode The hot-gas then enters the FCU-T again through the FCU-T wet return line since this is a top hot-gas feed fan-coil unit, where the hot-gas mixes with the cold refrigerant inside the FCU-T finned tubes and leaves the FCU T through the FCU-T liquid line. The mixed refrigerant leaving the FCU-T will be called here "defrost refrigerant" to differentiate it from the "heated refrigerant" mentioned before when describing the electric defrosting mode of the FCU A.

The mixing of the hot-gas with the cold refrigerant inside the FCU-T finned tubes will increase the pressure and temperature of the leaving defrost refrigerant. This increase in pressure will force the leaving defrost refrigerant to flow in a 5/8"OD copper tube and to pass through the defrost refrigerant solenoid valve (which is energized to open) the defrost refrigerant isolation valve, and the FCU-T defrost refrigerant strainer (Items 6, 46 and 24 respectively, in Figure 2.10) The defrost refrigerant solenoid valve is identical to the main hot-gas line solenoid valve (Items 6 and 7, respectively, in Figure 2.10) and is only energized to open when the FCU-T is operating under the hot-gas defrosting mode.

The FCU-T defrost refrigerant strainer is identical to the FCU-A heated refrigerant strainer (Items 24 and 37 respectively, in Figure 2.10) The defrost refrigerant will not be able to flow through the FCU-T defrost refrigerant pressure regulator (Item 17 in Figure 2.10) unless the saturated pressure of the defrost refrigerant reaches 70 psig, which is the preset inlet pressure value of this regulator The FCU-T defrost refrigerant pressure regulator is identical to the FCU-A heated refrigerant pressure regulator (Items 17 and 36, respectively, in Figure 2 10) This FCU-T defrost refrigerant pressure regulator (Item 17) starts to open at that saturated pressure value (70 psig) and modulates the defrost refrigerant flow to the defrost refrigerant separator (Item 34 in Figure 2.10). The FCU-T defrost refrigerant pressure regulator closes when the saturated pressure of the defrost refrigerant at its inlet drops below 70 psig This pressurizing process is needed here to hold the defrost refrigerant inside the FCU-T finned tubes for a suitable period of time in order to confirm and speed the removal of all the frost accumulated on the finned tubes and also to dry out the finned tubes.

A schematic showing the FCU-T operating under the refrigeration mode can be seen in Figure B 1, while a schematic showing the same unit operating under the hot-gas defrosting mode can be seen in Figure B 2 In these schematics, the refrigerant flow

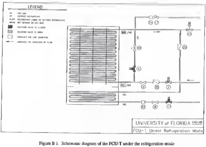
LEGEND
HG HOT GAS
DF DEFROST REFRIGERANT
RL/DR REFRIGERANT LIQUID OR DEFROST REFRIGERANT
WR/HG WET RETURN OR HOT GAS
SOLENOID VALVE IS CLOSED
SOLENOID VALVE IS OPEN
INDICATES THE LINE CONDITION
INDICATES THE DIRECTION OF FLOW
WR/HG
RL/DR
HG
HG
24
17
15
46
45
6
3
29
2
32
8
51
UNIVERSITY of FLORIDA CAD LAB
FCU-T Under Refrigeration Mode

Figure B.1 Schematic diagram of the FCU-T under the refrigeration mode

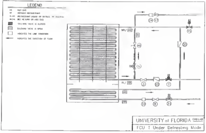
LEGEND
HOT GAS
DEFROST REFRIGERANT
SOLENOID VALVE IS CLOSED
SOLENOID VALVE IS OPEN
INDICATES THE LINE CONDITION
INDICATES THE DIRECTION OF FLOW
HG
RL
24
17
5
3
2
6
UNIVERSITY of FLORIDA CAD LAB
FCU T Under Defrosting Mode

Figure B.2 Schematic diagram of the FCU-T under the hot-gas defrosting mode

directions and the conditions of the solenoid valves are clearly identified. During the FCU-T refrigeration mode, the FCU-T liquid line solenoid valve and the FCU-T wet return stop solenoid valve are both open (Items 2 and 15, respectively, in Figure B.1) while the hot gas defrost solenoid valve and the defrost refrigerant solenoid valve are both closed (Items 31 and 6, respectively, in Figure B.1). During the FCU-T hot gas defrosting mode, the FCU-T liquid line solenoid valve and the FCU-T wet return stop solenoid valve are both closed (Items 2 and 15 respectively, in Figure B.2), while the hot gas defrost solenoid valve and the defrost refrigerant solenoid valve are both open (Items 31 and 6, respectively, in Figure B.2).

After passing through the FCU-T defrost refrigerant pressure regulator (Item 17 in Figure 2.10), the defrost refrigerant will flow into the defrost refrigerant separator (Item 34 in Figure 2.10) which works as a liquid vapor separator. This separator is manufactured in house and is shown in Figure B.3. The vapor leaves the top of the separator where then, it passes through the defrost orifice meter and a hand operated throttling valve (Items 33 and 27, respectively, in Figure 2.10). The liquid leaves the bottom of the separator, where then, it passes through the high-side float valve and the liquid refrigerant isolation valve (Items 53 and 45, respectively, in Figure 2.10). After leaving the liquid refrigerant isolation valve (Item 45), the liquid refrigerant mixes with the vapor refrigerant coming from the hand operated throttling valve (Item 27) before it connects to the 1 3/8 OD main wet return line.

The defrost orifice meter is identical to the hot gas orifice meter (Items 33 and 32, respectively, in Figure 2.10) and is manufactured in house (model M2). It is used to measure the mass flow rate of the refrigerant vapor. The high-side float valve (Item 53 in

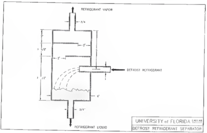

Figure B.3 Defrost refrigerant separator

Figure 2.10) is manufactured by Vilter Manufacturing Corporation (model number KT1018) and is used to provide a liquid seal to the bottom outlet of the defrost refrigerant separator, otherwise, some vapor refrigerant could exit from the bottom outlet of the latter at the late stages of the FCU-T hot-gas defrosting mode. Having a liquid seal to the bottom outlet of the defrost refrigerant separator is important in order to confirm the flow of all the vapor refrigerant through the defrost orifice meter (Item 33) for a correct vapor flow measurement.

A vent line connecting the top of the high-side float valve to the defrost refrigerant line upstream of the defrost refrigerant separator (Item 34) can be seen in Figure 2.10. This vent line is needed to equalize the vapor pressure inside the high-side float valve. The defrost refrigerant and liquid refrigerant isolation valves (Items 46 and 45, respectively, in Figure 2.10) are identical Superior ball valves (model number 586W-8ST). These valves along with a Superior hand operated throttling valve (Item 27 in Figure 2.10; model number 216-10ST) are employed in the system in order to be able to isolate the defrost refrigerant line and its components for service and maintenance. These valves are to be fully open when the system is in operation, and should be closed when the system is shut down in order to prevent the refrigerant from migrating to the main wet return line. A picture of the defrost refrigerant line and its components is shown in Figure B.4, where the FCU-T defrost refrigerant strainer and the FCU-T defrost refrigerant pressure regulator are seen in the center of the picture. The high-side float valve is also seen to the left of the strainer while the defrost refrigerant separator is seen at the upstream right of the pressure regulator.

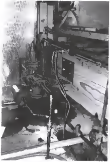

Figure B 4. Defrost refrigerant line and its components

All the refrigerant connections to the 1-3/8" OD main wet return line that were discussed before will lead the refrigerant to proceed inside the main wet return line until it enters the load compensation unit (LCU) as can be seen in Figure 2.10 The refrigerant will pass through the LCU wet return isolation valve (Item 40 in Figure 2.10) before it enters the LCU This isolation valve is a ball valve manufactured by Superior valve company (model number 592WA-13ST) and is always kept open (only closed when the load compensation unit is in need of service and maintenance). The load compensation unit is a pressure vessel used as a liquid refrigerant vaporizer in order to compensate for the hot-gas required during the FCU T hot-gas defrosting mode The LCU also serves as a liquid refrigerant storage drum and a liquid-vapor separator (Stoecker 1988)

As the wet return enters the LCU, its vapor leaves the top of the LCU through the 2-1/8"OD main suction line and passes through the LCU suction line isolation valve and the LCU pressure regulating valve (Items 42 and 13, respectively, in Figure 2 10) before entering the condensing unit. The liquid refrigerant accumulates inside the LCU until its level reaches the liquid overfeed outlet, where then, the overfeed liquid leaves the LCU through the 1 1/8"OD liquid line and passes through the LCU liquid line isolation valve and a schrader valve (Items 44 and 49, respectively, in Figure 2.10) before entering the surge drum A 7/8"OD drain line connects the bottom of the LCU with this liquid line at a point upstream of the schrader valve, where the LCU drain line valve (Item 43 in Figure 2.10) is installed on this drain line. This LCU drain valve is always closed, and only opens when there is a need to evacuate the LCU for service and maintenance The vapor inside the surge drum leaves the top of the latter through the 1 1/4"OD suction line and passes through the surge drum suction line isolation valve (Item 41 in Figure 2.10) before it connects with the main suction line as can be seen in Figure 2.10.

The surge drum and the LCU suction line isolation valves along with the LCU drain line and liquid line isolation valves (Items 41, 42, 43 and 44, respectively, in Figure 2.10) are all ball valves and are manufactured by Superior valve company (model numbers 592WA-13ST 594WA-21ST, 587W-14ST and 591WA-11ST, respectively) The isolation valves (Items 41, 42 and 44) are always kept open when the system is in operation, and are only closed when the system is shut down in order to store the liquid refrigerant inside the LCU The schrader valve (Item 49 in Figure 2.10) is used as a gage port to read the pressure of the liquid line, and is also used to charge and discharge refrigerant from the system (Pita 1991, Whitman and Johnson 1991)

A 5/8"OD liquid refrigerant bypass line connects the main liquid line from a point upstream of the turbine flow meter (Item 30 in Figure 2.10) to the main wet return line at a point downstream of the LCU wet return isolation valve (Item 40 in Figure 2.10) A hand operated throttling valve (Item 29 in Figure 2.10) is installed on this liquid bypass line. This Superior hand operated throttling valve (model number 255A-8S) is used when needed to adjust the pressure and temperature of the wet return going to the LCU

The LCU pressure regulating valve is manufactured by Sporlan Valve Company (model number ORIT 20-0/75) and has the capability of operating at pressure drops of less than one pound per square inch. This valve is sensitive only to its inlet pressure where it throttles to open as its inlet pressure rises above a preset minimum LCU pressure value and throttles to close as its inlet pressure drops toward the preset value The valve will be fully closed when the inlet pressure is equal to or lower than the preset minimum

LCU pressure value (Sporlan 1991a). Therefore, its function is not to hold a constant LCU pressure but to prevent a minimum LCU pressure from occurring (Tomczyk 1996b).

The LCU pressure regulating valve is a pilot operated valve, where it has a small pilot valve attached on top of the main valve. The pilot valve has an external equalizer connection of 1/4" OD which connects the pilot valve with the LCU suction line. The pilot valve also has a bleed orifice which leads to the main suction line through an outlet connection of 1/4" OD. The LCU pressure regulating valve is an externally adjustable type valve that utilizes an adjusting screw and spring assembly to preset a minimum LCU pressure value, where the pressure adjustment ranges from 0 to 75 psig. The LCU pressure regulating valve is employed with a pressure tap on its inlet connection, which allows the use of a pressure gage to check the setting of the inlet pressure (Sporlan 1991a).

The LCU pressure regulating valve is operated by the power of the hot-gas high pressure. The hot gas enters the valve through the pilot valve's hot-gas inlet, where the latter is equipped with a strainer to protect the pilot assembly from potential dirt (Sporlan 1991a). The hot-gas is supplied to the pilot valve by opening the hand operated throttling valve (Item 20 in Figure 2.10) located on a 1/4"OD pilot line extending from the main hot gas line to the pilot valve's hot-gas inlet as can be seen in Figure 2.10. The LCU pressure regulating valve is a normally-opened valve that operates in a mechanism, where it is closed by the hot-gas pressure bleed on the top of the main valve piston as long as the LCU pressure is equal to or below the valve setting. The LCU pressure regulating valve opens when the LCU pressure is above the valve setting by venting the hot-gas through the bleed orifice of the pilot valve and out to the suction line (Sporlan 1991a).

The hand operated throttling valve (Item 20 in Figure 2.10) is manufactured by Superior valve company (model number 254A-4S) and must be kept open as long as the system is in operation in order to supply the hot-gas to the pilot valve of the LCU pressure regulating valve This throttling valve must be closed when service and maintenance are needed for the LCU pressure regulating valve It is also closed for system pump down control, since closing the throttling valve will release the hot gas pressure on the top of the main valve piston of the LCU pressure regulating valve, which in turn keeps the regulating valve open during the pump down process (Sporlan 1991b)

As can be seen in Figure 2.10, there are five sight glasses and seven vibration isolators installed in the piping system The sight glasses are used to indicate the conditions of the liquid refrigerant, while the vibration isolators are used to reduce the effects of the compressor and motor vibrations on the other piping system components. All the suction lines have been insulated with 3/4" thick Rubatex, while the main liquid line is only insulated from the liquid refrigerant outlet of the surge drum up to the turbine flow meter (Item 30 in Figure 2 10) with 3/4" thick Rubatex

APPENDIX C
DESCRIPTION OF THE COMPRESSOR CAPACITY CONTROL SYSTEM

The compressor capacity control system is described here with reference to Figure 2.10 and Table 2.1 in Chapter 2. The system is employed in this refrigeration/defrost system in order to protect the compressor from low suction pressure and high suction temperature situations. This system is represented by a 1/2"OD hot-gas bypass line connecting the main hot-gas line with the main suction line, and a 1/2"OD liquid refrigerant bypass line connecting the main liquid refrigerant line with the main suction line as can be seen in Figure 2.10. In the case of a low suction pressure the hot gas bypass line is used to raise the suction pressure by flowing hot gas to the suction line. In the case of a high suction temperature the liquid refrigerant bypass line is used to drop the suction temperature by flowing liquid refrigerant to the suction line.

The hot-gas flows inside the hot-gas bypass line at a point upstream of the piercing valve (Item 54 in Figure 2.10), where then it passes through the hot gas bypass solenoid valve and the hot-gas discharge bypass valve (Items 9 and 10 respectively, in Figure 2.10) before it connects with the main suction line. The hot gas bypass line connects with the main suction line at a point upstream of the oil rich refrigerant line connection. The liquid refrigerant flows inside the liquid refrigerant bypass line at a point downstream of the schrader valve (Item 48 in Figure 2.10), where then it passes through the liquid bypass solenoid valve and the desuperheating thermostatic expansion valve (Items 11 and 12, respectively in Figure 2.10) before it tees with the hot-gas bypass line on its way to the main suction line.

The hot-gas discharge bypass valve and the desuperheating thermostatic expansion valve are both externally equalized valves, where each valve is equipped with a 1/4"OD external equalizer. The hot gas bypass valve's external equalizer tees with the other valve's external equalizer before it connects with the main suction line at a point closer to the condensing unit as shown in Figure 2.10. The desuperheating thermostatic expansion valve is employed with a sensing bulb located on the main suction line upstream of the equalizer connection (Sporlan 1992) and downstream of the oil rich refrigerant line connection.

The hot-gas bypass solenoid valve (Item 9 in Figure 2.10) is manufactured by Sporlan Valve Company (model number B10S2) and is a normally-closed valve that is energized to open as long as the refrigeration/defrost system is in operation. This valve is de-energized to close when the system is shut down or during system pump down process in order to prevent the flow of hot-gas to the main suction line.

The hot-gas discharge bypass valve (Item 10 in Figure 2.10) is manufactured by Sporlan Valve Company (model number ADRPE 3) and is used to prevent the suction pressure from dropping to a low value. It is a fully adjustable type valve which offers a spring assembly for pressure adjustment purposes in the range of 0 to 80 psig (Sporlan 1994b). This valve throttles to open as the suction pressure drops below the preset opening pressure value, and throttles to close as the suction pressure rises toward the preset opening pressure value. The valve will be fully closed when the suction pressure is equal to or higher than the preset valve opening pressure value. The flow of the hot-gas to the main suction line will raise the suction pressure in order to control the compressor capacity, while this process might overheat the compressor because of the high hot gas temperature. The role of the desuperheating thermostatic expansion valve comes here, where it will pass liquid refrigerant to the main suction line in order to drop the suction temperature (Sporlan 1994b).

As can be seen in Figure 2.10, the hot gas bypass line is also bypassed by a 1/2"OD hot-gas line that has a hand operated throttling valve installed on it (Item 23 in Figure 2.10). This valve is manufactured by Superior valve company (model number 255A-8S) and is used to provide hot-gas to the main suction line when there is a sudden drop in the suction pressure or when the suction pressure drop is more than what the hot-gas discharge bypass valve can handle.

The liquid bypass solenoid valve (Item 11 in Figure 2.10) is manufactured by Sporlan Valve Company (model number E9S240) and is a normally-closed valve energized to open as long as the system is in operation. This valve is de-energized to close when the system is shut down or during system pump down in order to prevent the flow of liquid refrigerant to the main suction line.

The desuperheating thermostatic expansion valve (Item 12 in Figure 2.10) is manufactured by Sporlan valve company (model number EGVE-1-1/2-Z) and is used to maintain a certain amount of superheat in the main suction line, where the valve is employed with an adjusting stem and spring assembly for that purpose (Sporlan 1993b). This control valve is employed with a thermostatic element, which is a sensing bulb connected to the top of the valve diaphragm by a capillary tube. The sensing bulb is filled with a thermostatic charge (type Z) sensitive to the suction temperature (Sporlan 1993b).

The operating mechanism of the desuperheating thermostatic expansion valve is based on three pressures acting on the valve's diaphragm. The spring and the equalizer pressures are the two pressures acting underneath the diaphragm in order to close the valve. The spring pressure is the adjustable pressure by the stem and spring assembly, while the equalizer pressure is the suction pressure. The third acting pressure is that of the sensing bulb which is acting on the top of the diaphragm in order to open the valve, where this pressure is a function of the thermostatic charge temperature. When the valve is in operation, the opening pressure must equal the closing pressure in order to maintain the desired amount of superheat in the main suction line (Sporlan 1993a).

The sensing bulb has a length of 3.5" and an outside diameter of 0.5", while it is connected to the desuperheating thermostatic expansion valve by a 5-foot standard capillary tube of 1/8"OD (Sporlan 1993b). When the suction temperature rises the heat transferred from the main suction line to the attached sensing bulb increases the thermostatic charge pressure within the bulb which causes the valve to open and the liquid refrigerant to flow to the main suction line in order to bring back the desired amount of superheat. On the other hand, when the suction temperature drops the thermostatic charge pressure drops with it and causes the valve either to modulate or to shut off depending on how low the drop in the superheat level was (Sporlan 1993a).

APPENDIX D
DESCRIPTION OF THE ARTIFICIAL LOAD GENERATION SYSTEM

The artificial load generation system is described here with reference to Figure 2.23 and Table 2.5 in Chapter 2 It is designed to provide the freezer with the required load in order to be able to manipulate the value of the load sensible heat ratio (LSHR) inside the freezer during the testing period This artificial load generation system provides both sensible and latent loads.

The generation of the sensible heat load is provided by an electric duct heater with integral limit control manufactured by Warren Technology (model number HO-10 00-16 x 16) with a total capacity of 10 kW (Item 78 in Figure 2 23) This heater is a 5 step heater where each step is 2000 Watts This heater is power controlled by an Omega silicon controlled rectifier (model number SCR73Z-230-M) which is an extremely fast controller capable of controlling the required sensible load setting to be provided to the freezer This controller can be operated by a computer, since the controller can accept input signals of 4-20 mA, as well as manually as it is employed with a manual module and a remote potentiometer (Omega 1992a, 1993)

The artifical latent heat load is generated by the water-vapor generator (WVG) shown as Item 77 in Figure 2.23 City water is allowed to flow into the system by opening the hand operated line valve (Item 70 in Figure 2.23), where the water starts to fill the McMaster-Carr polyethylene water tank (model number 3754K71) The tank has a capacity of 5 gallons and its dimensions are 16"L x 10"W x 8"H, and is employed with a brass float valve (model number 4607K41) to protect the tank from overflow (McMaster-Carr 1996).

The water then flows to an electronic diaphragm metering pump (Item 72 in Figure 2.23) which is manufactured by LMI-MILTON-ROY (model number A751 95T). The pump capacity ranges from 0.63 to 63 milliliter per minute, where its maximum capacity per day is 24 gallons. This metering pump has an adjustable speed which ranges from 5 to 100 strokes per minute while it also has an adjustable stroke length that ranges from 0 to 100% (Cole-Parmer 1995). A picture of the electronic diaphragm metering pump is shown in Figure D.1. The metering pump can be operated manually, where by adjusting the frequency and the stroke length, the pump will provide the exact amount of water at the desired flow rate in order to generate the required latent heat load. This pump can also be operated by a computer since it is employed with a Micropace analog to-digital converter (model number MP-100) which is an automatic controller that can receive an input analog signals of 4-20 mA. This will allow the computer to adjust the metering pump to discharge the required amount of water to the water-vapor generator (Item 77 in Figure 2.23).

The water flows through two check valves (Items 73 and 74 in Figure 2.23) after it leaves the metering pump. These valves serve the purpose of preventing the backflow of water to the metering pump. The first check valve (Item 73) is an injection valve that is part of the metering pump assembly, while the other check valve (Item 74) is a Superior valve (model number 802B 6S). A Sporlan water feed solenoid valve (model number E5S130) is located between the Superior check valve (Item 74) and the WVG (Item 77)

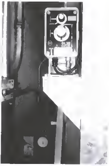

Figure D.1 Electronic diaphragm metering pump

This normally-closed solenoid valve (Item 76 in Figure 2.23) is energized to open when water is needed to supply the WVG, and de-energized to close otherwise.

The WVG is a liquid-injection type water vapor generator. It is a 1/4" thick steel constructed vaporizer that has a rectangular shape and inside dimensions of 27"L x 5.5"W x 1.5"H. The vaporizer is equipped with three heating elements strapped to its sides and bottom, and each heating element works at 700 Watts and 240 Volts. The vaporizer with its three heating elements are insulated with a 1" thick high temperature insulator and are all enclosed in an 18 gage galvanized sheet metal housing. The overall dimensions of the WVG housing are 32"L x 7"W x 6"H. A picture of the water vapor generator is shown in Figure D.2.

As can be seen in Figure 2.23, the water vapor generator is also equipped with a thermometer, a thermostat and a pressure relief valve. The thermometer is an Ashcroft thermometer (model number 2A609) that has a reading range of 50 to 550°F. The thermostat is a Vulcan Calstat thermostat (model number 1C1C9) that has an adjustable temperature range of 100 to 600°F, where its adjusting screw is used to adjust the thermostat to the desired set point (Vulcan 1992). The pressure relief valve is a Grainger valve (model number 5Z763) that has a cracking pressure range of 0 to 20 psig. The cracking pressure can be adjusted to the desired set point using the valve's adjustment screw.

The water injected to the WVG is heated to the desired temperature inside the vaporizer and is allowed to leave the WVG as steam through a 7/8" copper tube. This copper tube passes through the freezer wall to the steam outlet as shown in Figure 2.23. The process of injecting steam to the freezer occurs while the temperature inside the latter

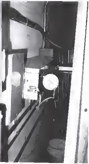

Figure D 2 Water vapor generator

is very low (below 0°F). To prevent the steam from freezing inside the copper tube, a Raychem electric heating cable (model number W51-12P) is wrapped around the copper tube inside the freezer. This electric heating cable is 12 feet in length and has a voltage range of 110-120 Volts and its power rating is 5 Watts per foot on a pipe at 40°F (Raychem 1994). The copper tube and the heating cable are both covered by a 3/4" thick Armaflex insulation. A "clean-up" strip heater is also attached to the bottom of the steam outlet in order to prevent the steam from freezing at the outlet which will then stop the flow of steam to the freezer. The strip heater has a voltage rating of 120 Volts and a power rating of 150 Watts.

The artificial load generation system is employed with a Dayton blower (model number 5C093A) that has a wheel of 10-5/8" diameter and a width of 8" (Item 79 in Figure 2.23). This blower is used to distribute the latent (steam) and the sensible heat loads inside the freezer. A picture of the artificial load generator is shown in Figure D.3, where the blower and the steam outlet can be seen. The blower is operated by a 1/2-hp motor that is mounted to the body of the blower in order to reduce vibrations. This motor operates at four different speeds and has a capacity of 1550 cfm when the motor is operating at a speed of 1050 rpm (Dayton 1992). As can be seen in Figure 2.23, the blower discharges the air through a discharge duct ending with a grill.

An alternate water vapor generation technique has also been tried in this research. This system is shown in Figure 2.23, and is represented by the Sporlan solenoid valve and the Omega formed ceramic radiant heater (items 75 and 80, respectively in Figure 2.23) where the latter surrounds a 2"OD copper tube. This tube is to be heated and is extended inside the discharge duct on both sides of the heater. The inside bottom of the 2"OD tube

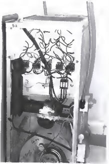

Figure D 3. Artificial load generator

is filled with a bronze wool blanket in order to absorb the injected water before it vaporizes. The Sporlan water feed solenoid valve (model number E3S130) is a normally-closed valve that is energized to open when water is needed to supply the copper tube inside the ceramic radiant heater and de-energized to close otherwise.

The Omega formed ceramic radiant heater (model number CRFC-312-240-C) is used for pipe heating, since it has a helical wound heating wire element embedded into the formed ceramic fiber. The ceramic radiant heater has a cylindrical shape with a length of 12" and an outside diameter of 5". The heater is employed with unheated vestibules on its sides which cause the inside diameter of the heater to equal 2". This ceramic radiant heater operates at 240 Volts and has a power rating of 1400 Watts (Omega 1992a). As can be seen in Figure 2.23 the water flows from the solenoid valve (Item 75) to the heater through the 1/4" copper tube. As the water is injected inside the heated 2"OD copper tube, it gets absorbed by the bronze wool blanket. The water then vaporizes and leaves the 2"OD copper tube from its right extension inside the discharge duct, since this extension has some nozzles on it to let the steam out to the freezer. The left extension of the 2"OD copper tube inside the discharge duct is bent 90° in a manner that allows the tube outlet to face the discharge section of the fan. This 90° bend will allow the air to flow inside the 2"OD copper tube in order to pick up the steam and discharge it through the nozzles of the right extension.

APPENDIX E
ORIFICE METERS

E.1. Performance Tests of the Orifice Meters

The hot-gas and the defrost orifice meters are identical and are manufactured in house. A schematic describing the shape and dimensions of the orifice meters can be seen in Figure 3.17 in Chapter 3. Both orifice meters are of the concentric type with sharp edges, and are employed with a D-and-D/2 taps. The inside diameter (D_i) of the pipe is 0.527", while the throat diameter (D_t) is 0.2625". The ratio (β) of the orifice throat diameter to the pipe inside diameter is 0.5.

The two orifice meters were tested for their perfomance, before their installation on the piping system, by forcing compressed air through them. The data from the performance tests are shown in **Table E.1**, where these data have been curve fitted by **POLFIT** polynomial curve fitting program (version 1.01) from Algor Interactive System, Inc. A polynomial equation has been developed for the volumetric flow rate as a function of the differential pressure across the orifice. This fifth order polynomial equation is shown below

$$\forall = C_0 + \left(C_1\,\delta P\right) + \left(C_2\,\delta P^2\right) + \left(C_3\,\delta P^3\right) + \left(C_4\,\delta P^4\right) + \left(C_5\,\delta P^5\right) \qquad \text{(E.1)}$$

where

$\forall$ = Volumetric flow rate in cubic feet per minute (ft^3/min)

Table E.1 Data From the Performance Tests

Volumetric Flow Rate (ft^3/min)	Differential Pressure Across the Orifice (inches of water column differential)	
	Hot-Gas Orifice Meter	Defrost Orifice Meter
0.18	0.1	0.1
0.35	0.2	0.2
0.71	0.5	0.5
1.06	1.2	1.2
1.41	1.8	2.0
1.77	2.8	3.0
2.12	4.2	4.2
2.47	5.8	5.6
2.65	6.6	6.6

δP = Differential pressure across the orifice meter in inches of water column differential (inches WCD)

C_i = Polynomial coefficients and are shown in Table E.2 for each orifice meter

E.2. Calculation Procedure for the Refrigerant Vapor Mass Flow Rate

The following procedure is used to calculate the mass flow rate of the refrigerant vapor:

1- From the measured value of the differential pressure across the orifice meter, calculate the volumetric flow rate ($\forall$) of the refrigerant vapor in cubic feet per minute using Equation (E.1)

2- Calculate the local average velocity ($\overline{V}$) in feet per minute of the refrigerant vapor upstream of the orifice using the following equation

$$\overline{V} = \forall / A \tag{E.2}$$

where

A = Inside cross sectional area upstream of the orifice in square feet, where the inside diameter (D_1) of the pipe is 0.527"

3- From the properties of R-22 refrigerant vapor calculate the Reynolds number (Re_D) as follows

$$Re_D = \frac{\rho_R (\overline{V}/60)(D_1/12)}{\mu g_c} \tag{E.3}$$

where

ρ_R = Density of the refrigerant vapor (lbm/ft^3)

Table E 2 Polynomial Coefficients

Polynomial Coefficient	Hot-Gas Orifice Meter	Defrost Orifice Meter
C_0	$8.8732835 \cdot 10^{-2}$	$6.8789129 \cdot 10^{-2}$
C_1	1.3515731	1.5020023
C_2	$5.6170389 \cdot 10^{-1}$	$-7.6861261 \cdot 10^{-1}$
C_3	$1.5420988 \cdot 10^{-1}$	$2.3729195 \cdot 10^{-1}$
C_4	$-2.1259177 \cdot 10^{-2}$	$-3.4148261 \cdot 10^{-2}$
C_5	$1.1271703 \cdot 10^{-3}$	$1.8147108 \cdot 10^{-3}$

μ = Dynamic viscosity of the refrigerant vapor (lbf sec/ft^2)

g_c = Constant of proportionality (32.2 ft lbm/lbf sec^2)

4- Calculate the dimensionless Discharge Coefficient (C_d) of the orifice meter using the following equation (Miller 1989, ASME 1981)

$$C_d = 0.5959 + 0.0312\beta^{2.1} - 0.184\beta^{8} + 0.039\frac{\beta^4}{\left(1-\beta^4\right)} - 0.0158\beta^{3} + \frac{91.71\beta^{2.5}}{Re_D^{0.75}} \tag{E 4}$$

where

β = Ratio of the orifice throat diameter to the pipe inside diameter; β is equal to 0.5

5- Calculate the dimensionless Flow Coefficient (K) of the orifice meter using the following equation (Miller 1989, Fox and McDonald 1992)

$$K = \frac{C_d}{\sqrt{1-\beta^4}} \tag{E.5}$$

6- Calculate the mass flow rate ($\dot{m}_v$) of the refrigerant vapor in pounds per hour using the following equation (ASHRAE 1993, Fox and McDonald 1992)

$$\dot{m}_v = 3600\left(K\ A\ \beta^2\sqrt{2\,g\,\rho_R\,\rho_{water}\,(\delta P/12)}\right) \tag{E.6}$$

where

ρ_{water} = Density of water (lbm/ft^3)

δP = Differential pressure across the orifice meter in inches of water column differential (inches WCD)

g = Acceleration of gravity (32.2 ft/sec^2)

APPENDIX F

CALCULATION PROCEDURE FOR THE LIQUID REFRIGERANT MASS FLOW RATE

A Signet turbine flow meter (model number MK 525) was used in this project in order to measure the mass flow rate of the liquid refrigerant. The following procedure is used

1- From the measured frequency of the output signals, calculate the maximum local velocity (V_{max}) of the liquid refrigerant in feet per second using the following equation:

$$V_{max} = \frac{f}{F_c} \qquad (F\ 1)$$

where

f = Measured frequency of the output signals (Hz)

F_c = Calibration factor of the turbine flow meter (15 Hz per foot per second) (Signet 1994)

2- Knowing that the maximum local velocity (V_{max}) of the liquid refrigerant is 25% higher than the local average velocity ($\overline{V}$) of the liquid refrigerant (Signet 1994), the following equation is used to calculate the local average velocity ($\overline{V}$) of the liquid refrigerant in feet per minute

$$\overline{V} = \frac{60\ V_{max}}{1.25} \qquad (F\ 2)$$

3- Calculate the mass flow rate ($\dot{m}_L$) of the liquid refrigerant in pounds per hour using the following equation:

$$\dot{m}_L = 60\overline{V}\rho_R A \qquad \text{(F 3)}$$

where

ρ_R = Density of the liquid refrigerant (lbm/ft^3)

A = Inside cross sectional area of the pipe housing the paddlewheel in square feet, where the inside diameter of the pipe is 0 995"

APPENDIX G
TESTING PROCEDURES

The testing procedures employed in this investigation are discussed here in detail with reference to Figures G.1 through G.3. These procedures will cover the initial positions of the system valves before starting up the system, the start up operating sequence to set the freezer to the desired testing conditions, the operating procedures of a complete refrigeration/hot-gas defrost cycle, and the shut down operating sequence.

G.1. Initial Positions of the System Valves

Before starting up the system, the initial positions of the system solenoid valves are shown in Table G.1, while the initial positions of the gate and ball valves are shown in Table G.2. The three hand operated throttling valves (Items 3, 5 and 8 in Figure G.1) are partially opened to their preferable opening positions, since all of them have been pre-adjusted to these opening positions during the trial operation of the system. The shut-off valve (Item 50 in Figure G.1) is fully opened before starting up the system.

G.2. Setting the Psychrometric Room to the Testing Conditions

The following steps of operations have been followed in order to set the psychrometric freezer room to the desired testing conditions.

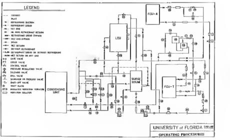

Figure G.1. Operating procedures -- piping system

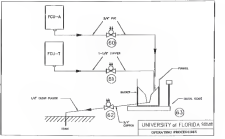

Figure G.2. Operating procedures -- melt weighing system

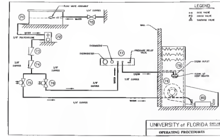

Figure G.3 Operating procedures – artificial load generation system

Table G.1 Initial Positions of the Solenoid Valves

Valve Name	Initial Position	Remarks
FCU-T Liquid Line Solenoid Valve	Closed	Item 2 in Figure G.1
FCU-A Liquid Line Solenoid Valve	Closed	Item 4 in Figure G.1
Defrost Refrigerant Solenoid Valve	Closed	Item 6 in Figure G.1
Main Hot Gas Line Solenoid Valve	Closed	Item 7 in Figure G.1
Hot-Gas Bypass Solenoid Valve	Closed	Item 9 in Figure G.1
Liquid Bypass Solenoid Valve	Closed	Item 11 in Figure G.1
FCU-T Wet Return Stop Solenoid Valve	Opened	Item 15 in Figure G.1
Main Liquid Line Solenoid Valve	Closed	Item 18 in Figure G.1
Oil Return Solenoid Valve	Closed	Item 21 in Figure G.1
Hot-Gas Defrost Solenoid Valve	Closed	Item 31 in Figure G.1
FCU-A Wet Return Stop Solenoid Valve	Opened	Item 38 in Figure G.1
FCU-A Melt Solenoid Valve	Closed	Item 60 in Figure G.2
FCU-T Melt Solenoid Valve	Closed	Item 61 in Figure G.2.
Drain Solenoid Valve	Closed	Item 62 in Figure G.2
Water Feed Solenoid Valve	Closed	Item 75 in Figure G.3
Water Feed Solenoid Valve	Closed	Item 76 in Figure G.3

Table G.2 Initial Positions of the Gate and Ball Valves

Valve Name	Initial Position	Remarks
Hand Operated Throttling Valve	Opened *	Item 3 in Figure G.1
Hand Operated Throttling Valve	Opened *	Item 5 in Figure G.1
Hand Operated Throttling Valve	Opened *	Item 8 in Figure G.1
Hand Operated Throttling Valve	Fully Opened	Item 20 in Figure G.1
Hand Operated Throttling Valve	Fully Closed	Item 22 in Figure G.1
Hand Operated Throttling Valve	Fully Closed	Item 23 in Figure G.1
Hand Operated Throttling Valve	Fully Closed	Item 27 in Figure G.1
Hand Operated Throttling Valve	Fully Closed	Item 29 in Figure G.1
Surge Drum Liquid Line Isolation Valve	Fully Opened	Item 39 in Figure G.1
LCU Wet Return Isolation Valve	Fully Opened	Item 40 in Figure G.1
Surge Drum Suction Line Isolation Valve	Fully Closed	Item 41 in Figure G.1
LCU Suction Line Isolation Valve	Fully Closed	Item 42 in Figure G.1
LCU Drain Line Valve	Fully Closed	Item 43 in Figure G.1
LCU Liquid Line Isolation Valve	Fully Closed	Item 44 in Figure G.1
Liquid Refrigerant Isolation Valve	Fully Closed	Item 45 in Figure G.1
Defrost Refrigerant Isolation Valve	Fully Closed	Item 46 in Figure G.1
Hand Operated Throttling Valve	Fully Closed	Item 47 in Figure G.1
Hand Operated Line Valve	Fully Closed	Item 70 in Figure G.3

* These valves are pre-adjusted to preferable partially opened positions during the trail operations of the system

1- Turn on electric power to all the measuring devices and the freezer's four fluorescent lamps.

2- Set the demand defrost system to the desired frost thickness.

3- Set the digital scale to zero reading (Item 63 in Figure G 2)

4- Set the electronic diaphragm metering pump to the desired water mass flow rate (Item 72 in Figure G.3)

5- Check the pressure setting of the condensing unit low pressure safety switch to be at 1 psi.

6- Turn on the two heating cables along the edges of the freezer doors.

7- Open fully the hand operated line valve (Item 70 in Figure G 3)

8- Turn on the heating elements inside the water-vapor generator (WVG), while energizing its water feed solenoid valve to open (Items 77 and 76, respectively, in Figure G 3) Wait until the temperature inside the water-vapor generator reaches a preset value then continue the following steps.

9- Open fully the hand operated throttling valve, the liquid refrigerant isolation valve and the defrost refrigerant isolation valve (Items 27 45 and 46, respectivaly, in Figure G 1)

10- Open fully the hand operated throttling valve, the surge drum suction line isolation valve, the LCU suction line isolation valve and the LCU liquid line isolation valve (Items 22, 41 42 and 44 respectively in Figure G 1)

11- Open the FCU-A dampers and turn on the dampers frames heating cables.

12- Energize the FCU A liquid line solenoid valve to open (Item 4 in Figure G.1) and start the FCU-A blower

13- Energize the main liquid line solenoid valve, the main hot-gas line solenoid valve and the oil return solenoid valve to open (Items 18, 7 and 21, respectively, in Figure G 1), while starting the oil pump (Item 51 in Figure G 1).

14- Operate the FCU-A under its refrigeration mode by starting the condensing unit and then immediately starting the liquid refrigerant pump (Item 52 in Figure G 1).

15- Energize the hot-gas bypass solenoid valve and the liquid bypass solenoid valve to open (Items 9 and 11 in Figure G 1).

16- Keep adjusting the four hand throttling valves (Items 22, 23, 29 and 47 in Figure G 1) and the surge drum suction line isolation valve (Item 41 in Figure G 1) to their best opening and/or closing positions until the desired system performance is reached. These five valves should always be checked and adjusted once the system performance starts to deviate from the desired performance in order to bring the system back to the desired performance.

17- Keep the system running until the desired FCU-T coil entering air dry bulb temperature (EAT) is reached, which is the desired testing condition inside the freezer.

18- At this point, the FCU-A should be switched to its electric defrosting mode, while starting the FCU-T in a complete refrigeration/hot gas defrost cycle. The operation steps required will be continued in the next section.

G.3. Refrigeration/Hot-Gas Defrost Cycle

In order to operate the FCU-A under the electric defrosting mode and starting the FCU-T in a complete refrigeration/hot-gas defrost cycle, the following steps of operations have been followed starting with step number 19

19- Energize the FCU-T liquid line solenoid valve to open (Item 2 in Figure G.1) and then immediately de-energize the FCU-A liquid refrigerant solenoid valve to close (Item 4 in Figure G.1)

20- Stop the FCU-A blower and immediately operate the FCU-A under its electric defrosting mode by closing the FCU-A dampers, energizing the FCU-A wet return stop solenoid valve to close (Item 38 in Figure G.1), turning off the dampers frames heating cables and turning on the defrosting heater elements.

21- Turn on the blower (Item 79 in Figure G.3), the heat cable, and the strip heater of the artificial load generator.

22- Begin the FCU-T refrigeration/hot-gas defrost cycle by operating the FCU-T under its refrigeration mode. This is done by turning on the electronic diaphragm metering pump (Item 72 in Figure G.3) and immediately starting the FCU-T fan.

23- Energize the FCU-A melt solenoid valve to open (Item 60 in Figure G.2) in order to collect the FCU-A melt in the funnel

24- When all the FCU-A melt has been collected and the FCU-A finned tubes have dried out, terminate the FCU-A electric defrosting mode by turning off the defrosting heater elements, de-energizing the FCU-A wet return stop solenoid valve to open (Item 38 in Figure G.1) and de-energizing the FCU-A melt solenoid valve to close

(Item 60 in Figure G 2) Keep the FCU-A unloaded until the FCU-T starts its hot-gas defrosting mode.

25- Measure the weight of the FCU-A melt using the digital scale (Item 63 in Figure G 2) and then energize the drain solenoid valve (Item 62 in Figure G 2) to open in order to drain all the melt.

26- When all the FCU-A melt has drained, de-energize the drain solenoid valve (Item 62 in Figure G 2) to close and set the digital scale (Item 63 in Figure G 2) to the zero reading again.

27- Keep the FCU-T operating under its refrigeration mode until the desired frost thickness is reached. At this point, the FCU-T should be switched to its hot gas defrosting mode, while starting the FCU-A under its refrigeration mode

28- Turn on the LCU band heaters and adjust their heating load to 70% using the silicon controlled rectifier, while the electronic diaphragm metering pump (Item 72 in Figure G.3) is turned off

29- Turn off the blower (Item 79 in Figure G.3), the heat cable and the strip heater of the artificial load generator

30- Open the FCU-A dampers and turn on the dampers frames heating cables

31- Begin the FCU-A refrigeration mode by energizing the FCU-A liquid line solenoid valve to open (Item 4 in Figure G 1) and starting the FCU-A blower At the same time begin the FCU-T hot-gas defrosting mode by stopping the FCU-T fan, de-energizing the FCU-T liquid line solenoid valve to close (Item 2 in Figure G 1), energizing the FCU-T wet return stop solenoid valve to close (Item 15 in Figure

G.1), energizing the hot-gas defrost solenoid valve to open (Item 31 in Figure G.1) and energizing the defrost refrigerant solenoid valve to open (Item 6 in Figure G.1)

32- Energize the FCU-T melt solenoid valve to open (Item 61 in Figure G.2) in order to collect the FCU-T melt in the funnel.

33- When all the FCU-T melt has been collected and the FCU-T finned tubes have dried out, terminate the FCU-T hot-gas defrosting mode by de-energizing the hot-gas defrost solenoid valve to close (Item 31 in Figure G.1), de-energizing the defrost refrigerant solenoid valve to close (Item 6 in Figure G.1), de-energizing the FCU-T wet return stop solenoid valve to open (Item 15 in Figure G.1), de-energizing the FCU-T melt solenoid valve to close (Item 61 in Figure G.2) and turning off the LCU band heaters. Keep the FCU-T unloaded until the FCU-A starts its next electric defrosting mode.

34- Measure the weight of the FCU-T melt using the digital scale (Item 63 in Figure G.2) and energize the drain solenoid valve (Item 62 in Figure G.2) to open in order to drain all the melt.

35- When all the FCU-T melt has been drained de-energize the drain solenoid valve (Item 62 in Figure G.2) to close and set the digital scale (Item 63 in Figure G.2) to the zero reading again.

36- Keep the FCU-A operating under its refrigeration mode until the previous desired FCU-T coil entering air dry bulb temperature (EAT) is reached. At this point, one FCU-T refrigeration/hot gas defrost cycle is completed.

37- If another FCU-T refrigeration/hot gas defrost cycle is needed then repeat the operation steps 19 to 36. Otherwise, begin the last FCU-A electric defrosting mode and terminate it while proceeding to shut down the system following the operation steps in the next section In the shut down process the refrigerant will be stored in the LCU, the two fan-coil units, and the receiver

G.4. System Shut Down

In order to begin the last FCU-A electric defrosting mode and terminate it while proceeding to shut down the system, the following steps of operations have been followed starting with step number 38

38- Energize the FCU-T liquid line solenoid valve to open (Item 2 in Figure G.1) and immediately de-energize the FCU-A liquid refrigerant solenoid valve to close (Item 4 in Figure G.1).

39- Stop the FCU-A blower and immediately operate the FCU-A under its electric defrosting mode by closing the FCU A dampers, energizing the FCU-A wet return stop solenoid valve to close (Item 38 in Figure G 1), turning off the dampers frames heating cables, and turning on the defrosting heater elements.

40- Start the FCU-T fan

41 Energize the FCU-A melt solenoid valve to open (Item 60 in Figure G.2) in order to collect the FCU-A melt in the funnel.

42- Close folly the two hand operated throttling valves (Items 27 and 29 in Figure G 1), the liquid refrigerant isolation valve and the defrost refrigerant isolation valve (Items 45 and 46, respectively in Figure G 1)

43- Close fully the surge drum suction line isolation valve the LCU suction line isolation valve and the LCU liquid line isolation valve (Items 41, 42 and 44, respectively in Figure G 1)

44- Wait for the condensing unit to stop itself due to the low suction pressure, and then immediately turn off the liquid refrigerant pump and the oil pump (Items 52 and 51, respectively, in Figure G 1) De-energize to close the main hot-gas line solenoid valve, the main liquid line solenoid valve, the hot-gas bypass solenoid valve, the liquid bypass solenoid valve, the oil return solenoid valve and the FCU-T liquid line solenoid valve (Items 7, 18, 9, 11, 21 and 2 respectively, in Figure G 1)

45- Close fully the three hand operated throttling valves (Items 22, 23 and 47 in Figure G 1) and the hand operated line valve (Item 70 in Figure G 3)

46 Stop the FCU-T fan.

47- Increase the pressure setting of the condensing unit low pressure safety switch to 10 psi. This will cause the compressor to cycle on and off in order to store the extra suction line refrigerant into the receiver.

48- Wait for the compressor to cycle on and off until the time of the compressor's off period reaches about 4-5 minutes. At that instant, stop the condensing unit and reduce the pressure setting of the condensing unit low pressure safety switch back to 1 psi.

49- When all the FCU-A melt has been collected and the FCU-A finned tubes have dried out, terminate the FCU-A electric defrosting mode by turning off the defrosting heater elements; de-energizing the FCU-A wet return stop solenoid valve to open

(Item 38 in Figure G.1) and de-energizing the FCU-A melt solenoid valve to close (Item 60 in Figure G.2)

50 Measure the weight of the FCU-A melt using the digital scale (Item 63 in Figure G.2) and then energize the drain solenoid valve (Item 62 in Figure G.2) to open in order to drain all the melt.

51 When all the FCU-A melt has been drained, de-energize the drain solenoid valve (Item 62 in Figure G.2) to close.

52- Turn off the two heating cables along the edges of the freezer doors.

53- Turn off the heating elements inside the water-vapor generator (WVG) and de-energize its water feed solenoid valve to close (Items 77 and 76 respectively, in Figure G.3)

54- Turn off the electric power to all the measuring devices and the freezer's four fluorescent lamps.

APPENDIX H
CALCULATION PROCEDURE FOR THE AVERAGE FROST TEMPERATURE

At any instant of time during the FCU-T refrigeration mode, it is assumed that the frost temperature (T_f) is equal to the average of the liquid refrigerant temperature (LRT) entering the FCU-T and the coil refrigerant temperature (CRT) leaving the FCU-T. In this project, an average constant single value for the frost temperature ($T_{f\ avg}$) is calculated for every run of the refrigeration/defrost system under a desired testing condition of a constant FCU-T coil entering air dry bulb temperature (EAT).

This average value ($T_{f\ avg}$) is calculated by averaging the frost temperatures over all the FCU-T refrigeration modes that occur during the operation of the refrigeration/defrost system under a desired testing condition of a constant FCU-T coil entering air dry bulb temperature (EAT). The following procedures are used to calculate the average frost temperature:

i- Calculate the frost temperature (T_f) in Fahrenheit for every measurement of the liquid refrigerant temperature (LRT) entering the FCU-T and the coil refrigerant temperature (CRT) leaving the FCU-T in every FCU-T refrigeration mode using the following equation

$$T_f = \frac{(\text{LRT} + \text{CRT})}{2} \qquad \text{(H.1)}$$

2 Calculate the average frost temperature for every FCU-T refrigeration mode ($T_{f\ mode}$) using the following equation

$$T_{f\ mode} = \frac{\sum_{i=1}^{Total} \left(T_f \right)_i}{Total} \tag{H.2}$$

where

Total = Total number of measurements during a single FCU-T refrigeration mode.

3- Calculate the average constant single value of the frost temperature ($T_{f\ avg}$) using the following equation.

$$T_{f\ avg} = \frac{\sum_{i=1}^{N} \left(T_{f\ mode} \right)_i}{N} \tag{H 3}$$

where

N = Total number of FCU-T refrigeration modes occurring during the operation of the refrigeration/defrost system under a desired testing condition of a constant FCU-T coil entering air dry bulb temperature (EAT).

REFERENCES

AC&R Components Inc 2-025-001 Oil Separator Installation Instruction Bulletin 2-025-001, rev H, AC&R Components Inc , Chatham Illinois.

AC&R Components Inc 2-025-012 Heat Element Instruction. Bulletin 2-025-012, AC&R Components Inc Chatham, Illinois

Alexiades V and A.D Solomon. 1993 Mathematical Modeling of Melting and Freezing Processes Hemisphere Publishing Corporation Washington, DC

Althouse, A.D , C.H. Turnquist, and A.F Bracciano 1988 Modern Refrigeration and Air Conditioning The Goodheart-Willcox Company, Inc., South Holland, Illinois.

ASHRAE 1992a. 1992 ASHRAE Handbook–HVAC Systems and Equipment. American Society of Heating Refrigerating and Air-Conditioning Engineers Inc , Atlanta, Georgia.

ASHRAE 1992b ASHRAE Research Project 622-WS. A Study to Determine Heat Loads Due to Coil-Defrosting American Society of Heating, Refrigerating, and Air-Conditioning Engineers Inc Atlanta, Georgia.

ASHRAE 1993 1993 ASHRAE Handbook–Fundamentals. American Society of Heating, Refrigerating, and Air-Conditioning Engineers, Inc , Atlanta, Georgia.

ASHRAE. 1994 1994 ASHRAE Handbook–Refrigeration Systems and Applications American Society of Heating Refrigerating, and Air-Conditioning Engineers, Inc Atlanta, Georgia.

ASME Fluid Meters Research Committee 1981 The ISO-ASME Orifice Coefficient Equation Mech. Eng. Vol 103, No 7 July pp 44-45

Bankoff S G 1964 Heat Conduction or Diffusion with Change of Phase Advances in Chemical Engineering Academic Press New York, Vol 5, pp 75 150

Boley B.A. 1963 The Analysis of Problems of Heat Conduction and Melting Proceedings of the 3rd Symposium on Naval Structural Mechanics Pergamon Oxford Edited by A M Freudenthal, B A. Boley and H. Liebowitz, pp 274-278 and 295-296

Brooks Instrument. 1991 Installation and Operating Instructions, Full-View Flowmeters. Bulletin X 1100, Issue 9 Brooks Instrument Division Emerson Electric Co , Hatfield, Pennsylvania, September

Cole R.A. 1989 Refrigeration Loads in a Freezer Due to Hot Gas Defrost and Their Associated Cost. ASHRAE Transactions Vol. 95, Part 2, June, pp. 1149-1154

Cole-Parmer Instrument Company 1995 Cole-Palmer 1995-1996 General Catalog Cole-Parmer Instrument Company, Niles Illinois

Coley, M B 1983. The Cost of Frost. ASHRAE Journal Vol. 82 No. 9, September pp 29-31

ComputerBoards Inc 1992a. CIO-EXP16 & EXP32, User's Manual, Revision 4. ComputerBoards Inc Mansfield, Massachusetts, July

ComputerBoards, Inc 1992b. CIO-DAS08, User's Manual Revision 5 ComputerBoards, Inc, Mansfield, Massachusetts, July

ComputerBoards, inc 1993 CIO-DAC16I: User's Manual Revision 1 0. ComputerBoards, Inc, Mansfield, Massachusetts, July

ComputerBoards Inc 1994a. Data Acquisition & Control, Volume 7, Five Year Anniversary Edition. ComputerBoards, Inc Mansfield, Massachusetts.

ComputerBoards Inc. 1994b. CIO-CTR, User's Manual, Revision 2. ComputerBoards, Inc, Mansfield, Massachusetts February

Copeland Corporation 1990a. 4D Discus Demand Cooling, Form No 90-131R2. Copeland Corporation, Sidney, Ohio

Copeland Corporation 1990b Copeland Discus Demand Cooling, Bulletin AE-1287-R1 Copeland Corporation, Sidney, Ohio December

Dayton Electric Mfg Co 1992. Operating Instructions & Parts Manual, Direct-Drive Blowers, Form 5S2447 Dayton Electric Mfg Co Chicago, Illinois June.

Dayton Electric Mfg Co 5S2709 Operating Instructions & Parts Manual: Linear Actuators Form 5S2709 Dayton Electric Mfg Co., Chicago, Illinois.

Demand Defrost Systems. 1990 Defrost Control Unit Switch (DCUS 100), Control Installation Instructions Form DDS-18 Division of Porpsil, Graziano & Associates Inc , Overland Park Kansas.

Demand Defrost Systems 1992 Commercial Frost Detector Head (CFDH 5), Installation Instructions. Form C5-6/89 Division of Pospisil, Graziano & Associates Inc. Overland Park, Kansas, October

Fox, R.W and A.T. McDonald 1992 Introduction to Fluid Mechanics, 4th ed., John Wiley and Sons, Inc., New York

Gatchilov, T.S and V.S Ivanova. 1979 Characteristics of the Frost Formed on the Surface of the Finned Air Coolers XV International Congress of Refrigeration, Venice, Paper # B2 71, pp 997-1003

Goodman, T.R 1958 The Heat Balance Integral and its Application to Problems Involving a Change of Phase. Transactions of the ASME Vol. 80, February, pp 335-342.

Goodman, T.R. 1964 Application of Integral Methods to Transient Nonlinear Heat Transfer Advances in Heat Transfer Academic Press New York Vol 1, pp 51-122

Goodman, T.R. and J.J Shea. 1960 The Melting of Finite Slabs. Journal of Applied Mechanics Vol 82, March, pp 16-24

Gupta, J.P 1973 An Approximate Method for Calculating the Freezing Outside Spheres and Cylinders Chemical Engineering Science, Vol 28, pp. 1629-1633

Hayashi, y., K. Aoki and H. Yuhara. 1977 Study of Frost Formation Based on a Theoretical Model of the Frost Layer Heat Transfer, Jap. Res. Vol. 6, No 3, July-September, pp. 79-94

HCR Incorporated. 1995a. Videotape Booklet. Form VT-1294 HCR Incorporated, Lewistown, Montana.

HCR Incorporated 1995b Model DCAV Conditioned Air Vestibule HCR Incorporated, Lewistown, Montana.

Hilpert, R. 1933 Warmeabgabe von geheizten Drahten und Rohren Forsch. Geb. Ingenieurwes. Vol 4 pp 220

Hosoda, T and H Uzuhashi 1967 Effects of Frost on the Heat Transfer Coefficient. Hitachi Review, Vol. 16, No 6, pp 254-259

Hyland, R.W and A. Wexler 1983 Formulations for the Thermodynamic Properties of the Saturated Phases of H_2O from 173 15 K to 473 15 K. ASHRAE Transactions, Vol 89, Part 2A, pp 500-519

Incropera, F.P and D.P DeWitt. 1996 Fundamentals of Heat and Mass Transfer. 4th ed., John Wiley and Sons, Inc New York.

Kerschbaumer, H.G. 1971. Analysis of the Influence of Frost Formation on Evaporators and of the Defrost Cycles on Performance and Power Consumption of Refrigeration Systems. XIII International Congress of Refrigeration, Washington D.C., Paper # 3.11, pp. 719-730

Khakimov, K.R. 1957. Problems in the Theory and Practice of Artificial Freezing of Soil. Publishing House of the Academy of Science, Moscow, USSR

Kondepudi, S.N. 1988. The Effects of Frost Growth on Finned Tube Heat Exchangers Under Laminar Flow. Ph.D. Dissertation, Department of Mechanical Engineering, Texas A & M University, December

Kondepudi, S.N. and D.L. O'Neal. 1987. The Effects of Frost Growth on Extended Surface Heat Exchanger Performance: A Review. ASHRAE Transactions, Vol. 93, Part 2, June, pp. 258-274

Kondepudi, S.N. and D.L. O'Neal. 1988. Performance of Triangular Spine Fins Under Frosting Conditions. Heat Recovery Systems & CHP. Vol. 8, No. 1, pp. 1-7

Kondepudi, S.N. and D.L. O'Neal. 1989a. Effect of Frost Growth on the Performance of Louvered Finned Tube Heat Exchangers. Int. J. Refrig., Vol. 12, No. 3, May, pp. 151-158

Kondepudi, S.N. and D.L. O'Neal. 1989b. The Effects of Frost Formation on the Thermal Performance of Finned Tube Heat Exchangers. AIAA Paper # 89-1741, AIAA 24th Thermophysics Conference, Buffalo, New York, June

Kondepudi, S.N. and D.L. O'Neal. 1989c. The Performance of Finned Tube Heat Exchangers Under Frosting Conditions. Collected Papers in Heat Transfer 1989, ASME Winter Annual Meeting, San Francisco, California, HTD-Vol. 123, December, pp. 193-200

Kondepudi, S.N. and D.L. O'Neal. 1990. The Effects of Different Fin Configurations on the Performance of Finned Tube Heat Exchangers Under Frosting Conditions. ASHRAE Transactions, Vol. 96, Part 2, June, pp. 439-444

Kondepudi, S.N. and D.L. O'Neal. 1991a. Frosting Performance of Tube Heat Exchangers with Wavy and Corrugated Fins. Experimental Thermal and Fluid Science, Vol. 4, No. 5, September, pp. 613-618

Kondepudi, S.N. and D.L. O'Neal. 1991b. Modeling Tube-Fin Heat Exchangers Under Frosting Conditions. XVIII International Congress of Refrigeration, Montreal, Canada, Paper # 242, August, pp. 1289-1292.

Krack Corporation. 1992a. Operating and Installation Instructions, Commercial Air-Cooled Condensing Units Model KB. Bulletin KB 1/92. Krack Corporation Addison, Illinois, January.

Krack Corporation 1992b Vertical Discharge Air-Cooled Condensing Units. Bulletin KB-392. Krack Corporation. Addison Illinois March.

LABTECH CONTROL 1995 LABTECH CONTROL On-Line Help, Version 5 1 Laboratory Technologies Corporation Wilmington, Massachusetts.

Lardner T.J. and F.V. Pohle. 1961 Application of the Heat Balance Integral to Problems of Cylindrical Geometry. Journal of Applied Mechanics, Vol 83, June, pp 310-312.

Lunardini, V.J. 1980 Phase Change Around a Circular Pipe CRREL Report No 80-27. U.S. Army Cold Region Research and Engineering Laboratory, Hanover, New Hampshire, December

Lunardini, V.J. 1981 Heat Transfer in Cold Climates Van Nostrand Reinhold Company, New York.

Lunardini V.J. and R. Varotta. 1981 Approximate Solution to Neumann Problem for Soil Systems Journal of Energy Resources Technology Vol. 103 March, pp 76-81

Mamac Systems, Inc 1990a. Pressure Transducer, Model PR-262, Form DN-262.1 Mamac Systems, Inc , Minneapolis, Minnesota.

Mamac Systems, Inc 1990b Low Pressure Transducer; Model PR-272, Form DN-272.5 Mamac Systems, Inc , Minneapolis, Minnesota.

Mamac Systems, Inc 1991 Static Pressure Probe, Model A 520, Form DN 520 2. Mamac Systems, Inc., Minneapolis, Minnesota.

McMaster-Carr Supply Company 1996 1996 Catalog McMaster-Carr Supply Company., Atlanta, Georgia.

Miller R.W. 1989 Flow Measurement Engineering Handbook, 2nd ed., McGraw-Hill Publishing Company. New York.

Mori A. and K Araki 1976 Methods for Analysis of the Moving Boundary Surface Problem International Chemical Engineering, Vol. 16, No 4, October pp 734-744

Muehlbauer, J.C and J.E. Sunderland, 1965 Heat Conduction with Freezing or Melting Applied Mechanics Reviews, Vol 18 No 12, December pp 951-959

Niederer D.H. 1976. Frosting and Defrosting Effects on Coil Heat Transfer. ASHRAE Transactions, Vol. 82, Part 1, February, pp. 467-473.

Ohio Semitronics Inc. 1992. Electrical Transducers and Monitoring Equipment, Catalog Number 1192. Ohio Semitronics Inc. Hilliard, Ohio.

Olivieri J., T. Singh and S. Lovodocky. 1996. Psychrometrics - Theory and Practice, ASHRAE Research Project 872-RP.

Omega Engineering, Inc. 1992a. The Electric Heater Handbook, Vol. 28. Omega Engineering, Inc., Stamford, Connecticut.

Omega Engineering Inc. 1992b. The Temperature Handbook, Vol. 28. Omega Engineering, Inc., Stamford, Connecticut.

Omega Engineering Inc. 1993. SCR71 and SCR73 Series: SCR Power Controllers, Operator's Manual M1112/0293. Omega Engineering, Inc., Stamford, Connecticut.

O'Neal, D.L. 1982. The Effect of Frost Formation on the Performance of a Parallel Plate Heat Exchanger. Ph.D. Dissertation. Department of Mechanical Engineering, Purdue University. December.

Ozisik M.N. 1993. Heat Conduction, 2nd ed., John Wiley and Sons, Inc., New York.

Ozisik, M.N. 1994. Finite Difference Methods in Heat Transfer. CRC Press, Inc., Boca Raton, Florida.

Padki, M.M., S.A. Sherif, and R.M. Nelson. 1989. A Simple Method for Modeling the Frost Formation Phenomenon in Different Geometries. ASHRAE Transactions, Vol. 95, Part 2, pp. 1127-1137.

Pita, E.G. 1991. Refrigeration Principles and Systems. An Energy Approach. Business News Publishing Company, Troy, Michigan.

Raychem Corporation Construction Group. 1994. Gard*n W51 Preassembled Electric Heating Cable, Installation Instructions, Form APP-924. Raychem Corporation Construction Group, Menlo Park, California.

Refrigerating Specialties Co. 1984. Hot Gas Defrost for Ammonia Evaporators, Bulletin 90-10B. Engineers Application Manual, Refrigerating Specialties Co., Broadview, Illinois.

Refrigerating Specialties Division. 1991a. Refrigerant Strainer: Type RSF. Bulletin 00-10E. Refrigerating Specialties Division, Parker Hannifin Corporation, Broadview, Illinois, May.

Refrigerating Specialties Division. 1991b Inlet Pressure Regulators, Type A4A, A4AK, A4AE, A4AR Bulletin 23-05 Refrigerating Specialties Division, Parker Hannifin Corporation. Broadview, Illinois, February

Refrigeration Research Inc 1996 Refrigeration Parts and Equipment, General Catalog Refrigeration Research Inc., Brighton Michigan.

Sanders C.Th 1974 The Influence of Frost Formation and Defrosting on the Performance of Air Coolers Ph.D Dissertation, Technische Hogeschool Delft University The Netherlands, October

Schlichting, H 1979 Boundary-Layer Theory, 7th ed. McGraw-Hill Book Company, Inc., New York.

Signet Scientific Company 1994 MK 525 METALEX Flowsensors and Fittings: Instruction Manual. Signet Scientific Company EL Monte California.

Smith, G R 1989 Theoretical Cooling Coil Calculations at Freezer Temperatures to Avoid Unfavorable Coil Frost. ASHRAE Transactions, Vol 95, Part 2, June, pp 1138-1148

Smith G R 1992 Latent Heat, Equipment-Related Load, and Applied Psychrometrics at Freezer Temperatures. ASHRAE Transactions Vol. 98, Part 2, pp 649-657

Sporlan Valve Company 1981 Thermostatic Expansion Valves, Bulletin 10-10 Sporlan Valve Company, St. Louis, Missouri, October

Sporlan Valve Company 1986 Head Pressure Control Valves Bulletin 90-30 Sporlan Valve Company, St. Louis, Missouri, September

Sporlan Valve Company 1989 Crankcase Pressure Regulating Valves: Installation and Service Instructions Bulletin 90-11 Sporlan Valve Company St. Louis, Missouri, January

Sporlan Valve Company 1990a, Sporlan Head Pressure Control Valves: Installation and Service Instructions Bulletin 90-31 Sporlan Valve Company, St. Louis, Missouri, January

Sporlan Valve Company 1990b Level Master Control Bulletin 60-15 Sporlan Valve Company St. Louis, Missouri, September

Sporlan Valve Company 1990c Thermostatic Expansion Valves, Installation, Field Service and Assembly, Bulletin 10-11 Sporlan Valve Company St. Louis, Missouri, May

Sporlan Valve Company 1991a. Evaporator Pressure Regulating Valves, Bulletin 90-20-1 Sporlan Valve Company St. Louis Missouri, August.

Sporlan Valve Company 1991b Evaporator Pressure Regulating Valves, Installation and Service Instructions Bulletin 90-21 1 Sporlan Valve Company St. Louis, Missouri, May

Sporlan Valve Company 1992. Sporlan Discharge Bypass Valves, Installation and Service Instructions Bulletin 90-41 Sporlan Valve Company, St. Louis Missouri, April.

Sporlan Valve Company 1993a. Thermostatic Expansion Valves, Theory of Operation, Application, Selection, Bulletin 10-9 Sporlan Valve Company, St. Louis, Missouri, January

Sporlan Valve Company 1993b Thermostatic Expansion Valves, Bulletin 10-10 Sporlan Valve Company, St. Louis, Missouri, January

Sporlan Valve Company 1994a. Crankcase Pressure Regulating Valves for Compressor Overload Protection, Bulletin 90-10 Sporlan Valve Company Washington, Missouri, October

Sporlan Valve Company 1994b Discharge Bypass Valves for System Capacity Control, Bulletin 90-40 Sporlan Valve Company, Washington Missouri, September

Stoecker W.F 1957 How Frost Formation on Coils Affects Refrigeration Systems. Refrigerating Engineering, Vol 65, No 2, February pp 42-46

Stoecker, W.F. 1960 Frost Formation on Refrigeration Coils. ASHRAE Transactions, Vol 66 February pp 91 103.

Stoecker, W.F 1988 Industrial Refrigeration Business News Publishing Company, Troy Michigan.

Stoecker W.F., J.J Lux and R.J. Kooy 1983 Energy Considerations in Hot-Gas Defrosting of Industrial Refrigeration Coils Final report. ASHRAE RP 193

Threlkeld, J.L. 1970 Thermal Environmental Engineering, 2nd ed., Prentice Hall, Inc. Englewood Cliffs, New Jersey

Tomczyk, J 1996a. Crankcase Pressure Regulators or CPR Valves. RSC, Vol 64 No 2, February, pp 7 and 10

Tomczyk, J 1996b Evaporator Pressure Regulator Valves RSC Vol 64, No. 4, April, pp. 10-11

Validyne Engineering Corporation. 1988. Sine Wave Carrier Demodulator: CD15. Form VESC-CD15-3/88 Revised. Validyne Engineering Corporation, Northridge, California.

Validyne Engineering Corporation. 1993. General Operating Instructions, Validyne Variable Reluctance Pressure Transducers. Form VEC OIGT-05/93-Revised. Validyne Engineering Corporation, Northridge, California.

Validyne Engineering Corporation. 1994. Ultra Low Range Wet-Wet Differential Pressure Transducer: DP103. Form VESC-DP103-07/94-Revised. Validyne Engineering Corporation. Northridge, California.

Viking Pump, Inc. 1987. Technical Service Manual, Installation, Start Up, Trouble-Shooting, Preventative Maintenance, Do's and Don'ts, Series SG-04, SG-05 and SG-07 Spur Gear Pumps. Section TSM340. Viking Pump Inc., A Unit of IDEX Corporation. Cedar Falls, Iowa.

Vulcan Electric Company. 1992. Take Total Control With The Vulcan Calstat Thermostat. Vulcan Electric Company, Kezar Falls, Maine.

Wang, S.K. 1993. Handbook of Air Conditioning and Refrigeration. McGraw-Hill, Inc., New York.

Whitman, W.C. and W.M. Johnson. 1991. Refrigeration and Air Conditioning Technology, 2nd ed. Delmar Publishers Inc., Albany, New York.

Wile, D.D. 1944. Psychrometry in the Frost Zone. Journal of the ASRE, Vol. 48, No. 4, October, pp. 291-302.

Zakrzewski, B. 1984. Optimal Defrost Cycle for the Air Cooler. Int. J. Refrig., Vol. 7, No. 1, January, pp. 41-45.

BIOGRAPHICAL SKETCH

The author is a citizen of Kuwait and was born in Lebanon on September 26, 1961. Upon graduation from Oregon State University in 1984 with a B.S. with honors in mechanical engineering, he accepted a position as mechanical maintenance engineer with the Kuwait Ministry of Electricity and Water at Az-Zour South Power Station, lasting until May, 1987.

In May, 1987, the author was invited to join the staff of Kuwait University as a scientific assistant, where then he was awarded a scholarship from the University to pursue his graduate studies in the U.S.A. The author completed his M.S. in mechanical engineering from Oregon State University in 1989. He completed an initial Ph.D. course work and research at the University of Washington, then he transferred to the University of Florida in May, 1993, to work for his Ph.D. in mechanical engineering under the supervision of Dr. S. A. Sherif. The author was admitted to Ph.D. candidacy in 1997.

I certify that I have read this study and that in my opinion it conforms to acceptable standards of scholarly presentation and is fully adequate, in scope and quality as a dissertation for the degree of Doctor of Philosophy

S.A. Sherif

S.A. Sherif, Chairman
Associate Professor of
Mechanical Engineering

I certify that I have read this study and that in my opinion it conforms to acceptable standards of scholarly presentation and is fully adequate, in scope and quality as a dissertation for the degree of Doctor of Philosophy

William E. L

William E. Lear
Assistant Professor of
Mechanical Engineering

I certify that I have read this study and that in my opinion it conforms to acceptable standards of scholarly presentation and is fully adequate, in scope and quality, as a dissertation for the degree of Doctor of Philosophy

H.A. Ingley III
Associate Professor of
Mechanical Engineering

I certify that I have read this study and that in my opinion it conforms to acceptable standards of scholarly presentation and is fully adequate, in scope and quality, as a dissertation for the degree of Doctor of Philosophy

Ali Seireg

A. A. Seireg
Ebaugh Professor of
Mechanical Engineering

I certify that I have read this study and that in my opinion it conforms to acceptable standards of scholarly presentation and is fully adequate in scope and quality as a dissertation for the degree of Doctor of Philosophy

Fazl T Najafi

Fazl T Najafi
Associate Professor of Civil
Engineering

This dissertation was submitted to the Graduate Faculty of the College of Engineering and to the Graduate School and was accepted as partial fulfillment of the requirements for the degree of Doctor of Philosophy

August, 1997

Winfred M Phillips
Dean College of Engineering

Karen A. Holbrook
Dean, Graduate School